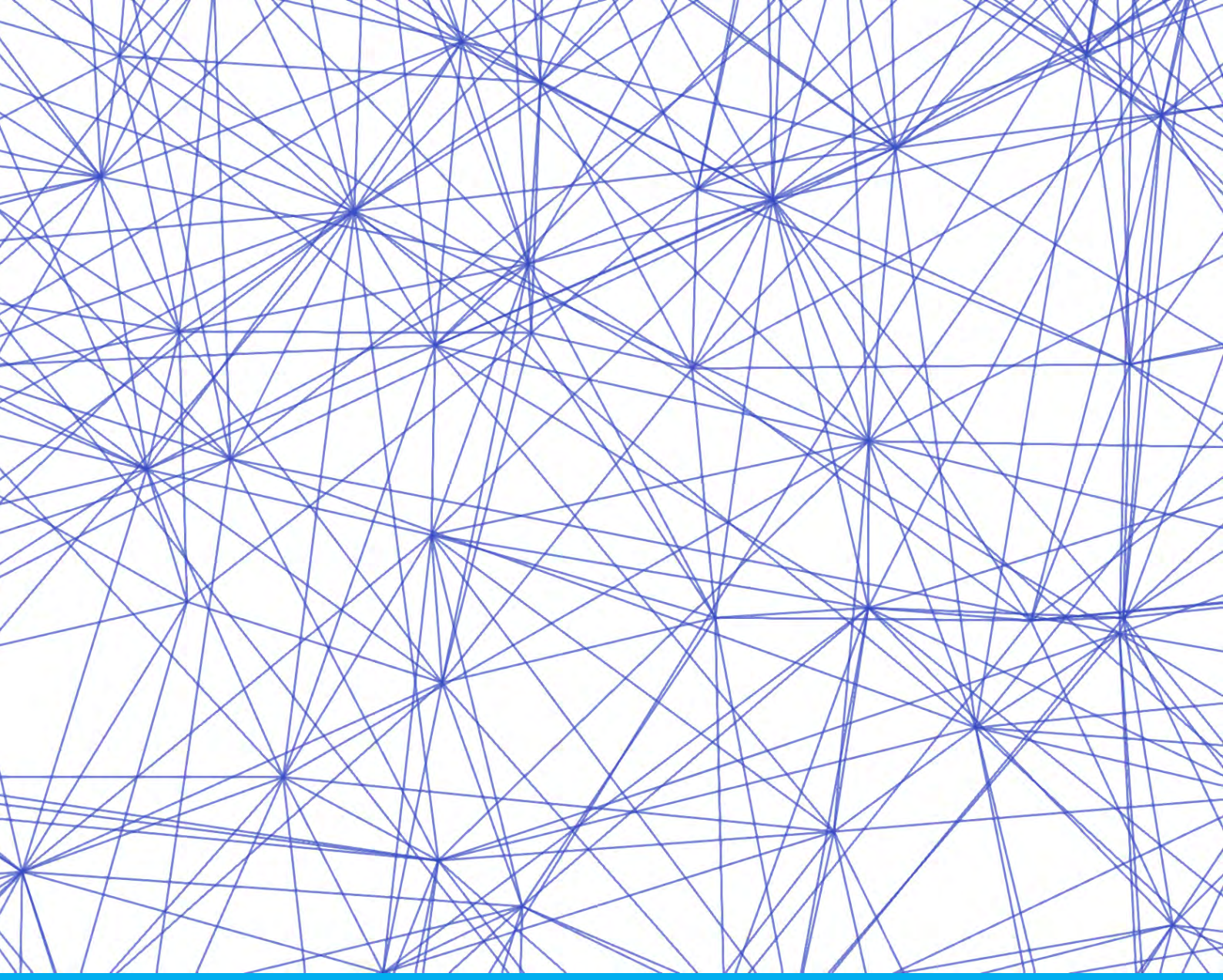

Effect of NSC-SHCC interface in different bond tests using the lattice model

E.J.H. Westerbeek

Technische Universiteit Delft

TU Delft

Effect of NSC-SHCC interface in different bond tests using the lattice model

A numerical and parametric study

by

E.J.H. Westerbeek

to obtain the degree of Master of Science
at the Delft University of Technology,

Student number:	4695445
Project duration:	March, 2022 – January, 2023
Supervisors:	Dr. Ir. M. Luković
	Dr. B. Šavija
	Ir. S. Mustafa

TU Delft

Preface

I hereby present my master thesis. This thesis is written to obtain the degree of Master of Science at the University of Technology in Delft at the faculty of Civil Engineering and Geosciences. This thesis is written to fulfil the requirements of the master track in structural engineering with a specialisation in concrete structures. Apart from fulfilling the requirement, the thesis shows the academic growth and interest gained in past years studying at the university. What cannot be expressed in words in this thesis is the confidence gained in becoming an engineer.

A research oriented thesis about the effect of changing interface properties between different concrete and SHCC using the lattice model is presented. This thesis is a follow up on the experiments carried out by O. Harrass. The experiments are used to compare the simulation results to the experimental observations. This thesis is of interest for anyone working with or planning to work with interfaces in both a theoretical and experimental way. This research provides knowledge and understanding in the behaviour of interfaces and the effect of the interface properties on the structural behaviour.

Preliminary knowledge on concrete and finite element modelling is required, but the concept of interfaces, machine learning and regression analysis will be explained. Machine learning for processing the data is a main part of the research, while unknown to me before starting this thesis. This shows how different disciplines come together. New skills are gained in acquiring information and making a subject my own.

Before moving on to my research I would like to dedicate this section to express my gratitude to a few people.

I would like to thank my supervisors for working with me over the past year. Thank you, Dr. Ir. M. Luković, for providing me with the topic and allowing me to work under your supervision again after the bachelor thesis. Your enthusiasm for the topic and what you do, stimulates students to get the best results possible.

I want to thank my supervisor Dr. B. Šavija for your critical thinking and sharing your knowledge and ideas in the meetings. Your ideas broadened my horizon and expand my knowledge in other fields.

And lastly, Ir. S. Mustafa for your help on a daily basis. Thank you for your flexibility and time for our discussions, even until late.

You all helped me to bring my academic skills to good use. The discussions motivated me to dig deeper, to be curious and to work hard.

I want to thank my fellow students and friends Youri, Regino and Peter. You have been there from the start. And now that we all have gone our separate ways, I appreciate the time we spent even more. Thank you for your support, interest and mostly for making me laugh.

I want to close off by thanking my family: Peter, Jacqueline, Sven and Dennis. I am grateful for all of you in my life. You are always willing to help in any way possible. You know when to give advise, encourage or just listen. You support my decisions and my goals. I am glad to be the youngest and to have such examples to learn from and look up to. The secured place you provided, allowed me to develop myself to the fullest. I know you will always have my back and I cannot thank you enough for doing so.

E.J.H. Westerbeek
Pijnacker, January 27, 2023

Abstract

There is an ongoing demand for concrete structures to become more sustainable. This can be achieved by repairing and strengthening of existing structures to increase the capacity and durability. Strain hardening cementitious composites (SHCC) can be used for this goal. SHCC has a strain hardening behaviour with dense micro-cracking, which makes it more ductile compared to conventional concrete. In new structures SHCC can be used in the tension zone to limit reinforcement needed for crack width control and conventional concrete can be used in the non-critical locations. In each cases a hybrid system is established, where an interface is formed in between the two concrete layers. Different chemical processes take place when forming the interface. As a result, the concrete-concrete interface contains voids, cracks and a higher amount of hydration products. This results in the interface being the weakest link in the system, governing the structural performance. Research is needed to relate the interface properties to the global behaviour of hybrid structures. More specifically, it is interesting to gain insight into the influence of the individual interface properties on the global behaviour. The lattice model is a discrete element model that allows to model the complex behaviour of interfaces with using only the fundamental parameters including the interface stiffness and interface tensile strength. Previous results using the lattice model were found to be promising with respect to the cracking behaviour of hybrid systems. Therefore, the lattice model is used to investigate the effect of the interface tensile strength and interface stiffness on the structural behaviour in different bond tests between normal strength concrete (NSC) and SHCC.

First, small-scale tests were carried out on NSC-SHCC specimens to gain insight into the effect of the changing interface properties for direct tension and shear resistance. Also, the effect of increasing the interface roughness was investigated by modelling a profiled interface. The interface tensile strength and stiffness were altered separately to investigate the effect of the individual interface properties. The effect of the different interface properties was also investigated using a large-scale test, the notched-beam test. In the notched-beam test the SHCC is situated in the tension zone with a notch in the centre and concrete on top. In this test both tension and shear stresses are present in the interface when the structure is loaded under four-point bending. From the notched-beam test a data set was created from the information about the displacement, load, interface opening and joint opening at failure. The data set was investigated to conclude on the effect of the interface properties on the global behaviour. To gain an even better insight into the dependency of the different interface properties a regression analysis is carried out on the notched-beam data. The interface properties are used as input and the behaviour at failure as output. The output considered were the failure load, displacement, interface opening and joint opening. To carry out a regression analysis the data was first split into categories based on the failure modes. Three failure modes can occur, namely concrete failure, interface failure or partial (mixed-mode) failure. A part of the data was used for classification with time series k-means clustering. In this method three dimensions are used: displacement, ratio of failed damaged coupling rebar bond elements and ratio of failed damaged interface elements. After the classification, additional data was generated to provide for stable results of the regression analysis. Time series classification is a time-consuming method to classify the additional data. Therefore, support vector machine is used to find the classification boundaries. This method allows for classification of additional data based on the already classified data. The regression analysis was carried out on the interface and partial failure classes only. For concrete failure the interface is not governing anymore and was, therefore, not part of the regression analysis. Four regression models were used: LASSO, ridge, SVR and regular linear regression. LASSO can shrink the regression coefficients to zero in case there is no effect of the interface properties.

In the small-scale tests adjacent materials were activated at increased interface tensile strength and decreased interface stiffness. In case of interface failure a linear relation is obtained between the interface tensile strength and load capacity for the direct tension and direct shear test on a smooth interface. With higher interface tensile strength cracking of the adjacent materials increased the load capacity, but the mechanical properties of the adjacent materials started to become governing. The application of a profile on the interface increased the capacity even further and resulted in an increased softening. For a profiled interface the effect of changing interface properties was limited in most cases compared to the effect on a smooth inter-

face. This was due to the activation of the adjacent materials at lower interface properties compared to the smooth interface. A decrease in interface stiffness resulted in a scatter of failed elements over the interface, increasing the ductility in the direct tension tests. Findings were similar as found in literature. Except, that the lattice model was found to have a brittle behaviour for modelling the interface with one row of elements. This caused an underestimation of the fracture energy in the direct tension tests. For the direct shear test the results showed decreased softening compared to literature. This could also be due to the modelling of the interface with one row of elements or the elements under compression dominating the behaviour.

Similar trends were found between the structural behaviour and interface properties for the notched-beam test. Only the application of a profile did not increase the load and displacement compared to the smooth interface. To validate the lattice model, the results were compared to experimental results. The lattice model was able to provide the same load-displacement and crack pattern at failure as observed in experiments. For the cases where SHCC was activated the beam stiffness was overestimated. This is a result of the SHCC behaviour modelled in the lattice model. This leads to a deviation from experimental results.

After classifying the data obtained from the beam simulations, the effect of the interface properties on the behaviour in different failure modes is investigated. From the classification it was found that with a smooth interface higher interface properties can be reached before the failure mode would change from interface to partial failure or from partial to concrete failure compared to a profiled interface.

The regression analysis results supported the overall trends. An increase in interface tensile strength and decrease in interface stiffness increase the load and displacement. For both a smooth interface and a profiled interface the same relation between the interface properties and the output values was obtained. A strong dependency of the interface tensile strength and a minor dependency on the interface stiffness was found. For the interface opening no conclusions can be given, because the data was very scattered due to the local behaviour of this output feature. Also, due to the categorization, the remaining data sets were small. Still the R2-scores were above 0.7 in most cases, indicating an accurate prediction of the models. One exception is for partial failure of beams with a smooth interface, for which all models could not predict the simulation values accurately. This was not a result of the data set being too small, but due to the nature of the behaviour of these beams. Beams with a smooth interface showing partial failure had more drops in load in the load-displacement curves from cracking. Beams with a profiled interface showed a more consistent curve for this type of failure. The dependency on the interface properties for different interface geometry and failure modes can be distinguished with the regression analysis results. For interface failure a larger dependency of the interface stiffness is observed for a smooth interface compared to the profiled interface. For the interface tensile strength the dependency is very similar for a smooth and profiled interface. For partial failure this is also observed. However, the regression coefficients are reduced compared to interface failure. This is to be expected, since concrete starts to play an increasing role in the partial failure mode.

All bond tests led to the same overall conclusion about the effect of the interface properties. Only the effect of a profile on the load capacity and displacement is more significant in the small-scale test compared to the notched beam test. The range of interface properties that can be investigated for interface failure is increased with the notched-beam test. This means that in both modelling and experimental testing, the notched-beam test will be able to have failure localized in the interface for higher interface properties. Also, the cracking behaviour can be observed with the notched-beam test. However, the notched-beam test was found to be more time-consuming compared to the small-scale tests in terms of computational time. By carrying out experiments, the notched-beam test will require a larger test set-up and more used materials.

For further research it is recommended to improve the model to predict the experimental results more accurately. The lattice model currently overestimates the stiffness of SHCC. This results in an overestimation of the stiffness of the notched-beam in case the SHCC is activated. This means the model can be improved or a different model should be used to also suffice for cracking of SHCC. Also, modelling of the interface with one row of elements in the small-scale tests leads to a more brittle behaviour. The use of the lattice model is on top of that time consuming due to the large computational time. With the insight on the interface properties of this report, different, faster, models could be used that include these and other properties to broaden the field of research. With a faster model it would be easier to gain a larger data set. Due to the limited time, different profiles were not investigated, although an effect of the profile was indicated in literature for small-scale tests. Investigating the most efficient profile on beams could be of interest in future studies.

Nomenclature

Abbreviations

CH	Calcium hydroxide
CSH	Calcium silicate hydrate
DBA	Dynamic time warping barycentre averaging
DIC	Digital image correlation
DTW	Dynamic time warping
ITZ	Interfacial transition zone
LASSO	Least absolute shrinkage and selection operator
LVDT	Linear variable differential transformers
MAE	Mean absolute error
MSE	Mean squared error
NSC	Normal strength concrete
PoF	Point of failure
RMSE	Root mean squared error
RSS	Residual sum of squares
SF	Silica fume
SHCC	Strain hardening cementitious composite
SS	Sum of squares
SVM	Support vector machine
SVR	Support vector regression
UHPC	Ultra-high performance concrete
UHSC	Ultra-high strength concrete

Symbols

α	Bending influence factor
χ	Uni-axial tensile strength
δ	Measured displacement
$\hat{\beta}$	Regression estimates
$\hat{y}_i$	Predicted value
λ	Langrange's multiplier
μ	Friction coefficient

ν	Poisson's ratio
$\overline{y}$	Mean of the data
ϕ	Friction angle material
ϕ_{eff}	Effective friction angle
ψ	Dilatancy angle
σ_n	Normal stress
τ	Shear stress
A	Area
a	Slope, Regression coefficient
b	Intercept
C	Cluster centre
c	Cohesion
d	Diameter
$D(x)$	Distance function
d_{wk}	Warping path distance of k'th element
E	Young's modulus
e, ϵ	Error
F	Applied load
f_s	Shear strength (no material specified)
f_t	Tensile strength (no material specified)
f_{cm}	Mean concrete compression strength
$f_{ctm,split}$	Tensile splitting test stress
f_{ctm}	Mean concrete tensile strength
G	Shear modulus
K	Stiffness, Warping path length
L	Langragian form, Length, Measuring length
M	Bending moment
p	Probability
R^2	Coefficient of determination
t	Tuning parameter
$t_{c,bond}$	Interface thickness
$t_{n,s,t}$	Traction stress
u	Displacement in normal direction
v	Displacement in tangential direction

W	Section modulus
w	Crack opening, Normal vector SVM
x	Independent variable
y	Dependent variable

Contents

1

Introduction

With the current demand for structures to become more sustainable and efficient use of materials, innovations in concrete are needed. Efficiency in material usage can be reached by using multiple materials in one structure with high quality materials at the susceptible location and lower quality concrete at non-critical locations. An example of such hybrid structures is the use of strain hardening cementitious composite (SHCC) in the tension zone and conventional concrete elsewhere. SHCC has a strain hardening behaviour, making it more ductile due to dense micro-cracking compared to conventional concrete [1]. The strain hardening behaviour of SHCC allows to control crack widths. As a result, reinforcement needed to control crack widths can be limited, saving reinforcement [2]. With this innovation more efficient use of materials can be achieved. On top of that SHCC has been concluded to have improved durability compared to conventional reinforced concrete [3].

SHCC can also be used to strengthen or repair existing structures. Using SHCC for repairing structures allows for bridging between existing and new cracks due to the increased ductility of the material. SHCC can also be implemented as strengthening material to increase the (shear) load bearing capacity of slender structures. With both strengthening or repairing reinforced concrete with SHCC has shown to improve the durability of the structures [4].

Both repairing structures and new hybrid structures result in the formation of an interface between the different types of concrete or the same type of concrete cast at different ages. The interface is often the weakest link in the hybrid system and has a governing role in the structural performance [5]. The structural behaviour of hybrid structures is mostly defined by the bonding of the interface. Different parameters affect the bonding properties of the interface. The parameters affecting the interface are among others the surface preparation, the compressive strength of the weakest concrete and the stress state at the interface [6]. Due to the importance of the interface and the many parameters effecting the behaviour, the concrete-concrete interface is of interest in ongoing research.

In order to predict the behaviour of hybrid structures, the interface should be understood properly. From a research point of view a simple model is required with a limited number of parameters. It is of interest to change one physical parameter at a time to model the effects of the properties individually. However, if interface failure is not achieved, the result cannot be linked to specific interface properties. Once a correct model is obtained, it is a beneficial tool to gain a quick insight into the interface properties and behaviour. Such a model allows for a larger number of simulations in a short period of time compared to experiments. The different parameters can be tuned to create a data set. With a data set it might be possible to observe trends using a regression analysis. With the data of a simple model more insight can be gained into effects shown in experimental studies. It is, however, difficult to select the right test set-up to base a model on, as different bond tests provide different results [7]. The notch beam test used in the master thesis of Harrass [8] has a more complicated stress state in the interface since both tension and shear stresses are present. A structural behaviour can be modelled with the notched-beam test, but insight into the different variables can maybe already be obtained with simple tests. In that case the simple test would be more beneficial.

In [8] the program DIANA was used to model a concrete notched beam with a SHCC layer in the tension zone. Interface elements with a Mohr-Coulomb friction envelope for the interface properties was used. This did

not obtain correct results due to the limitations of DIANA in modelling the SHCC and insufficient knowledge about the non-linear stress distribution in the interface. In an earlier master thesis [5] the same program with a Mohr-Coulomb friction envelope was used to model a concrete beam with SHCC in the tension zone. Also, in this thesis correct material and interface behaviour was not found. These findings imply that a different approach for modelling the interface can be useful to gain more insight into the interface behaviour.

Recently the lattice model was used to model structures on macro scale with promising results for normal concrete behaviour. In [2] the same beams of Singh [5] were modelled using the lattice model. The behaviour of the hybrid beam was overly stiff due to the difficulties of modelling the SHCC behaviour. The interface strength is modelled using a reduced concrete strength. But due to the promising results when it comes to the cracking behaviour, the lattice model could help in modelling the influence of the interface properties on the interface behaviour.

1.1. Goal and research questions

The goal of this thesis is to study the role of different interface parameters on the interface behaviour in hybrid structures. Therefore, the research question is:

What is the effect of the interface properties between NSC and SHCC in different bond tests using the Lattice model?

The answer to this question is given by answering the following sub-questions:

What is the effect of the interface tensile strength on the load capacity and ductility in different bond tests?

What is the effect of the interface stiffness on the load capacity and ductility in different bond tests?

What is the influence of interface roughness on the load capacity and ductility in different bond tests?

What is the interface parameter with the most significant effect on the load capacity and ductility in different bond tests?

What bond test is recommended for investigating the effect of different interface properties?

1.2. Methodology

In this thesis the lattice model is used to study the role of the interface in different bond tests. First, the simple direct tension and direct shear tests are modelled to investigate the effect of the interface properties on the load capacity and ductility on a small scale. Both a smooth and profiled interface will be investigated. Next, three beams tested in the experiments of Harrass [8] are used as a reference for modelling the notched-beam test. One beam with a smooth surface, one with a profile and one with an epoxy layer in the interface are modelled. The hybrid structure consists of normal strength concrete on top and SHCC in the tension zone. In this thesis the simulations will be limited to two beams: one with a smooth interface and one with a profiled interface. The use of an epoxy layer is modelled by changing the strength and stiffness of the interface. The role of the bond strength, stiffness and roughness are investigated. All results will be compared to literature to validate the lattice model and to link interface properties to experimental findings.

With the results of the beam simulations a data set is created with the information at failure. A method is proposed to classify the data into different failure modes. Within each class a regression analysis will be carried out to find the most influential parameter for the interface behaviour.

1.3. Scope

In this thesis the focus is on the interface behaviour, meaning the modelling of the material behaviour is out of the scope of this thesis. The lattice model only allows for altering the tensile strength, compressive strength and elastic modulus. Other parameters cannot be investigated. The influence of other interface effects, for example curing, are investigated in the literature study and will not be modelled explicitly.

1.4. Outline

In Chapter 2 a literature study is carried out to investigate concrete-concrete interfaces on a micro-structural level. Factors influencing the interface behaviour will be explained. Different tests and models to capture the interface behaviour are discussed. In Chapter 3 the lattice model is used to simulate direct tension and direct shear tests. The set-up of the models is explained as well as the effect of changing different parameters of the bond behaviour. Chapter 4 will continue with the notched-beam tests, where the structural behaviour will be modelled. A classification of the data will be carried out. Chapter 5, will focus on the regression analysis with which the most influential parameter will be found. Lastly, Chapter 6 will provide the answer to the research question and recommendations for future work.

2

Literature review

This chapter displays previous research carried out on concrete-concrete interface. First, the interface is explained on a micro-structure level. Next, different influencing factors for the interface behaviour are explained. In the third and fourth section of the literature review the focus switches to testing and modelling methods of interfaces found in literature. Lastly, the lattice model will be explained.

2.1. Micro-structure interface

The interface between concrete and SHCC is of interest in this thesis, but the current literature on NSC-SHCC is limited. Therefore, the concrete-concrete interface will be explained in this literature review.

2.1.1. Concrete-concrete interface

In reinforced concrete different interfaces are present. On meso-scale there is the interface between aggregate particles and the cement paste. This interface is called the interfacial transition zone (ITZ). The ITZ is a weak link that is of importance for the crack initiation and propagation in concrete. Among others this is influenced by the aggregate shape and water-to-cement ratio [9].

The interface discussed in this thesis is the interface between two layers of concrete. This interface arises when old concrete is repaired or strengthened with a new layer or in case of new structures where the first concrete is hardened (partially) before the second concrete layer is poured. The layers could be made of different types of concrete. The interface is the weakest link in the hybrid system, governing the structural behaviour [5]. The concrete-concrete interface is investigated on a micro-scale level to see what mechanisms determine the interface behaviour. The interface between old and new concrete shows similar features as the ITZ [10]

In [11] a model is described in which the interface is divided in three layers. The model indicating the different layers is shown in Figure 2.1. The first layer is the penetration layer, which is on the top of the old concrete layer. The new concrete can partly fill the pores of this layer, increasing the density of this penetration layer. The strength of this layer will thus be positively influenced by the new concrete depending on how much the pores are filled. The second layer is the boundary between old and fresh concrete. The second layer is the weakest link due to the presence of voids, cracks and a high amount of the hydration products calcium hydroxide (CH) and ettringite. The formation of these crystals is the results of the increased water-cement ratio present in the interface layer due to the hydrophilicity of the substrate. In the hydration process with a higher water to cement ratio larger crystals of calcium hydroxide and ettringite are formed, leading to a looser microstructure at the interface [12]. This phenomenon is similar as the interfacial transition zone between aggregates and the cement paste within concrete itself. The third layer is within the new concrete and is hardly affected by the processes taking place in the formation of the interface [11].

Other mechanisms leading to the weaker behaviour of the interface are due to the presence of larger aggregates. When larger aggregates are used the cement can be blocked from penetrating the substrate, the positive effect of the penetration layer will then be limited. Larger aggregates can sink when poured on top of the substrate and blocking the cement from penetrating. This mechanism leads to more gaps in the boundary layer [12].

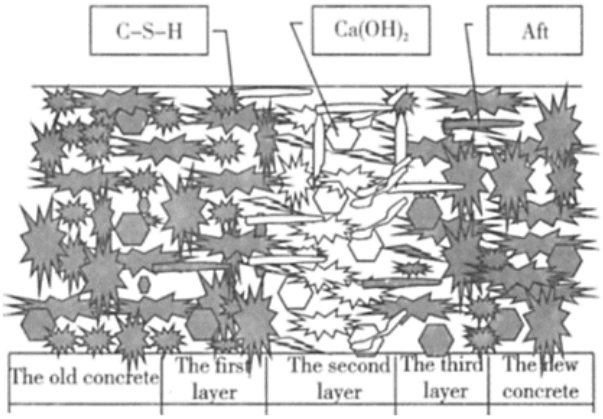

Figure 2.1: Concrete-concrete interface layer model, retrieved from [11].

2.1.2. Concrete-UHPC interface

Other research carried out by [13] investigates the interface on a microstructural level between a concrete substrate and concrete repair layer. The results were compared to a substrate with UHPC as a repair material. Images of the interfaces were made using backscattered electrons (BSE) and are shown in Figure 2.2. In the concrete-concrete interface more gaps were present between the two concrete layers. Also, more cracks had been formed. The microstructure of the UHPC was very dense. Due to the low water to binder ratio and low amount of water the number of pores was reduced. This results in a smaller width of the interface in the UHPC repair layer. In that layer there is high pozzolanic activity due to the presence of silica fume (SF). Silica fume reacts with calcium hydroxide (CH) to form calcium silicate hydrate (CSH) resulting in an increased density of the repair interface. In general, in the interface the CH-content was higher than in the other areas. The decrease of CH-content over the interface towards the repair material was used to compare the width of the interface for concrete and UHPC. The interface covered 55 μm in case of the concrete repair layer and 35 μm in case of the UHPC repair layer. Also, the porosity in the UHPC was found to stabilize at a smaller distance compared to the concrete repair layer.

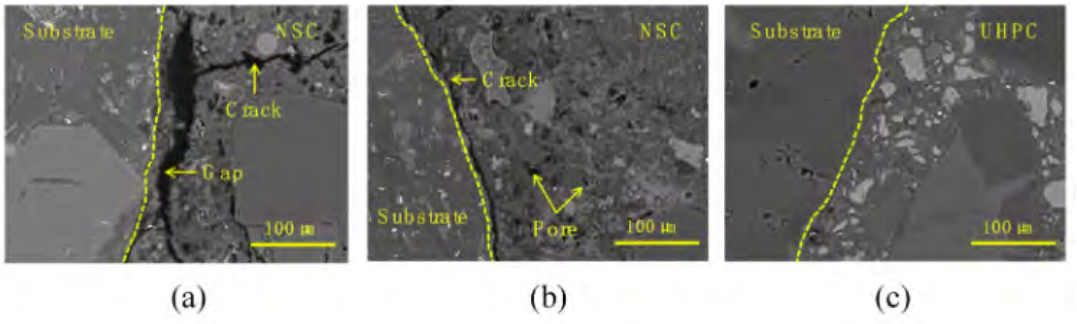

Figure 2.2: BSE images of repair interface of substrate and concrete (a and b) and substrate and UHPC (c), retrieved from [13].

2.1.3. Concrete-SHCC interface

A denser repair layer is also found if SHCC is used as a repair layer. In that case due to the fluidity of the SHCC it can fill pores and microcracks at the surface of the substrate. The bonding mechanisms are comparable to the mechanisms for concrete-concrete interfaces [14].

In [17] two different SHCC mixes were used as an overlay repair layer to concrete. One mix contained slag and the other fly ash. Both caused a chemical reaction with the calcium hydroxide in the concrete substrate to form calcium silicate hydrate. By allowing a secondary reaction between calcium hydroxide and pozzolana to take place the density increases. This improves the microstructure of the interface. This study also emphasizes the possibility of the SHCC to fill the pores and cracks in the substrate due to the fluidity of the mixture.

2.2. Parameters influencing concrete-concrete interface behaviour

In this section the influence of different interface properties and parameters are discussed for concrete-concrete interfaces. Where possible the effect for concrete-SHCC will be included.

According to [6] the interface behaviour depends on the surface preparation, the use of bonding agents, the compressive strength of the weakest concrete, but also the general mechanical properties of the layers, the moisture content of the substrate, curing conditions, the stress state at the interface, the presence of cracking and the amount of reinforcement crossing the interface. The surface roughness is part of the surface preparation. For each of these influencing factors, the effect is explained.

2.2.1. Surface preparation and roughness

Roughness has a classification according to Eurocode 2 [15]. The Eurocode distinguishes four categories: very smooth, smooth, rough and profiled. Very smooth is the side poured against the casting material, smooth the open side without treatment, rough when the open surface is treated and lastly a profiled surface is when a roughness is applied in forms of (ir)regular patterns. Adding a roughness to the concrete surface can be done by for example removing the top layer to allow the aggregates to be visible at the surface. Each classification has a friction coefficient and cohesion value assigned to it. If looked at the Mohr-Coulomb failure envelope, Equation 2.1, it can be observed that an increase in roughness leads to an increase in shear strength.

$$\tau = c + \sigma_n \cdot \mu \tag{2.1}$$

With τ the shear stress, c the cohesion, σ_n the normal stress and μ the friction coefficient.

In this thesis roughness and profiles are stated as micro and macro roughness respectively. In both cases the mechanical interlocking and bonding area is increased, resulting in a better performance of the interface. In literature the addition of a surface roughness is often investigated with one or more of the other influencing parameters, making it difficult to attribute the effect to the roughness only.

One research that focuses on roughness only is carried out by Wagner [16]. A wedge splitting test is carried out to test the effect of the interface roughness between high strength concrete and SHCC. It was found that the bond strength depended strongly on the roughness if the roughness value was low. In that case failure happened at the interface without affecting the SHCC. With a higher interface roughness, the SHCC was affected leading to a post-peak hardening and higher fracture energy. If the bond strength is high, the influence of the roughness is cancelled out, since the cracks will form in the SHCC.

A splitting prism test was carried out in [17] on three samples with different SHCC mixes on a concrete substrate. Compared to a smooth interface an applied roughness increased the interface bond strength. For the three different mixes used an increase in strength of 5 to 12 % was found due to the roughness compared to a smooth interface. The different percentages mean that the roughness alone will not always give the same effect but will have different effects with the different mixes used.

In [8] different profiles were used at the interface. A micro-roughness of epoxy and sand led to an increased bearing capacity and a reduction in the interface opening. The holed and profiled surfaces had an equal or higher bearing capacity respectively. Both showed lower vertical displacement compared to the sand and epoxy surface, but still higher compared to the sample with a smooth interface. In the case of the epoxy-resin interface the failure mechanisms was not at the interface between the two concrete types, but in the interface of the reinforcement in the top layer and the concrete.

2.2.2. Use of bonding agents

Bonding agents are materials that are used to join concrete layers and make the hybrid structure act as one. Examples of such bonding agents are cement-based slurries, epoxies and latex emulsions. By adding a bonding agent or primer on the substrate the interface bond strength can be increased. An increase in bond strength is only achieved if the bonding agent is compatible with the substrate and the repair material [18]. The increase in bond strength can be explained by looking at the effect of bonding agents and primers on the microstructure of the interface. The use of bonding agents or primers results in a less pore microstructure due to a combination of filler, packing and pozzolanic effects. The microstructure improves due to the reaction of silica fume in the primers with the CH in the old concrete forming CSH and densifying the interface.

Adding a bonding primer helps to close the gaps from settling aggregates at the interface. Primers also fill the pores in the substrate before poring the new concrete layer [19].

An increase of CSH, which densifies the interface and increases the bond strength, is also described in [20] for the use of cement-based bonding agents. A two-layer, three-zone model, shown in Figure 2.3 is used to describe the effect. The transition zone (interface) between the substrate and the repair material consists of the permeable layer of the substrate and reaction layer of the new concrete. The roughness effects the permeable layer and the bonding agents the reaction layer. In the reaction layer chemical reactions take place between the bonding agent and cement hydrates. This is the same as described in [19]. In [20] it is, however, described that the polymers in the bonding agent form films that are cross-linked. These fill the cracks and holes on the surface of the substrate, increasing the mechanical interlocking and density. Additionally, the polymers will prevent cracks from expanding. If a high roughness of the substrate is present the repair material can permeate the cracks and holes even better.

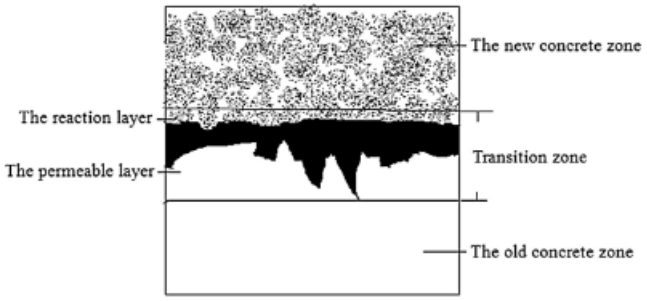

Figure 2.3: Three-zone model new-to-old-concrete interface, retrieved from [20].

The effect of bonding agents is affected by different parameters. The main parameter is the roughness of the interface. A very rough surface will limit the effect of using bonding agents, because the roughness will be the most influential parameter for increasing the bond strength [18, 21]. Another factor influencing the effect of bonding agents is the surface moisture content. It is found that bonding agents work best on a dry surface [21] but this is not always supported by other studies. If case epoxy resin is used as a bonding agent the influence of the roughness and wetness of the interface is negligible, because the failure is often not found at the interface [6]. This is also found in the failure mechanisms in the experiments in [8] with the sand and epoxy resin applied at the interface as described earlier.

Other factors influencing the effect of bonding agents is the applied thickness and properties of the primer. The thicker the applied layer the higher the bond strength. Also, the higher the compressive strength of the primer the higher the bond strength [19].

2.2.3. Compressive strength weakest concrete

In hybrid structures the concrete is cast at different times. This means that even in the case of the same mixture there is a difference in concrete compressive strength and elastic modulus. The weakest compressive strength will influence the behaviour of the hybrid system. Increasing the compressive strength will increase the bond strength and the contribution of cohesion for the shear strength [21].

2.2.4. Moisture content substrate

Moist is absorbed from the repair mortar if the substrate surface is dry. This leads to a denser microstructure and an enhanced bond strength. However, if the surface is too dry the hydration at the interface could be incomplete, reducing the strength of the interface. This latter indicates a surface dry state for the substrate to be preferable. From the investigation of Bentz [22] it was found that a dry substrate has higher moisture transport than the saturated surface dry state. For pull-off testing the consolidation of the repair mortar into the rough profile of the saturated surface dry substrate led to higher bond strength. The combination of a dry substrate with a higher surface roughness leads to an increase of interface strength in the case of slant shear tests. The same relation was found for a bi-surface shear test, as carried out in [21]. A saturated substrate would cancel out the effect of applying a bonding agent or surface roughness due to the lowered bond strength. A dry substrate achieved higher bonding strength. This indicates that for different loading

conditions different moisture content of the substrate is desired.

2.2.5. Stress state interface

In the service life of the repair or hybrid system the interface will experience different stress states due to mechanical and environmental loading. The environmental loading causes a stress state to be present even before the mechanical loading is added. The stress state can influence the interface behaviour and capacity. If the concrete is not cast at the same time the materials will have different elastic moduli leading to additional stresses at the interface [21]. But also due to the different state in the hydration process there will be a difference in shrinkage (both plastic and drying shrinkage) and hydration heat leading to stresses [6]. A way to limit the differential shrinkage is by applying a proper curing method. The effect of curing is discussed next.

2.2.6. Curing conditions

Curing of concrete is the processes that controls temperature and moisture movement from and into concrete. The goal of curing is to keep the concrete saturated to allow for the capillary pores to have filled with hydration products. There are two categories of curing methods to limit the moisture movement: wet curing and membrane curing. In the first method the concrete surface is in constant contact with water. With this method the evaporation of water is prevented. In the second method the loss of water is reduced by applying a barrier [23].

In the experiments of Harrass [8] two different curing conditions were tested. One method used the application of a barrier. During the hardening phase a plastic sheet covered the sample in the mould. In the other curing method, the sample was placed in a humidity-controlled room with a relative humidity of 50% during the hardening process. From the experimental testing the same load bearing capacity was obtained. However, the second method resulted in a reduced initial stiffness.

In hybrid structures there will always be some stress due to differential shrinkage and difference in elastic modulus. However, considering the curing process properly the effect of environmental loading and the accompanying stress state in the interface can be limited. If done properly the curing process will prevent debonding or micro-cracking. For hybrid structures it is important to limit the effect of differential shrinkage as a cause of the different layers being in different phases of the hydration process, for example hardened and hardening in case of repairing structures [6]. It is, therefore, recommended to start curing immediately after casting of the added concrete to improve the bond strength [21].

2.3. Experimental bond tests

In the previous sections different test methods have been used for investigating the interface. Different test set-ups lead to different values of the bond behaviour [7]. The standard test set-ups modelled in this thesis, other standard test-set-ups and the notched beam test set-up will be described.

In this thesis the direct tension, direct shear and notched beam test are used to investigate the different interface properties using the lattice model. The direct tension and direct shear test are straightforward tests which focus on only one fracture mode. There are three fracture modes to distinguish, mode I is for tension, mode II for shear and mode III is a combination of the two. Mode I is achieved with the direct tension, mode II with direct shear and the notch beam test has mode III failure. These test and other test or applications of the methods are described below.

2.3.1. Mode I tests

The standard and most used tension tests are direct tension, pull-off and tensile splitting test as shown in Figure 2.4. In the direct tension test the different materials are cast on top of each other, resulting in a horizontal interface. The specimen is pulled from the top. In this test-set-up there is due to practical issues always some bending moment. The bond strength is often underestimated and the results show a larger scatter compared to other test set-ups [7]. In the tensile splitting test the specimen is compressed perpendicular to the interface. Due to the expansion of the specimen a tensile stress occurs at the interface in the centre, but a compression stress is present at the point where the load is applied. This leads to a non-uniform stress distribution at the interface. The tensile strength from the splitting test can be calculated using the following formula:

$$f_{ctm,split} = \frac{2F_{ult}}{\pi L d} \tag{2.2}$$

With F_{ult} the maximum applied load, L and d the length and diameter of the specimen respectively.
The tensile splitting test is also used for regular homogeneous concrete without interface. In that case the coefficient of variation of the test is much lower compared to the case where an interface is applied [24].

The pull-off test is used for overlay systems mostly. The scatter is large due to local effects. In this test failure does not always happen in the interface, making it less reliable [7].

Lastly, the wedge splitting test can be used. In that case the interface is vertically oriented. The different materials are cast next to each other and the notch is present at the bottom in the interface. This is a short and vertical oriented version of the notched beam, however, because of the vertical orientation of the interface mostly tension will be present, resulting in a mode I fracture instead of the mixed-mode fracture of the notched beam, which will be discussed in Section 2.3.3.

The direct tension test is used to have the lower limit of the behaviour and a simple model set-up.

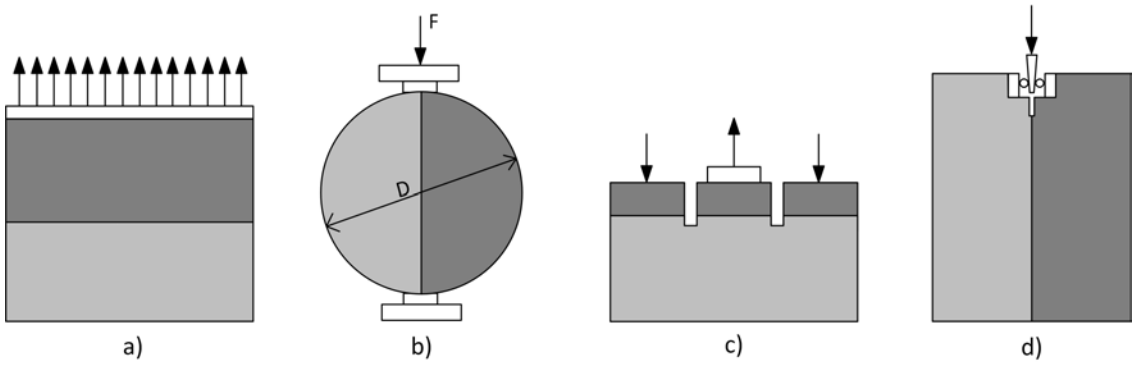

Figure 2.4: Mode I bond tests: a) direct tension test, b) splitting test, c) pull-off test and d) wedge splitting test.

2.3.2. Mode II tests

For shear the bond tests push-out/pull-through, bi-surface shear and L-shaped shear are test methods that are used besides the direct shear test. All test set-ups are shown in Figure 2.5. The push-out generally provides lower values, since no compression and purely shear applies. This test also has a larger scatter due to local effect and stress disturbances. In the bi-surface shear the same set-up as the push-out test is used, but there is only one interface present. The L-shaped test also has one interface but the test set-up allows for only two applied loads to apply compression instead of the three or four needed for the push-out and bi-surface shear. Altering the L-shaped test so that the interface is in a slant will make the test set-up as the slant shear test, which is a mixed mode test [7].

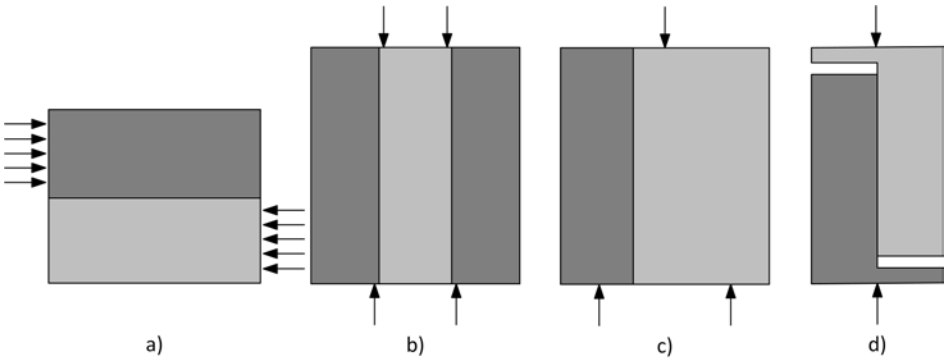

Figure 2.5: Mode II bond tests: a) direct shear test, b) push-out test, c) bi-surface shear test and d) L-shaped test.

2.3.3. Mixed mode tests

For mixed-mode test for crack propagation of regular concrete different test are proposed in literature based on an asymmetrical test set-up and a notch in the shear region [25, 26]. A symmetrical set-up will lead to mode I fracture similar to the wedge splitting test of Section 2.3.1. The test set-up with the crack pattern for mixed mode cracking is shown in Figure 2.6.

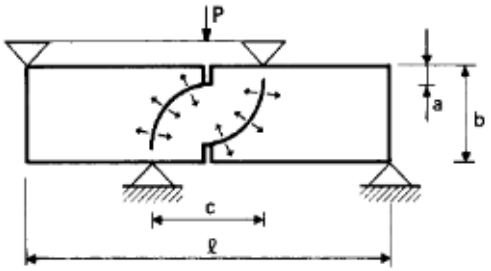

Figure 2.6: Mixed mode fracture test with crack pattern, retrieved from [25].

The use of a notch in a beam is also proposed by [27] for testing mixed mode on concrete-concrete interfaces. In this study a test set-up has been proposed based on a four-point bending test with a notch at the top. The test-set-up is shown in Figure 2.7. A steady state crack propagation was found with this test. In developing this test model, a FEM model analysis was compared with experimental results. It was found that the friction of the supports and the initial stress state in the interface effected the energy release rate. The initial stress state resulted from a difference in thermal expansion between the used layers.

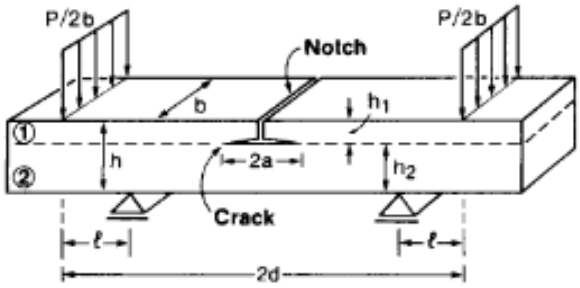

Figure 2.7: Mixed mode bond test, retrieved from [27].

In this thesis a notched beam under four-point-bending will be used based on the test set-up from Harrass [8]. In the experiments SHCC was positioned in the tension zone and concrete on top. The notch will reach up to the concrete. Due to the composite structure and horizontal orientation of the interface, there will be both tension and shear in the interface. Apart from the occurring stresses due to the test geometry, there are interface stresses present as described in Section 2.2.5 due to shrinkage, temperature etc. The stress distribution along the interface of the notched beam due to the composite lay-out and mechanical loading is shown in the Figure below.

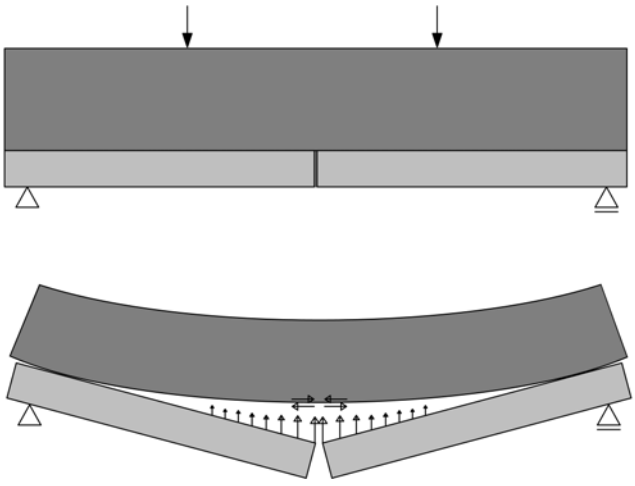

Figure 2.8: Mixed mode bond test: notched beam test set up (top) and resulting stress distribution along the interface (bottom).

A different, small-scale test for mixed mode tests is the slant shear test. The set-up of this test can be seen in Figure 2.9. The slant shear test is a combination of shear and compression. In this test a slant is present between the two concrete layers. Applying a compression force on the sample a stress state at the interface of both normal and shear stresses occurs. Due to the presence of the slant the interfacial friction plays a role and the angle of the slant determines the ratio between shear and normal forces. This test often provides a high resistance [7].

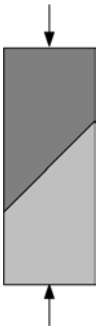

Figure 2.9: Mixed mode bond test: slant shear test.

2.4. Modelling of interfaces

In this section it is explained how in literature interfaces have been modelled. In early studies bond behaviour was mostly based on Mohr-Coulomb and Carol cracking envelopes. In [8] the Mohr-Coulomb envelope is used in the interface elements of DIANA. These cracking envelopes will be explained first and how they are incorporated in modelling of interfaces. Next, more recent models are discussed. The model used in this thesis, the lattice model, will be explained at the end of this chapter.

2.4.1. Cracking models

The Mohr-Coulomb failure criterion is stated in Equation 2.1. The angle of the failure envelope is determined by the internal friction angle of the material, ϕ. The inherent shear strength is described by the cohesion (c), which determines how much off-set the envelope has. The envelope describes the combination of normal and shear stress at which an isotropic material will fail. The normal and shear stress can also be the major and minor principle stress, but here the normal and shear stress will be used. This is the contribution of Coulomb which is based on a linear failure envelope, which describes the combinations of shear and normal forces that lead to failure. Mohr stated that the failure plane could be linear or non-linear [28]. The formula above results in a linear plane, but other authors describe a non-linear plane, which will be discusses later on.

The failure curve by Carol [29] follows up on the Mohr-Coulomb friction envelope for cracking of quasi-brittle materials under normal and shear loading. A model based on fracture mechanics, that shows a work-softening elastoplactic behaviour, was introduced. In Equation 2.3 this criterion is shown.

$$F = \tau^2 - (c - \sigma_n \tan\phi)^2 + (c - \chi \tan\phi)^2 \tag{2.3}$$

With F the force, τ the shear stress, χ the uni-axial tensile strength at the intersection of hyperbola with normal stress, c the cohesion, ϕ the friction angle and σ_n the normal stress.

The model can be used in interface elements for discrete crack analysis. The curve has a hyperbolic shape to provide a transition between the two limit states: pure tension and pure shear. The hyperbolic curve reaches the Mohr-Coulomb curve in the shear region. The hyperbola in the tension region describes the crack state under tension with the kinematic condition that both sides of the cracks can separate from each other. The work of the fracture process is used as a process to determine the propagation of the cracking surface in both modes. In the work of the fracture process the dilatancy angle was used. The dilatancy angle decreased with increasing compression strength and increasing degradation of the crack surface. The latter is represented by zero cohesion.

2.4.2. Interface models

The models discussed above are to be used for cracking or failure within a material. The interface between different materials is the weakest link and will, therefore, often crack first and could be used to model the interface. Models used explicitly to describe the cracking or failing of the interface between different materials will be discussed next.

Failure envelope of interface

In [30] the failure curve of concrete-SHCC interface is described using three regions to accommodate for the material behaviour of SHCC. The failure curve is depicted from experimental testing on wedge splitting tests and slant shear tests. The formulas that describe the three regions of the failure envelope are stated in Equation 2.4.

$$F(\sigma,\tau)=\begin{cases}\left(\frac{\sigma_n}{f_t}\right)^2+\left(\frac{\tau}{f_s}\right)^2-1=0 & for\ 0\le\alpha^{\sigma}\le\alpha^{\sigma_n}_{con}\\ \tau-\sqrt{f_s^2-\frac{f_s^2\sigma^2}{f_t^2}}+\frac{\tan\phi_{eff}}{(\sigma_n-\sigma_{n,limit})^{-1}}=0 & for\ \alpha^{\sigma_n}_{con}<\alpha^{\sigma_n}<\frac{\pi}{2}\\ \tau+\tan\phi_{eff}\sigma_n-c=0 & for\ \alpha^{\sigma_n}\ge\frac{\pi}{2}\end{cases} \tag{2.4}$$

With f_t the tensile strength, f_s the shear strength, τ the shear stress, σ_n the normal stress, ϕ_{eff} the effective friction angle, which is the sum of the friction angle and the effective dilatancy angle. The region where the stress plane is at is distinguished by α^{σ} and α^{σ}_{con}. The first is the direction of the stress resultant and the second the contact angle in the stress space, which depends on the deformation and the stiffness (K) in the loading directions.

$$\alpha^{\sigma_n}_{con}=\tan\left(\frac{K_v}{K_u}\frac{v}{u_{Dil}(v)}\right) \tag{2.5}$$

With u for the displacement in normal direction and v in tangential direction.

In the compression region the Mohr-Coulomb failure curve is applied. In the tension region an elliptical curve is used to describe the failure envelope. The transition region depends on the dilatancy angle. The dilatancy angle describes the crack opening occurring due to crack slip from the irregularities along the crack plane under shear loading. These irregularities are often described using saw-teeth [29]. A schematized overview of the saw-teeth is shown in Figure 2.10.

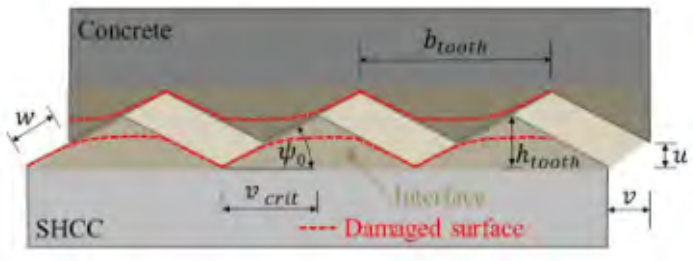

Figure 2.10: Saw-teeth model for interface roughness, retrieved from [30].

The effective dilatancy angle is determined by Equation 2.6. In this equation a distinction is made between two situations. The first where damage of the saw-teeth is considered if present. In the second the presence of a normal displacement leads to a decrease in effectiveness of the saw-teeth due to a reduction in contact stresses. The turning point between these two situations is presented by v_{crit}.

$$\tan\psi_{eff}=\begin{cases}\tan\psi_0\cdot\left(1-\frac{e^{\alpha_{Dil}\cdot v}}{(e^{\alpha_{Dil}}-1)v+v_{crit}}\right) & for\ 0\le v\le v_{crit}\\ 0 & for\ v_{crit}\le v\end{cases} \tag{2.6}$$

With α_{Dil} the damage parameter.

In this method a change in friction angle will not affect the strength in the tension region. The use of this model is compared to the curve of Carol and Mohr-Coulomb. The model of Wagner [30] leads to lower shear strength values, because of the implementation of the saw-teeth. Compared to the other cracking models the

tension strength showed the lowest standard deviation with the model proposed by Wagner [30].

Carol's formula for describing the concrete-concrete interface failure envelope is also stated by [7]. It is required to use both the slant shear and splitting bond test to obtain the coefficients for the formula. The values for the coefficient are extrapolated using data fitting. The same method is described by [31] apart from the cohesion, which is stated to be derived from theoretical considerations. The formula below is from rewriting Carol's formula knowing the force in the crack is zero.

$$\tau = \sqrt{(c - \sigma_n \tan\phi)^2 - (c - f_t \tan\phi)^2} \tag{2.7}$$

Failure envelope for interface elements in FEM

In [24] Carol's formula is used together with the FEM program Abaqus. Cohesive elements were used to model the interface. The standard Abaqus damage traction was changed to make the failure envelope pressure-dependent. This leads to the use of Carol's formula in case the normal stress is in compression and the use of the shear strength if the normal stress is in the tension region. With this process Carol's curve is adjusted in the tension part of the curve. The formulas in Equations 2.8 and 2.9 describe this envelope. Figure 2.11 shows the change between Carol's curve and the curve used in the program. For the post-cracking behaviour, the traction is calculated taking into account a damage factor.

$$\left(\frac{\langle t_n \rangle}{f_{ctm}}\right)^2 + \left(\frac{t_s}{\tau'^{ult}(t_n)}\right)^2 + \left(\frac{t_t}{\tau'^{ult}(t_n)}\right)^2 = 1 \tag{2.8}$$

With:

$$\tau'^{ult}(t_n) = \begin{cases} f_s & if\ t_n \leq 0 \\ \tau^{ult}(t_n) & if\ t_n < 0 \end{cases} \tag{2.9}$$

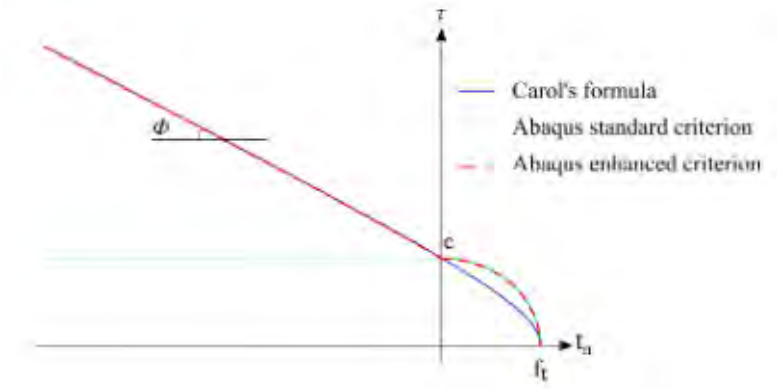

Figure 2.11: Failure curves from Carol, Abaqus criterion and enhanced Abaqus criterion, retrieved from [24].

In this model as input values for the interface element the stiffness of the weaker concrete is used. For the interface tensile strength, the strength was in most cases than 50% of the weakest concrete.

Debonding models

In the above cases the behaviour of the interface elements is described by using a failure envelope. The failure envelope is deducted from Mohr-coulomb and Carol, which both describe the stress state and cracking behaviour inside a material, while in interfaces cracking and debonding occurs. Therefore, more recent models focus on this debonding for modelling the interface.

In [32] a UHPC-concrete beam was modelled using finite element modelling. LS-DYNA was used for a 3D model under 3-point bending using eight-node solid elements for the normal and UHPC concrete layers and two-node beam elements for the reinforcement. The UHPC layer was situated in the tension zone. For modelling a perfect bond, the materials shared nodes and an interface was not explicitly modelled. In case of an unbonded interface the nodes were not shared and the interface had a single surface contact algorithm

to prevent penetration of the elements. A third case was modelled taking the interface bond strength into account by using beam elements rather than friction of cohesive elements. The beam elements are placed in longitudinal direction trough each node at the interface and no elements are placed in transverse direction. The elements had elastic-plastic characteristics. The element properties assigned were the young's modulus and yield strength (bond strength) and were assumed to be dependent on the weaker concrete layer.

The young's modulus was defined as an equivalent beam element to describe the interface accurately. In the equivalent state the stiffness of the weaker concrete is the same as for the interface, leading to the following derivation for the equivalent interface stiffness, $E_{b,eq}$:

$$K_c = \frac{G_c A_c}{t_{c,bond}} \tag{2.10}$$

$$K_{eq} = \frac{E_{eq} A_{eq}}{L_{eq}} \tag{2.11}$$

$$E_{b,eq} = \frac{E_c}{2(1+\nu)} \frac{A_c}{A_{eq}} \frac{L_{eq}}{t_{c,bond}} \tag{2.12}$$

The bond strength is defined as:

$$f_{y,eq} = \frac{\tau_{max} A_c}{A_{eq}} \tag{2.13}$$

With for the maximum bond strength, the value suggested by the ACI committee for intentionally roughened surfaces is used.

The model showed for the case with interface beam elements a good agreement with experiments for the bond performance in terms of peak load, load-deflection curve and effective plastic strain. When the post-peak performance did not coincide with experiments, this could be due to the longitudinal rebar bond performance being modelled as fully bonded. Also, the post-peak ductile behaviour of the model was discussed to allow for improvement.

In [33] a test developed by the authors was used for experiments and accompanying modelling of the debonding of the interface of an overlay system. The test set-up of the authors is shown in Figure 2.12. When an overlay system cracks, the same debonding mechanism and stress distribution in the interface exists as in the notched beam. There is, however, a difference in the applied load. In the notched-beam test static loading in four-point bending is applied. In case of an overlay system dynamic loading from vehicle and soil settlements is present. Also, overlays are often slabs instead of beams.

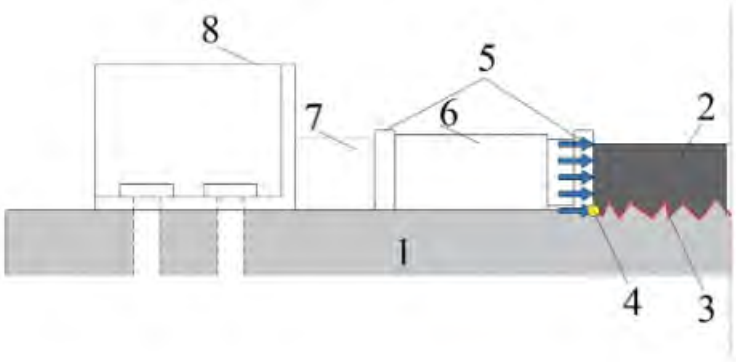

Figure 2.12: Overlay test set-up with substrate (1), overlay (2), interface (3), slip point measured by LDTV (4), bearing plates (5), loading device (6), force transducer (7), rigid support (8), retrieved from [33].

A cohesive FE model is used to model the overlay system with the software program Strand7. The load is applied as an imposed displacement. Truss elements in both vertical and horizontal direction are used to model the interface's peeling-opening and shear-slip respectively. The energy balance concept of fracture mechanics is used to predict the loading capacity and the crack propagation. To prevent the substrate and repair layer to penetrate in the model a master-slave link provided by the code is used. This link is not an

element but provides infinite stiffness to the interface so that the individual materials cannot penetrate each other. It causes the nodes in the link to have the same displacement.

The final non-linear expressions of the cohesive law are found by iterating until the model would provide the output equal to the experimental results. To model the non-linear material behaviour, the material properties were expressed using multiple points on the stress-strain curves for both normal stresses and shear stresses. The material properties of the interface elements only have stresses and strains as input parameters to describe the interface behaviour.

2.5. Lattice model

In this thesis the lattice model is used to simulate the behaviour of hybrid structures. The last two models discussed in the previous section already have aspects that occur in the lattice model. In this section the lattice model will be explained. Figure 2.13 shows a 2D version of the following steps to turn a structure into a lattice model [2]. The following steps need to be performed

- Divide the structure or specimen into equal sized boxes called voxels. The size of the voxel depends on the size of the modelled structure and available computational power.
- A sub-voxel is defined within each voxel. The size of the sub-voxel is determined by the specified randomness. The nodes will be placed randomly within the sub-voxel. Specifying a randomness of zero means the node will only have one available position, which is the centre of the voxel. A randomness of one allows the node to be generated anywhere in the voxel. The randomness of the nodes results in heterogeneity of the model, which is beneficial to model concrete and the cracking behaviour.
- Delaunay triangulation is used to connect the nodes to form the lattice elements. Each node is connected to the nodes closest to it from the adjacent voxels. In a 2D model the connected nodes will form triangles.
- Each node is assigned material properties depending on the material it represents. In this way also elements can be assigned to be interface elements. The interface elements are situated between nodes of different materials. The interface is not modelled with a different type of element as seen in literature. The distinction between materials and interfaces is solely due to the assigned material properties.
- To add reinforcement, extra elements are generated. The nodes of these elements are situated where the rebar crosses a voxel edge. The interface between the rebar and concrete is simulated by the elements that connect the rebar nodes to the closest material node. The type of elements remains the same.
- A profiled interface for a macro-roughness on the interface is simply added by assigning the materials to the nodes in such a way that a profile between the different materials occurs. The interface is defined as before, which will now follow the profile.

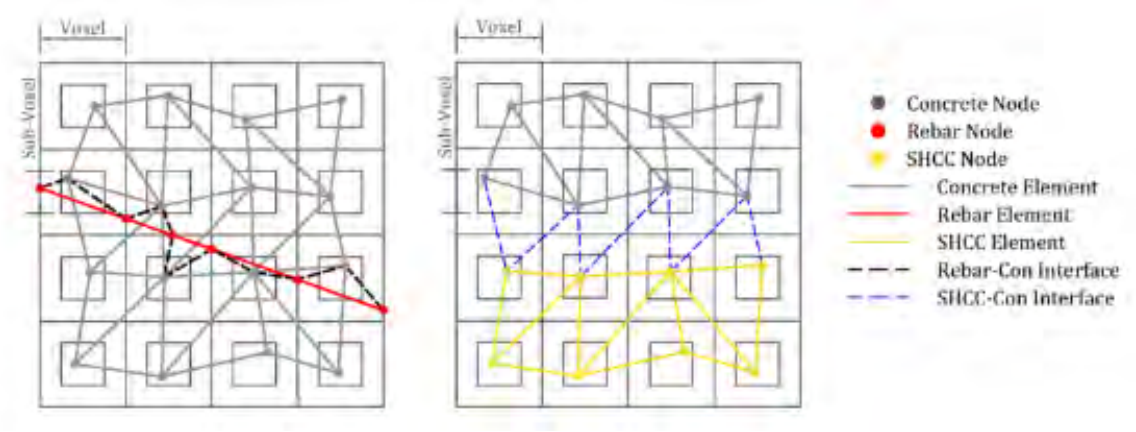

Figure 2.13: Lattice model aspects for reinforced concrete (left) and concrete-SHCC with an interface (right), retrieved from [2].

Apart from the set-up of the model, there are more choices that need to be made to accurately represent the real-life behaviour and that need to be assigned for defining the element properties. It should be chosen how the elements will break. This has to do with the stress state. It can be decided to have the elements failed in tension, compression, both or not fail at all. Elements can be defined to be unbreakable. This can be done at the positions of the loading and support plates to avoid damage due to a locally sharp increase in stress.

Conducting the simulation, the elements will be loaded. The generated stresses are linear elastic and calculated with Equation 2.14.

$$\sigma = \frac{F}{A} + \alpha \frac{M}{W} \tag{2.14}$$

With A the cross-sectional area of the element, W the section modulus and α being the bending influence factor. This factor determines which portion of the stress due to bending is considered. The bending influence factor influences the tail in the load-displacement curve of a specimen. The value should be based on experimental testing. Most often the factor is chosen to be 0 or 0.05 [34]. With zero meaning the bending stresses will not be considered. A normal force influence factor can be added before the first term of the stress formula above. This is almost always taken as 1, taking into account the full normal force.

When the model is simulated, the structure is loaded by an applied load or imposed deformation. The element that after loading has the highest stress to strength ratio above 1 will be removed. After this, the model will be reloaded and iterative procedure is repeated until failure occurs or other stop criteria are met. The material properties can be described using segments. Using one segment means the that after removing the element, the element has no strength left and has thus failed. Multiple segments can be used to describe elastic-plastic material behaviour of reinforcement steel. Material properties are assigned for each segment. If the first segment fails, the material properties of the second segment are used in the next iteration. This allows for modelling ductility of materials.

The elements can be assigned to be beam elements or truss elements. Beam elements are often chosen because they can transfer bending moments. Truss elements do not accurately describe rotation of the material that connect cracks [35].

The elements can be chosen to be square of circular. Here a circular shape is used, which means a radius should be assigned. This radius influences the stiffness of the elements and thus the behaviour of the model. But also the randomness causes different lengths and orientations of the elements. Because of these features the input values for the elements deviate from the output values. The stress calculated in each beam element from Equation 2.14 differs from the stress calculated for the global specimen tested. Not only because of the different cross-section, but also because the orientation of each beam element differs. This means a different stress is obtained in each element. Relating the element input properties to the global output properties is difficult due to the randomness of the element orientation. Therefore, the input properties should be calibrated for the correct output properties using small specimens.

The ITZ is around 10 - 100 μm [10] and the interface in an overlay is around 100 μm [33]. In [13] the interface between UHPC and NSC was investigated and an interface width of 35 μm was found. In the same research the NSC-NSC interface was found to be 55 μm. The interface between different concrete layers will in practice thus not be larger than 1 mm. This means that for large models, where a mesh size of 10 mm is common, the interface element properties are influenced by the adjacent materials. The effect of this phenomena accounts the elastic modulus. The principle is explained using a spring model with the spring in series, which is illustrated below. The phenomenon also counts for lattice models used for meso-scale models of concrete, where the interface element represents the ITZ, which is influenced by the matrix and aggregates [36].

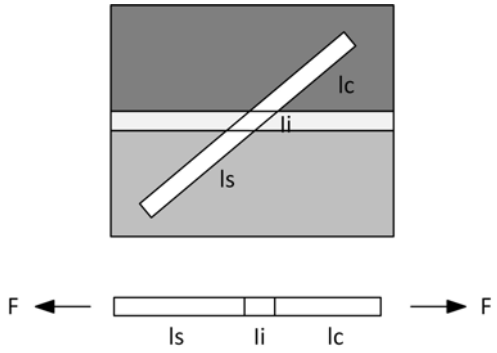

Figure 2.14: Interface element representing multiple materials.

Each segment represents a part of the lattice beam element. The spring stiffness of the interface element depends on the stiffness of the individual materials. The lattice beam elements are calculated linear elastically making it possible to use the Hooke's law for the beam equations. The equivalent beam stiffness is calculated using Equation 2.15. Changing the stiffness of the interface element would mean that the contribution of a material is changed or the width of the interface region is different.

$$\frac{l}{E_{b,eq}} = \frac{l_s}{E_s} + \frac{l_i}{E_i} + \frac{l_c}{E_c} \tag{2.15}$$

For the tensile strength the mechanism differs. The materials are in series, meaning it could be seen as a chain in which the weakest link will break first and is governing for the behaviour. Therefore, the assigned interface tensile strength is the actual tensile strength of the interface. There is no contribution of the adjacent materials to this strength.

3

Small-scale tests

In this chapter the set-up and results of the small-scale simulations will be presented. The tests carried out are the direct tension and direct shear test, which are explained in the previous chapter. The results of the simulations are shown and the effect of changing the interface stiffness and tensile strength will be discussed. The focus is on the failure mechanisms, fracture energy and stress-strain or stress-crack opening curve. The results will be compared to results found in literature. A conclusion is given on the suitability of the small-scale tests for investigating the interface.

3.1. Set-up of the model

The set-up of the model is based on a direct tension and shear test carried out in [37] for a concrete-to-concrete interface. Here, the tests will be simulated for concrete-to-SHCC specimens. The tests are carried out on prisms with a size of 30x30x12 mm with the top 6 mm made of concrete and the bottom 6 mm made of SHCC. In between the layers, the interface is present. The used mesh size is 1 mm. The dimensions of the test set-up are shown in Figure 3.1.

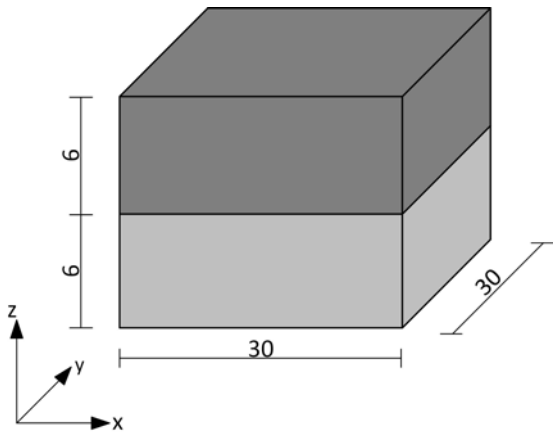

Figure 3.1: Dimensions small-scale test specimen in millimetres.

3.1.1. Material properties input

For the material properties the experiments of Harrass [8] are used. Since tests are carried out, the mean values of the material properties are used. The concrete stiffness is calculated from the known strength class using the Eurocode formula shown in Equation 3.1 and the corresponding shear modulus with Equation 3.2, using a Poisson's ratio (ν) of 0.2.

$$E_{cm} = 22\left(\frac{f_{cm}}{10}\right)^{0.3} \tag{3.1}$$

$$G = \frac{E_{cm}}{2(1+\nu)} \tag{3.2}$$

Due to the randomness of the lattice beam elements the input values of the model do not correspond with the output values. This was explained in Section 2.5. In order to achieve the same material properties in the simulations the input values for the concrete material properties are determined by using prisms with a size of 10x10x20 mm and mesh size of 1 mm. The input is calibrated to provide the output values corresponding to the material properties from the experiments. These are stated in Table 3.1 together with the input values needed to obtain these material properties.

The material properties for SHCC are stated in Table 3.2. It can be seen that multiple segments with different input values are stated. The lattice model allows non-linear material behaviour to be accounted for by using segments. For SHCC three segments are needed to represent the material behaviour. How the segments are defined for SHCC are shown in Figure 3.2 for a generalized form of the stress-strain curve of SHCC. The first segment is defined at the end of the elastic region, the top of the curve is used for the third segment, and the second segment is in between these points. Because the behaviour of SHCC does not only depend on the tensile strength and stiffness, but also on the crack formation. The first elastic part can be calibrated using a prism as was done with concrete. For the other segments the input is defined to ensure for crack widths that are presenting SHCC cracking behaviour. The input for the material properties of SHCC are used as defined in [2]. For concrete only one segment is defined, because of the brittle material behaviour of regular concrete. The softening of concrete is not considered in the lattice model to limit computational time.

Table 3.1: Concrete material properties model input and output and from experiments.

	Model input	Model output	Properties from [8]
f_{ctm} (MPa)	3.7	2.895	2.9
f_{cm} (MPa)	70	40.5	40
E_{cm} (MPa)	32836	32584.04	32836

Table 3.2: SHCC material properties model segment input and output.

	Segment 1	Segment 2	Segment 3	Output (max)
$f_{t,SHCC}$ (MPa)	3	3.75	4.5	4
$f_{c,SHCC}$ (MPa)	-60	-75	-90	-62.3
E_{SHCC} (MPa)	18500	9250	1125	1392.75

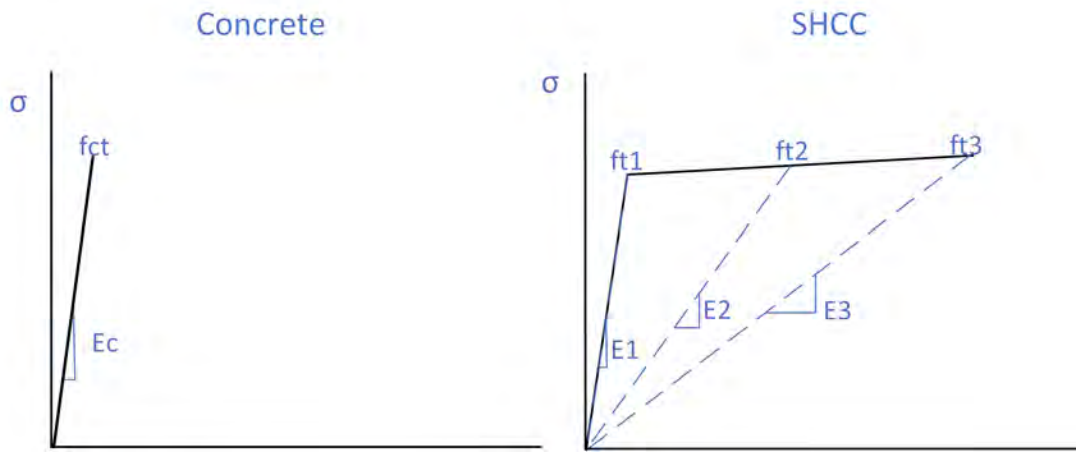

Figure 3.2: Defining segments for material properties of concrete (left) and SHCC (right).

3.1.2. Interface properties

The interface is often the weakest link in the hybrid system. The interface properties are, therefore, lower compared to the individual materials. The interface properties are taken as a percentage of the material properties of the weakest adjacent material. The concrete tensile strength is lower compared to the maximum tensile strength of SHCC, but the stiffness of the SHCC is lower. To simplify the notation of the interface properties one layer is chosen, namely concrete. This means a higher stiffness will be assigned to the interface layer. The interface element stiffness will represent all material layers, allowing for a higher interface stiffness as was explained in 2.5. A higher interface stiffness will consider the contribution of the concrete stiffness in the interface element.

The last interface property that needs to be determined is the compression strength. The effect of changing the compression strength will not be investigated in this thesis, but the magnitude does influence the results. The compression strength of the interface used in the simulations of the small-scale tests are calibrated in order to provide an output shear stress that is at least twice the tension stress. This ratio between the tensile and shear stress is obtained in [38] for small-scale tests carried out between concrete and SHCC. To obtain this ratio the compression strength of the interface elements can be altered. In the reference tests of [37] the ratio between tension and compression strength in the input values is 10. Due to the difference between input and output material properties this means an output ratio of around 7.4. In reality the ratio is around 15, depending on the concrete strength class. The reason why the concrete compression strength needs to be reduced, is because in shear multiple interface elements are loaded in compression and govern the resistance of the interface. Failure of the interface only happens if all the elements are broken. The compression strength should be limited, which results in deviating values compared to the actual concrete material properties. However, for the goal of these simulations this is not an issue. Investigating the effect of changing interface properties is the goal of this thesis, rather than simulating a behaviour as close to the actual case as possible. Therefore, the ratio of 10 between the input of the interface tensile strength and interface compressive strength is used. For all the samples used the interface properties are stated in Appendix A. The same sample numbers and corresponding interface properties will be used for all small-scale test simulations.

Apart from changing interface properties, also the lay-out of the interface is altered. A distinction is made between a smooth surface and a profiled surface. A profiled surface is used to represent a macro roughness. Squares of 2 by 2 mm are used to form a profile between the concrete and SHCC. In the experiments of Harrass [8] a profile is among one of the different cases that are tested. The profile is included here to investigate the effect of this profile on a smaller scale. The interface will follow the profile between the concrete and SHCC. The visualisation of the smooth and profiled interface in the lattice model are shown in Figures 3.3a and 3.3b.

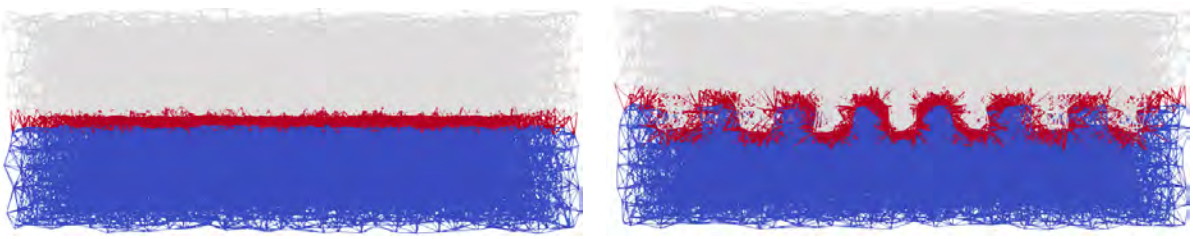

(a) (b)

Figure 3.3: Lattice model smooth interface (a) and profiled interface (b), with white representing concrete, blue SHCC and red the interface.

3.1.3. Model parameters

In all cases a radius of 0.42 mm is used for the beam elements representing concrete, SHCC or the interface. The factors for calculating the stress as was stated in Equation 2.14 in Section 2.5 are 1 and 0 for the normal force influence factor and the bending influence factor respectively. All elements next to the supports are prevented from failing, meaning neither tension nor compression will result in failure of the elements. This is done to prevent failure due to locally high forces in the model. When doing this the user should be careful not to include any interface element in this region in the direct shear test. This will prevent the specimen from failing in the interface, which will provide incorrect results. All other elements are allowed to fail in both

tension and compression.

The analysis is displacement controlled. An imposed displacement is defined in the model as 1 mm with a scaling search approach to a scaling limit of 10. This means that if the displacement would reach 10 mm, the simulation is aborted. If the specimen has failed prior to reaching the scaling limit, the simulation will stop.

3.2. Fracture energy

One parameter to investigate the effect of changing the interface properties is the fracture energy. The fracture energy is the area under the complete stress-crack opening curve [39]. Figure 3.4 indicates where often the stress-crack opening curve is cut off for calculating the fracture energy, while the fracture energy should be represented by the area under the complete curve. In this thesis the curves are also cut-off at a certain crack opening to increase the visibility of the curves. In that case both the cut-off and total fracture energy will be stated.

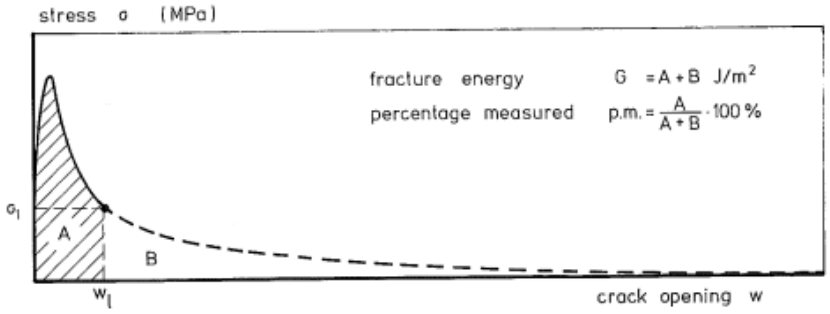

Figure 3.4: Stress-crack opening curve, with A the area mostly used as fracture energy and A+B the area of the actual fracture energy, adapted from [39].

The lattice model provides the displacement of the boundaries as output of the simulation. Measuring directly next to the crack will provide the crack opening immediately. However, it is in concrete not known beforehand where the crack will initiate. Therefore, a larger distance is taken over which the deformation is measured. This is also called the measuring length. When the displacement is measured over a larger distance the elastic deformation of the materials next to the crack is taken into account. The larger the distance over which the displacement is measured the larger the measured displacement [39]. Figure 3.5 provides a visualisation of the effect of increasing measuring length on the stress-displacement curves.

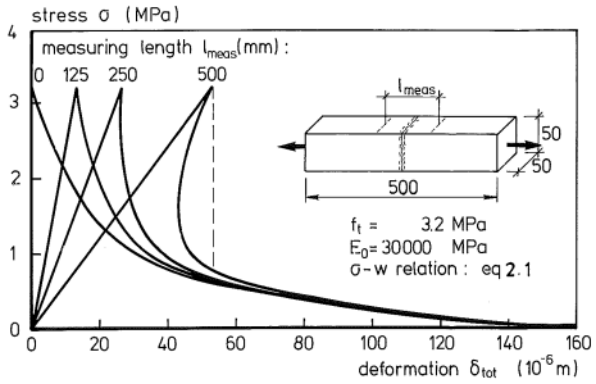

Figure 3.5: Stress-displacement curve for different measuring length, from [39].

To deduct the crack opening from the given displacement with a measuring length larger than the crack, the initial elastic displacement should be removed from the obtained displacement. A visualisation of the separation of the stress-displacement curve from this initial elastic deformation is shown in Figure 3.6. The formula for calculating the resulting crack opening is given with Equation 3.3 from Akita [40].

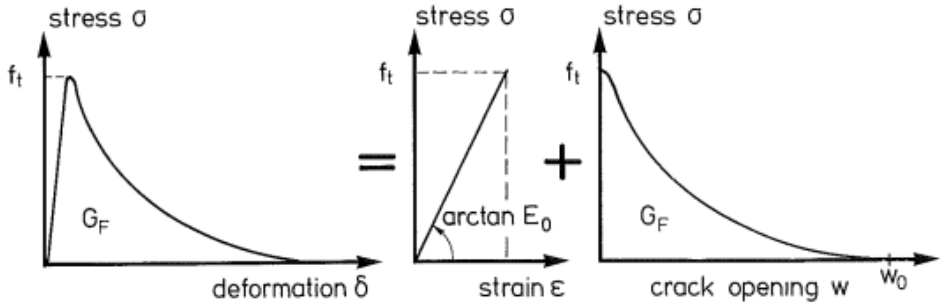

Figure 3.6: Stress-displacement curve split into elastic strain and crack opening, from [39].

$$w = \delta - \frac{FL}{EA} \tag{3.3}$$

With w the resulting crack opening, δ the displacement from the model output, F the applied load, L the measuring length, which is in this case the height of the specimen minus one mesh height, E the initial elastic modulus, which can be calculated by dividing the stress with the strain obtained in the elastic region and A is the cross-sectional area of the test specimen.

In the next sections the results for each test are shown and discussed. For the results of the direct tension tests, the initial elastic deformation will be removed in order to calculate the fracture energy with the area under the curve. For the direct shear tests the fracture energy will not be calculated. For those tests the stress-strain curve will be used and there will be no removal of the initial elastic deformation.

The effect of the interface properties will be discussed individually per test method and interface surface. The results will be compared with literature. An overall conclusion is given at the end of this chapter on the effect of the interface properties on the load capacity, fracture energy and the use of the small-scale test for investigating the interface behaviour.

3.3. Direct tension test smooth interface

For the direct tension tests the boundary conditions at the bottom are set fully restrained. At the top an imposed deformation is set upwards. The boundary conditions are indicated in Figure 3.7. The interface stiffness and tensile strength will be altered and investigated respectively in the next sections.

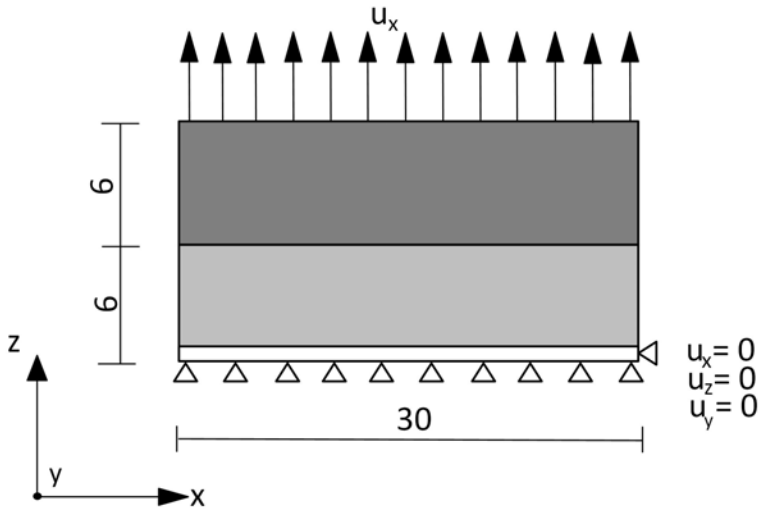

Figure 3.7: Test set-up and boundary conditions direct tension test with dimensions in millimetre.

Different results will be shown to explain the effect of altering the interface properties. The focus is on the stress-crack opening curve, the fracture energy and the damaged model for different loading stages along the stress-crack opening curve to track the crack propagation and indicate the final failure mode. The damaged model output indicates the failure of elements up to the indicated loading stage on the stress-crack opening curve. Before starting the simulation, the user should identify after how many failed elements the information for the damaged model should be provided. For the small-scale tests this is after 100 failed elements. For each point shown in the damaged model output a dot is added to the stress-crack opening curve. From the results, the effect of changing the interface stiffness and interface tensile strength is discussed respectively.

The fracture energy is shown in a bar plot. In some cases, there is a value stated on top of the bar plot. In Figure 3.4 it was shown that the stress-crack opening curve is often cut-off, while the complete area should be taken for the fracture energy. In this chapter the curves are also cut-off at a certain crack opening for the visibility of the curves. For the area under this curve the fracture energy is calculated and indicated in the accompanying bar plots. The total fracture energy is stated on top of the bar plot if the total value is higher than the cut-off value. The total values are stated to provide an indication of the behaviour after the curve is cut-off. The partial value is stated to compare the fracture energy between the different samples up to the point where the graph is cut-off.

3.3.1. Influence of interface stiffness

First, the effect of the interface stiffness on the load capacity and ductility in the direct tension test is discussed. The sample numbers and their interface properties used for investigating the effect of the interface stiffness are indicated in Table 3.3. The properties of the interface tensile strength and stiffness are stated as a percentage of the concrete material properties.

Table 3.3: Model input interface properties of samples used for interface stiffness in direct tension test on smooth interface.

Material	Sample number	Stiffness (MPa)	Tensile strength (MPa)	Compressive strength (MPa)
Concrete	all	32836	3.7	-70
Interface	1	100%	30%	-10*ft interface
Interface	2	50%	30%	-10*ft interface
Interface	3	20%	30%	-10*ft interface

In Figure 3.8a the stress-crack opening curve is shown for the samples 1 to 3 with changing interface stiffness. Each sample has two curves. Both curves have the initial elastic strain removed as was explained in the previous section. One curve is the curve with spikes. These spikes are the direct output of each iteration carried out in the lattice model. The second curve is the envelope that is drawn over the spikes and is represented by a thicker line of the same colour. This curve is considered the stress-crack opening curve.

In the stress-crack opening curve of Figure 3.8a it is shown that for a changing stiffness the maximum stress differs only slightly. The maximum stress increases from 1.03 MPa to 1.097 MPa to 1.16 MPa for the interface stiffness of 100%, 50% and 20% respectively. By decreasing the interface stiffness, a small increase in strength is obtained. The main difference between the stress-crack opening curves is the softening response. The sample with an interface stiffness of 20% of the stiffness of concrete shows a distinct different curve compared to the other two graphs. This distinct difference can also be observed from the fracture energy of the three samples, which are indicated in Figure 3.8b. In Section 3.2 it was explained how the fracture energy should be calculated by the area under the stress-crack opening curve. The area under the presented curve is calculated for the fracture energy, the total fracture energy is stated with the number on top of the bar plot. Sample 3, with the lowest interface stiffness, has significantly higher fracture energy compared to the other two cases. Not only the area under the curve is already much larger, but also the total fracture energy is almost ten times the fracture energy of sample 1 with 100% interface stiffness. The total fracture energy of sample 3 is more than three times the fracture energy of sample 2. Between sample 1 and 2 the fracture energy does not show such increase. This indicates that with a decrease in interface stiffness the fracture energy increases. The increase is more significantly for low interface stiffness. The failure mechanisms behind the different samples will be investigated next to indicate where this increase comes from.

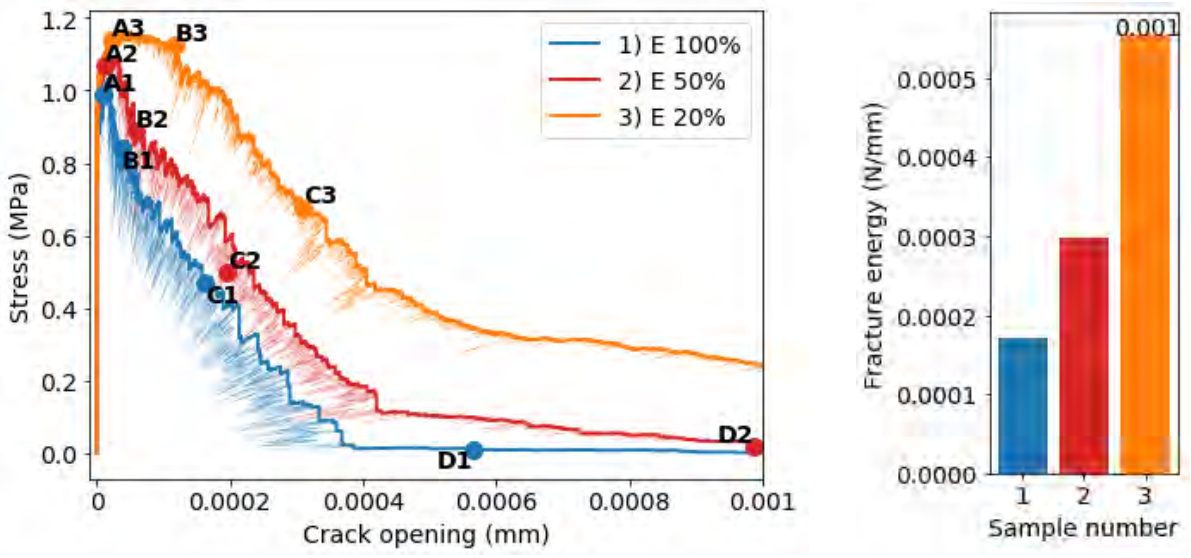

(a) (b)

Figure 3.8: Stress-crack opening curve under direct tension with a smooth interface and different interface stiffness for samples 1, 2 and 3 (a), with accompanying fracture energy from area under the curve and number in bar plot indicating total fracture energy (b).

To get a better insight into the failure mechanisms of these three cases, the damaged elements of the lattice model are observed at different loading stages. The stress-crack opening curve indicates the points at which the damaged model is extracted with dots for the steps A-D. For sample 3 point D is outside the limit of the curve. For point D of samples 1-3 the side view of the deformed damage is shown in Figure 3.9. In this side view the deformation and broken elements are shown. The only difference between these images, that can be observed, is the difference in deformation. In all cases the damaged elements are located in the interface.

From the top view of the damaged lattice in Figure 3.10 the crack propagation can be observed. In all cases only interface elements are broken. At points A1, A2 and A3, which are situated at the maximum stress during loading, only a few damaged elements in the interface can be observed. For the points on the softening side of the curves (B-C) the difference in crack propagation can be observed. In case of a high interface stiffness (sample 1 and 2) the damaged elements are grouped, meaning the crack localizes. While for sample 3 with a low interface stiffness the damaged elements are spread over the cross section. This can be attributed to the higher deformability of the interface as a result from the lower stiffness.

A decrease in interface stiffness in the direct tension test with a smooth interface increases the fracture energy and crack opening. This is the result of the higher deformability of the interface increasing. With very low interface stiffness the fracture energy was increased significantly. From the damaged model it can be seen that with low interface stiffness the failed elements are scattered over the interface instead of localized as is the case with higher interface stiffness. In case of localized cracking, the behaviour is more brittle. With lower interface stiffness values the localized cracking is replaced with a scatter of failed elements over the interface. This results in an increased ductility and explains the increase in fracture energy.

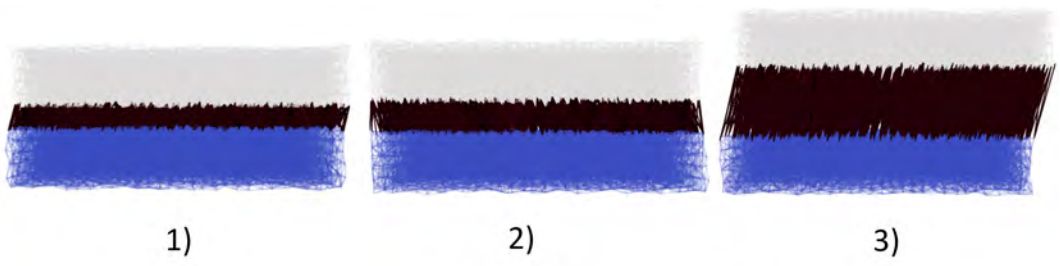

Figure 3.9: Side view deformed damaged lattice for direct tension with smooth interface for final loading stage (D) of samples 1-3. Deformation scaling factor x2000. Blue is SHCC, white is concrete and black is broken interface elements.

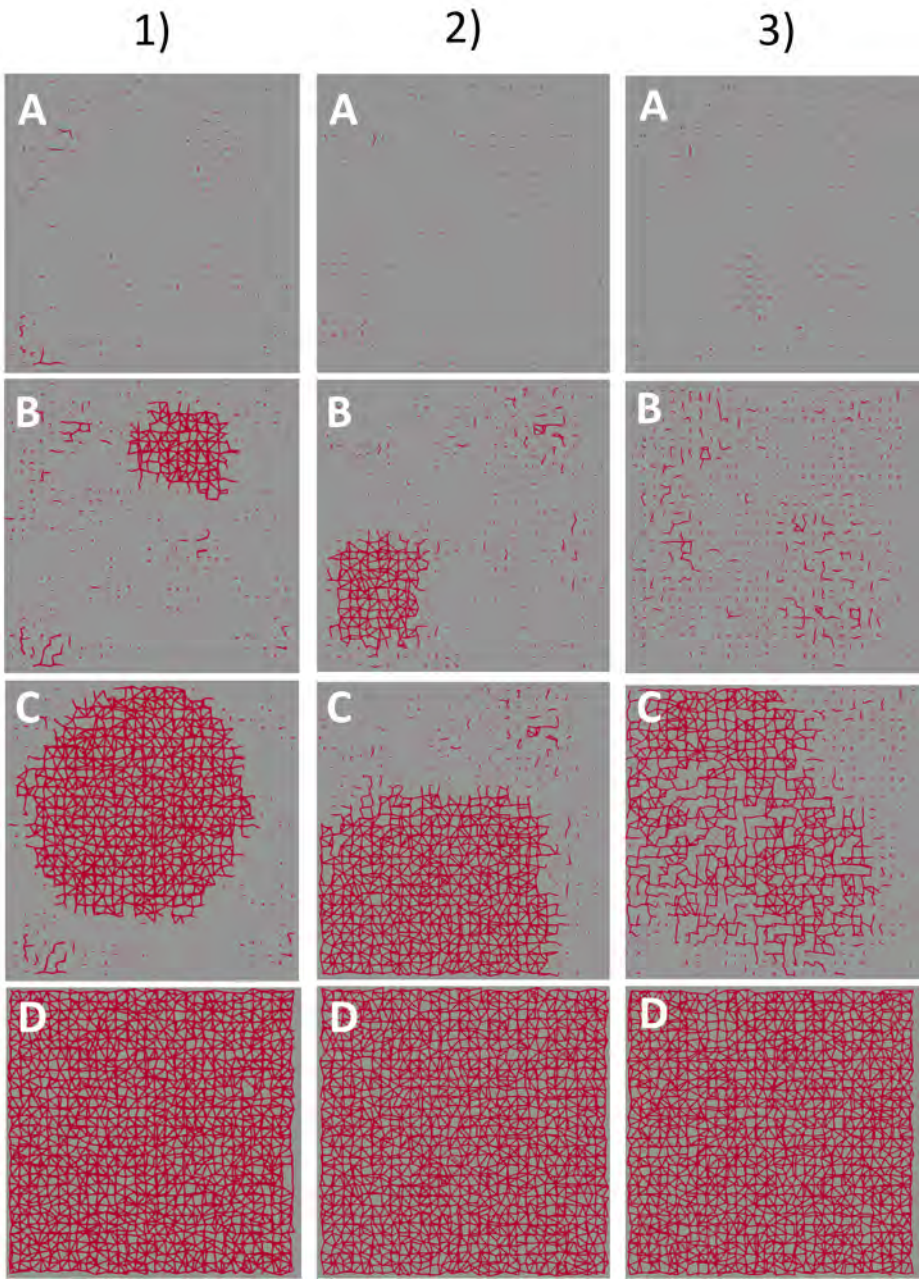

Figure 3.10: Top view indicating damaged elements for direct tension with smooth interface for different loading stages (A-D) of samples 1-3 with red indicating failed interface elements.

3.3.2. Influence of interface tensile strength

The same test set-up is used for investigating the effect of the interface tensile strength on the behaviour of the direct tension test. The samples and their interface properties used for investigating the effect of the interface tensile strength are indicated in Table 3.4. First all samples are discussed after which samples 1, 13 and 14 are compared more in depth.

Table 3.4: Model input interface properties of samples used for interface tensile strength in direct tension test on smooth interface.

Material	Sample number	Stiffness (MPa)	Tensile strength (MPa)	Compressive strength (MPa)
Concrete	all	32836	3.7	-70
Interface	5	100%	7.5%	-10*ft interface
Interface	4	100%	15%	-10*ft interface
Interface	1	100%	30%	-10*ft interface
Interface	11	100%	50%	-10*ft interface
Interface	13	100%	70%	-10*ft interface
Interface	14	100%	90%	-10*ft interface
Interface	12	100%	100%	-10*ft interface

Figure 3.11a shows the envelope of the stress-crack opening curves for the different samples with varying interface tensile strength from 7.5% to 100% of the concrete tensile strength. Sample 12 with 100% interface tensile strength should provide the same curve as there would be no interface modelled and only concrete and SHCC. In that case the cracks are located in the concrete, which is the weakest material. It is seen that this curve shows increased softening compared to the other curves of samples which have mainly cracked in the interface. Cracking in the interface shows a more brittle behaviour. From the fracture energy bar plot in Figure 3.11b it can be seen that the fracture energy of sample 12 is already higher compared the other samples. The number on top of the bar indicates the total amount of fracture energy, which can be seen to increase the value with a factor 10. This indicates that the ductility and softening of cracking in concrete is much higher compared to the samples with interface failure.

In general, an increase in interface tensile strength is shown to increase the load capacity, crack opening and fracture energy. With low interface tensile strength the curves have similar shape and a linear relation between the interface tensile strength and the different structural behaviours can be observed. With increasing interface tensile strength the stress-crack opening curve starts to show a deviation in the first part towards the peak of the curve. The bend in the beginning of the curve increases with an increase in interface tensile strength accompanied with an increase in fracture energy. To get a better insight in what causes this difference, samples 1, 13 and 14 are investigated in more detail.

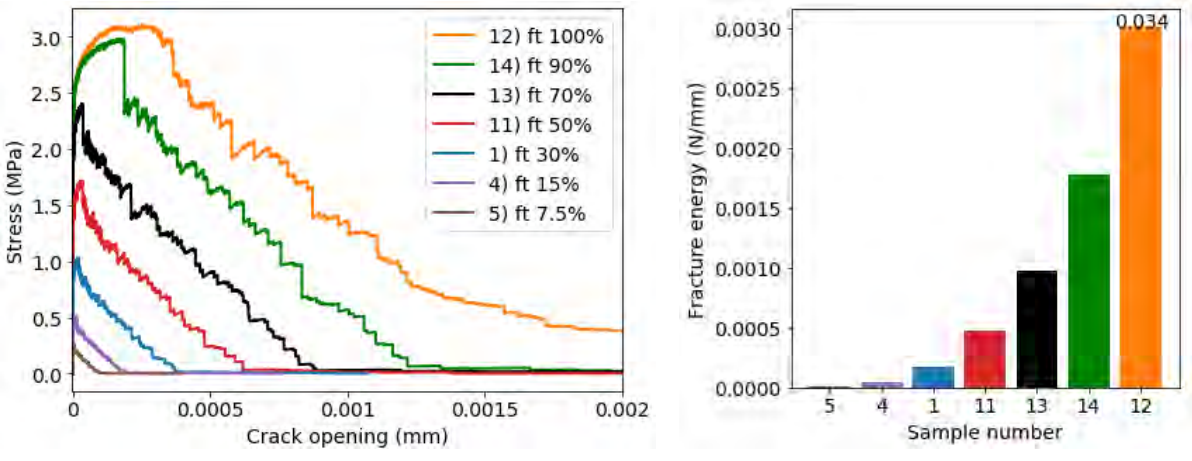

(a) (b)

Figure 3.11: Stress-crack opening curve direct tension with a smooth interface and different interface tensile strength (a), with accompanying fracture energy for area under the curve and the number above the bar plot for the total fracture energy (b).

Figures 3.12a and 3.12b show respectively the stress-crack opening curve and fracture energy of the three samples 1, 13 and 14. Comparing the fracture energy for these three cases it can be seen that the fracture energy is less than doubled between sample 13 and 14, while the fracture energy is increased with a factor 5 between samples 1 and 13. This means a significant increase of fracture energy can be obtained with increasing the interface tensile strength to higher values, but after a certain threshold, the increase in fracture energy is reduced. What contributes to this higher fracture energy will be investigated by looking at the damaged elements for different points on the stress-crack opening curve.

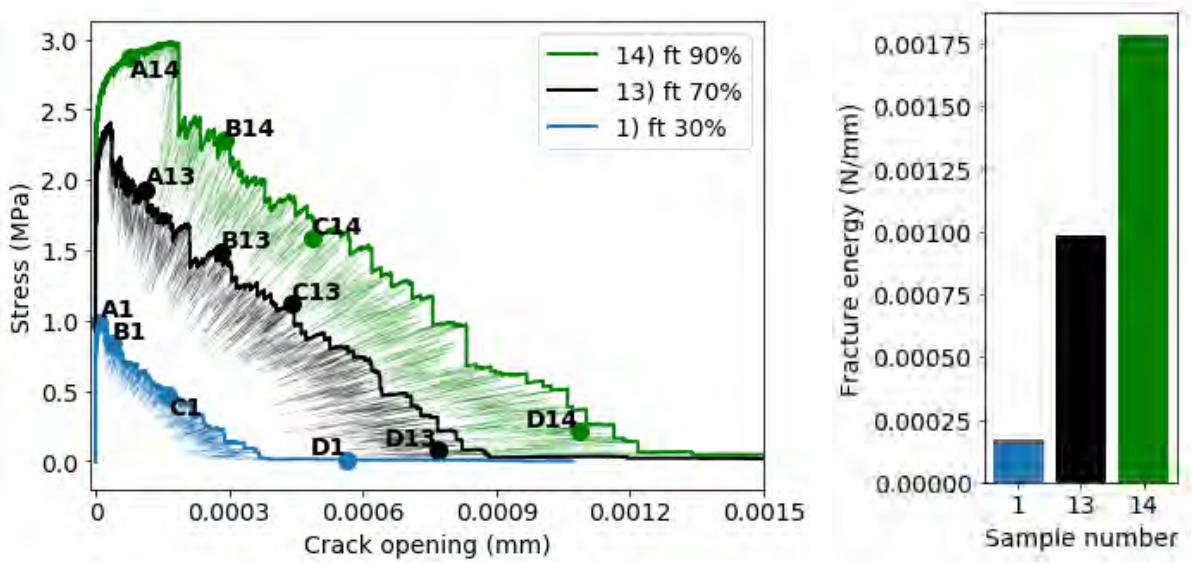

(a) (b)

Figure 3.12: Stress-crack opening curve direct tension with a smooth interface and different interface tensile strength for samples 1, 13 and 14 (a), with accompanying total fracture energy (b).

Looking at the side view of the deformed damaged lattice of point D in Figure 3.14 it can already be seen that in sample 1 only interface elements are broken, but in samples 13, and in higher amount in sample 14, the concrete and SHCC show failed elements. Sample 14 shows even intact interface elements. The damaged elements for the different points A-D are indicated from a top view in Figure 3.13. From these images it can be observed that for sample 13 and 14 the SHCC elements start to break in an early stage, point A, and contribute to the strength of the sample. The cracks in the interface still localize in all cases. The failure of the concrete is mainly present in sample 14 at points B and C, which are on the declining part of the stress-crack opening curve. The main contributor to the fracture energy and the load capacity is thus the SHCC. After a certain threshold of interface tensile strength, the SHCC is activated, governing the behaviour. The failure of SHCC elements reduce the increase in fracture energy and load capacity. An even higher interface tensile strength close to the concrete tensile strength will activate the concrete. For 90% interface tensile strength, the crack still localizes in the interface, causing brittle behaviour. With 90% interface tensile strength, the interface is still the weakest layer.

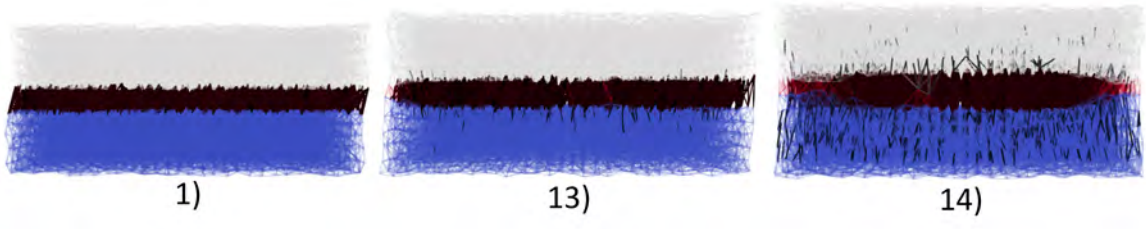

Figure 3.13: Side view deformed damaged lattice for direct tension with smooth interface for final loading stage (D) of samples 1, 13 and 14. Deformation scaling factor x2000. Red is interface, blue is SHCC, white is concrete and black is broken elements.

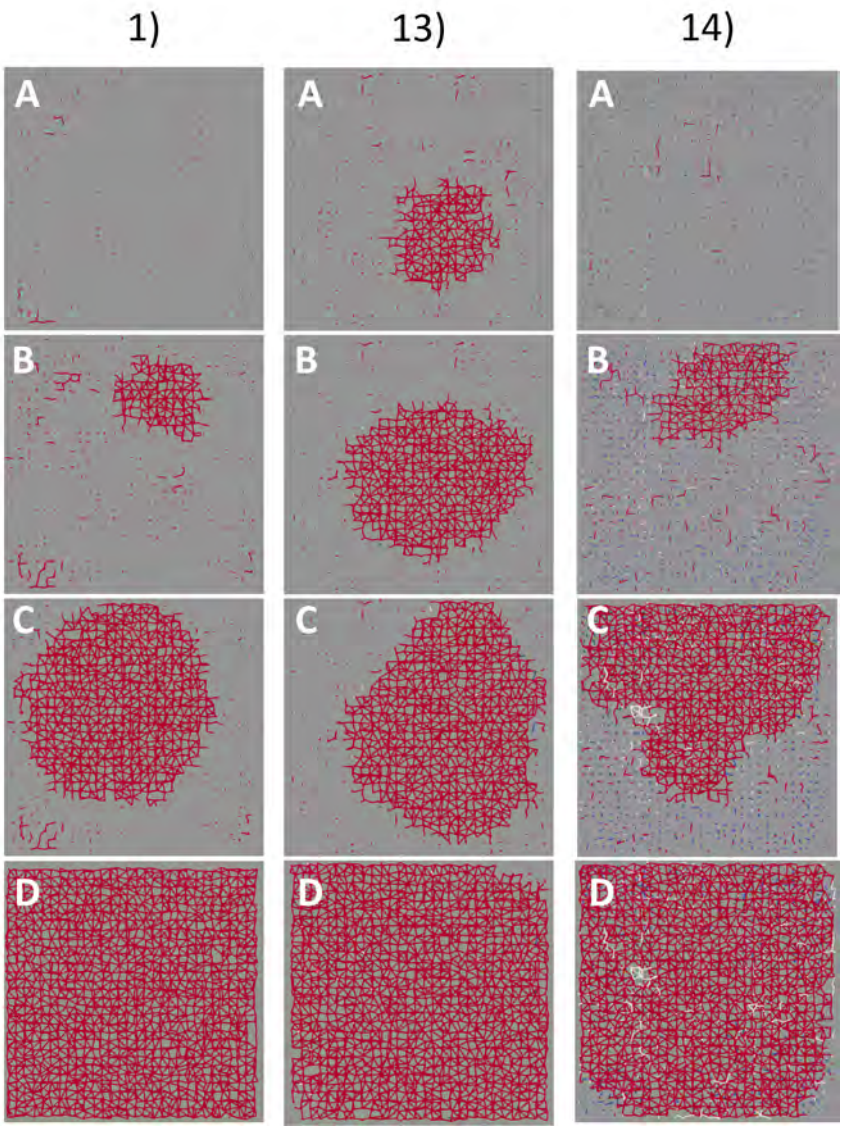

Figure 3.14: Top view indicating damaged elements for direct tension with smooth interface for different loading stages (A-D) of samples 1, 13 and 14 with red indicating failed interface elements, blue failed SHCC elements, white failed concrete elements.

3.4. Direct tension test profiled interface

The direct tension test is also carried out on a specimen with a profiled interface. In this section it is assumed that for the calculation of the fracture energy there is only one crack present. In the bar plot the partial fracture energy value is stated as area under the shown curve. The total fracture energy is stated in a number on top of the bars.

3.4.1. Influence of interface stiffness

Table 3.5 shows the input of the material properties shown for the samples used in this section.

Table 3.5: Model input interface properties of samples used for interface stiffness in direct tension test on profiled interface.

Material	Sample number	Stiffness (MPa)	Tensile strength (MPa)	Compressive strength (MPa)
Concrete	all	32836	3.7	-70
Interface	1	100%	30%	-10*ft interface
Interface	2	50%	30%	-10*ft interface
Interface	3	20%	30%	-10*ft interface

From the stress-crack opening curves in Figure 3.15a it can be seen that two peaks are present. The mechanism that causes this second peak will be discussed when the damaged model is analysed. In the stress-crack opening curve a decrease in stiffness increases the magnitude of the first peak. Sample 1 with 100% interface stiffness has a stress at the first peak that is approximately equal to the maximum stress in the direct tension test with a smooth interface for equal interface properties. For the other two samples this is not the case and a higher increase of the first peak is obtained with decreasing interface stiffness compared to the increase obtained in the direct tension test with a smooth interface. It will be pointed out with observing the damaged model what contributes to this increase. This will be discussed after investigating the fracture energy.

The fracture energy for the three cases can be compared using Figure 3.15b. The crack opening was limited to 0.002 mm for calculating the area under the curve. The total fracture energy is indicated on top of the bar plot of each sample. The trend that can be observed is: a slight increase in fracture energy is obtained with a decrease in interface stiffness up to a crack opening of 0.002 mm. Looking at the total fracture energy, there is only limited difference between the samples. Compared to the smooth interface, the fracture energy of sample 1 is increased times ten for a profiled interface for the area under the curve and even a factor 50 for the total fracture energy. The increase in fracture energy between the samples is low compared to the simulations with a smooth interface, where a sharp increase in fracture energy was obtained for a low interface stiffness.

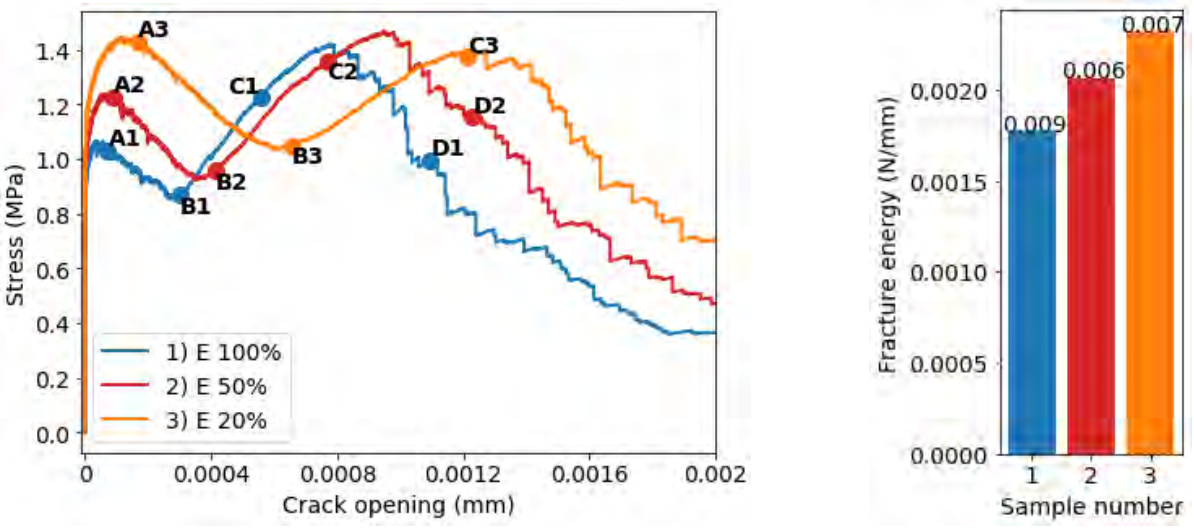

(a) (b)

Figure 3.15: Stress-crack opening curve direct tension with a profiled interface and different interface stiffness (a), with accompanying fracture energy for area under the curve and the number above the bar plot for the total fracture energy (b).

To see what contributes to the increase in the first peak and what the failure mechanism is, the side view of the deformed damaged lattice is compared for different points on the stress-crack opening curve. This time only the side views are shown and not the top views, because the behaviour can be considered the same through the depth of the specimen. This is because the damage localizes around the profile and the profile is the same through the depth. The propagation of the damage can be viewed best from the side. The deformed damaged lattice is shown in Figure 3.16 for the three samples for different points along the stress-crack-opening curve. The first points (point A1-A3) are located around the top of the first peak. From the damaged lattice it can be seen that the interface at the bottom of the profile start to fail first. This determines the magnitude of the first peak. The bottom of the profile starts failing before the top because the SHCC has a larger deformability compared to the concrete. With a decrease in interface stiffness the deformability of the interface increases and the stiffness difference between the SHCC and interface is reduced. With a lower interface stiffness the failed interface elements are positioned at both the top and bottom. An equal spread of the load over the top and bottom of the profile is the result, increasing the stress of the first peak.

At the lowest point between the two peaks the interface of both the top and bottom side of the notches have failed. The second peak can now be allocated to the failure on the shear side of the notches. Points C indicate the top of the second peak, where mainly the interface on the shear side start to fail. But also, some elements in the concrete and SHCC start to break. The points D indicate the declining part of the stress-

crack-opening curves after the second peak. It can be seen that in this step the cracks on top of the profile propagate through the concrete, indicating the failure of the samples. A few SHCC elements also fail in this process, but are not the main failure mechanism indicating the decrease in bearing capacity.

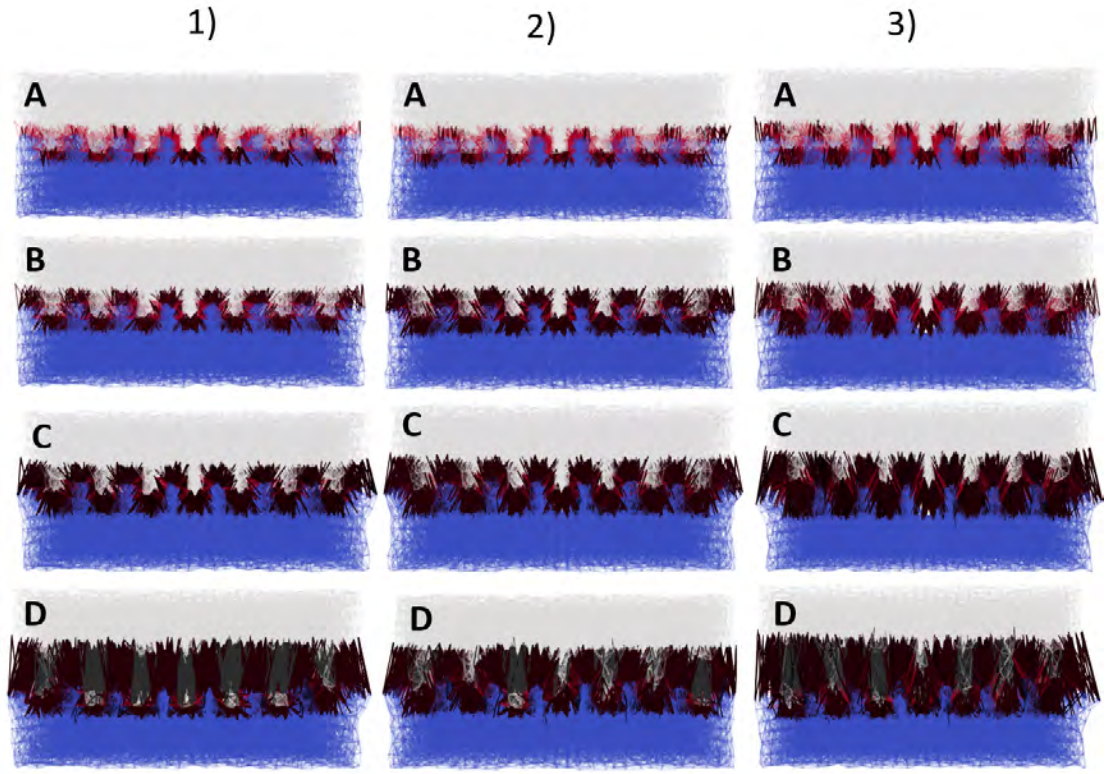

Figure 3.16: Side view deformed damaged lattice of direct tension with profiled interface for different loading stages (A-D) of samples 1-3. Deformation scaling factor x2000. Red indicates interface, blue SHCC, white concrete and black failed elements.

3.4.2. Influence of interface tensile strength

Table 3.6 shows the samples for investigating the effect of the interface tensile strength for the direct tension test on samples with a profiled interface. The envelopes of the stress-crack opening curves of these samples are shown in Figure 3.17a with the accompanying fracture energy in Figure 3.17b. Samples 1, 5 and 13 will be considered more in depth.

Table 3.6: Model input interface properties of samples used for interface tensile strength in the direct tension test on profiled interface.

Material	Sample number	Stiffness (MPa)	Tensile strength (MPa)	Compressive strength (MPa)
Concrete	all	32836	3.7	-70
Interface	5	100%	7.5%	-10*ft interface
Interface	4	100%	15%	-10*ft interface
Interface	1	100%	30%	-10*ft interface
Interface	11	100%	50%	-10*ft interface
Interface	13	100%	70%	-10*ft interface
Interface	14	100%	90%	-10*ft interface
Interface	12	100%	100%	-10*ft interface

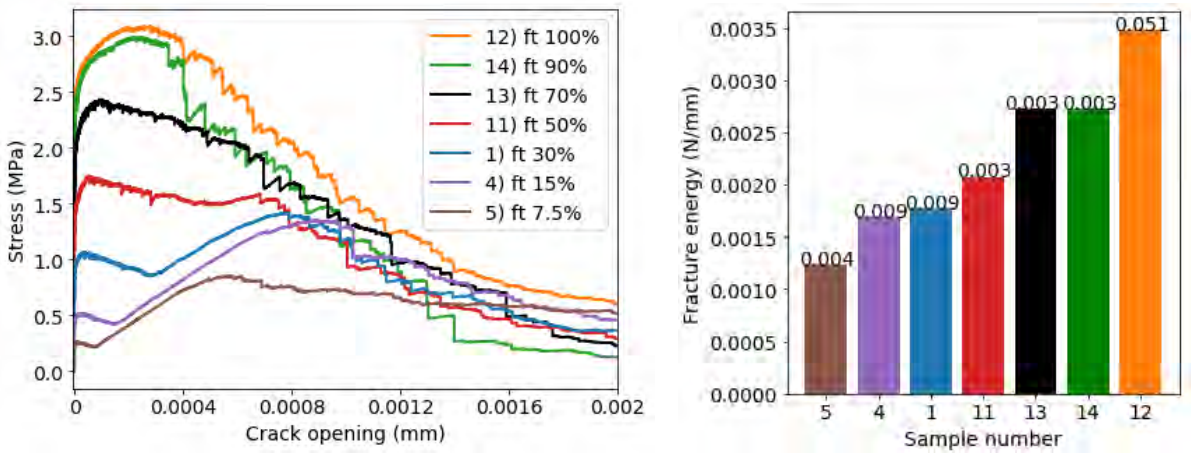

(a) (b)

Figure 3.17: Stress-crack opening curve direct tension with a profiled interface and different interface tensile strength (a), with accompanying fracture energy for area under the curve and the number above the bar plot for the total fracture energy (b).

Again a second peak is present in the stress-crack opening curve of multiple samples. It can be seen that the second peak vanishes with increasing interface tensile strength. From around 50% interface tensile strength the second peak already is lower compared to the first peak. With an even higher interface tensile strength the second peak is not present anymore. For samples 1, 4 and 11 the height of the second peak is comparable. Sample 5 with a very low interface tensile strength shows a decreased height of the second peak compared to samples 1, 4 and 11. Comparing the fracture energy obtained from the area under the curve only a general trend can be obtained. An increase in fracture energy is the consequence of the higher interface tensile strength. However, the total fracture energy does not show much difference. To gain more insight what causes the second peak to vanish, the samples 1, 5 and 13 are considered more closely. Figures 3.18a and 3.18b shows the stress-crack opening curve and fracture energy respectively for these samples.

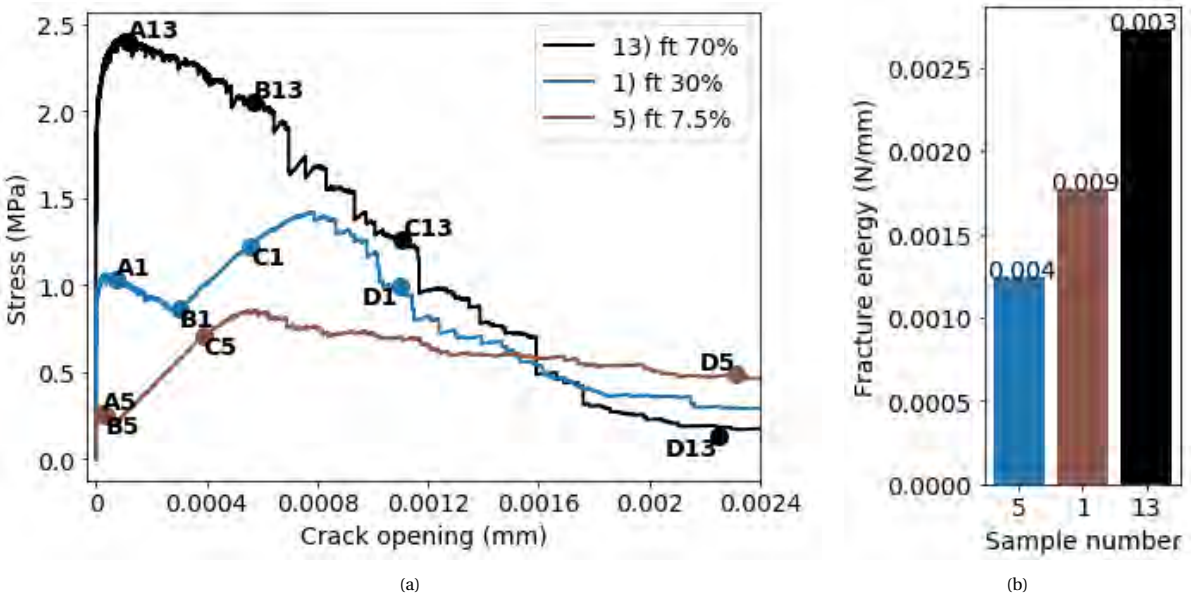

(a) (b)

Figure 3.18: Stress-crack opening curve direct tension with a profiled interface for different interface tensile strength for samples 1, 5 and 13 (a), with accompanying fracture energy for area under the curve and the number above the bar plot for the total fracture energy (b).

Comparing the deformed damage lattice of the samples 1, 5 and 13 from Figure 3.19 three different failure modes are observed. In case of the lowest interface tensile strength, sample 5, the interface at the bottom of the profile cracks first, resulting in the first peak. After this the top and shear planes start to break. This is the

contributor for the second peak. With the low interface properties no other elements outside the interface fail, making the interface the only material determining the stress-crack opening curve. In sample 1 the failure mechanisms start the same with cracking on the bottom side of the notches. The second peak is also affected by the concrete and SHCC elements that start to fail, before the interface elements on the shear planes are fully broken. Although, now more materials are activated, the second peak stress is around 1.5 times the first peak stress, while for sample 1, where only the interface effects the strength, the second curve peak stress is 3 times the first peak. For sample 13 the second peak stress is even lower compared to the first peak. From the deformed damaged model it is observed that in point A of sample 13, which is located at the top of the stress-crack opening curve, already some SHCC elements have failed. In the second step this amount has increased and also concrete elements start to fail. Some interfaces on the shear planes have already failed, while there are interface elements on the top of the notched that are still intact. Eventually, at point D it can be seen that the failure mechanism comes from failure on top of the notches through the interface and concrete. But in this point also the bottom of the profile has started to show connecting cracks through the SHCC. Lastly, what can be notices from the deformed model is the contribution of the SHCC in the total deformation in sample 13. The blue part (SHCC) has become larger compared to the white part (concrete) in the first points A and B. After point B there are more drops in the stress-crack opening curve present as a result from crack formation.

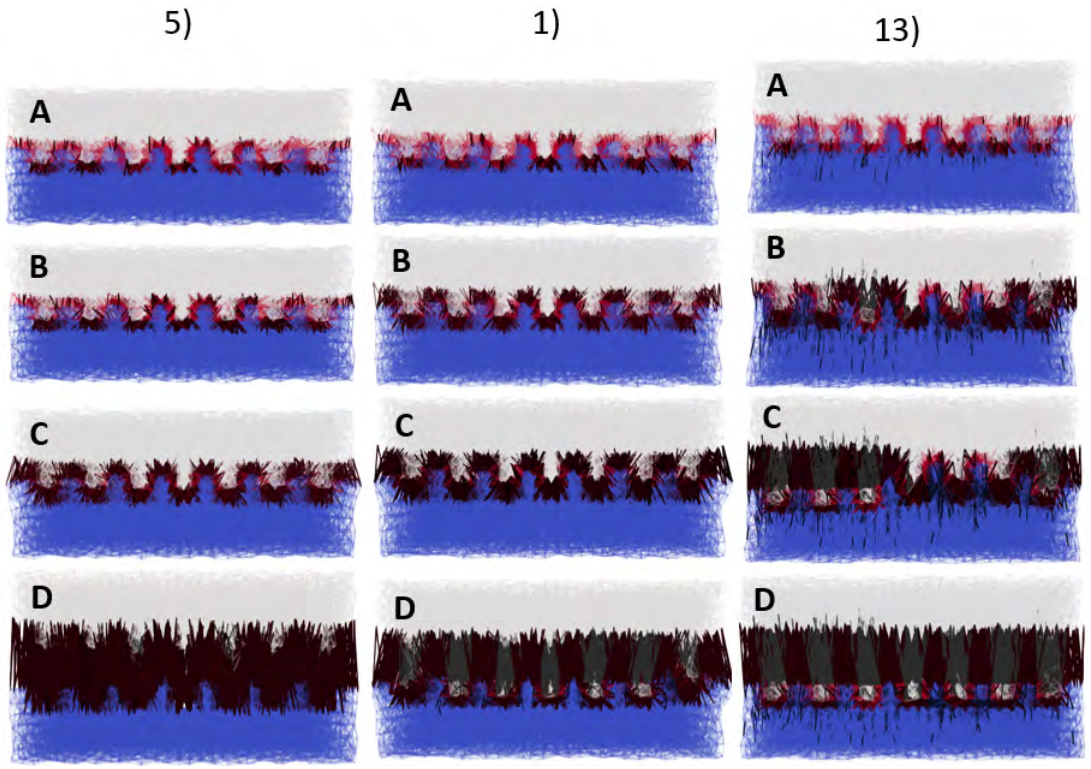

Figure 3.19: Deformed damaged lattice of direct tension with profiled interface for different loading stages (A-D) for samples 1, 5 and 13. Deformation scaling factor x2000. Red indicates interface elements, blue SHCC, white concrete and black are broken elements.

3.4.3. Influence of profiled interface

The influence of the profiled interface will be discussed by comparing the results between the direct tension test on a smooth and profiled interface. The focus is on the effect of the profile on the maximum stress and fracture energy. Next to the data shown in the above section, additional simulations have been carried out. The complete data of all samples are presented in Appendix A.

The maximum stress of all samples is plotted against the interface properties in Figures 3.20a and 3.20b. For the profiled interface it was seen that under direct tension the stress-crack opening curve shows two peaks. In results of Figures 3.20a and 3.20b the maximum stress is used. This means a shift from the second peak to the first peak is present in the results moving towards higher interface tensile strength. The same data is used in both figures, but the axes are reversed to show the effect of interface tensile strength and interface stiffness respectively.

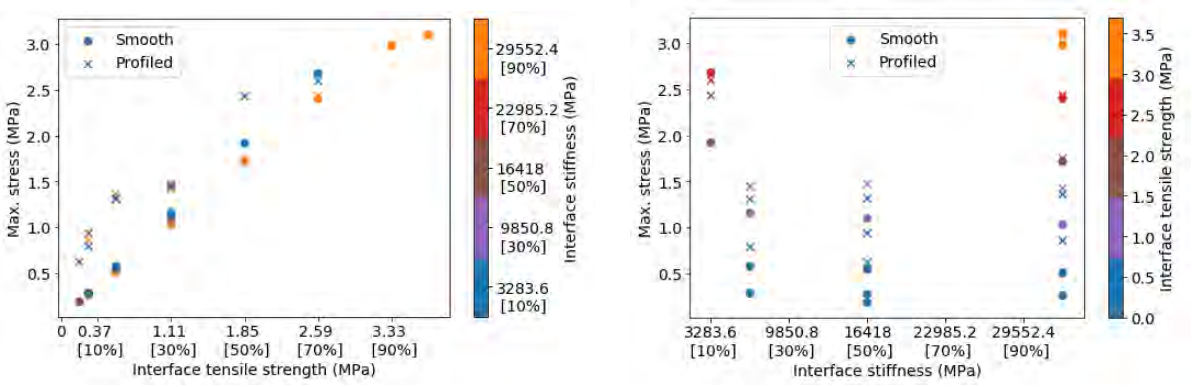

(a) (b)

Figure 3.20: Scatter plot of maximum stress vs. interface tensile strength (a) and maximum stress vs. interface stiffness (b) for all samples under direct tension of both smooth and profiled interface.

From the plot it can be seen that for low interface tensile strength adding a profile benefits the load capacity. However, with increasing interface tensile strength this benefit vanished since the adjacent materials are activated influencing the failure mechanism and the load capacity of the specimen.

Looking at Figure 3.20b the best way to conclude on the effect of the interface stiffness between smooth and profiled interface is to look at the purple dots, since these points have the same interface tensile strength. It is seen that for a decreasing interface stiffness the trend of an increase in maximum stress is stronger for a smooth interface compare to a profiled interface. The increase in peak stress from adding a profiled interface decreases with decreasing interface stiffness. This can be indicated by the reduced distance between the dots and crosses for lower interface stiffness compared to the distance at high interface stiffness.

From the fracture energy bar plots of a smooth interface it was seen that the fracture energy increases in a linear way, doubling the fracture energy if the interface tensile strength is doubled. This counts for the lower range in interface tensile strength. For the profiled interface the fracture energy is closer together, which is the result of the activation of the adjacent materials. The activation of the adjacent materials with a smooth interface happens at much higher interface tensile strength compared to the profiled interface. Also, for the decrease in interface stiffness a sharp increase in fracture energy is obtained in case of a smooth interface. For the profiled interface this increase is limited. However, adding a profile will increase the fracture energy in case of 100% interface stiffness and 30% interface tensile strength with a power 10 compared to the smooth interface. This difference decreases with increasing interface tensile strength, since the adjacent materials will be affected.

3.4.4. Comparison with literature

The results of the direct tension test and the conclusions found on the effect of the roughness are compared with experimental and numerical findings in literature to support the results obtained.

As a reference for the small-scale test the results of Luković [37] were used. In this study concrete-concrete interfaces are modelled with the lattice model. Direct tension and shear tests are modelled with both smooth and profiled interfaces. Comparing the stress-displacement curves of the study and the ones obtained here for profiled interfaces will indicate the effect of a profiled interface apart from the used materials. Also, in the study of Luković different profiles are modelled. From this the effect of changing the profile lay-out can be investigated. Figures 3.21a and 3.21b show the different profiles used and the accompanying stress-displacement curves. In the smooth curve there is no second peak obtained, this is the same as found in this thesis. Profiles 1 and 4 have the same height to width ratio as the profile in this thesis, but a different size. For these profiles a second peak is shown similar to the shape obtained here. However, here the second peak is in most of the cases higher compared to the first peak. From the literature results it can be seen that an increase in size of the profile leads to a higher fracture energy with a higher ductility due to the second peak. The shape of the profile thus influences the second peak. The presence of the second peak is a result of the profile shape and the shape of the stress-crack opening curve is a result of the height to width ratio of the notches together with the material properties and model input. It is not clear if in literature a bending influence factor of zero is used. If not, the shear planes of the profile can fail at a lower stress level, since bending will be considered in the stress state of the elements. With an increased bending influence factor these elements will fail sooner.

This would decrease the second peak stress in the cases where the shear planes are governing. In other cases the concrete was governing, showing a final crack through the interface and concrete on top of the profile.

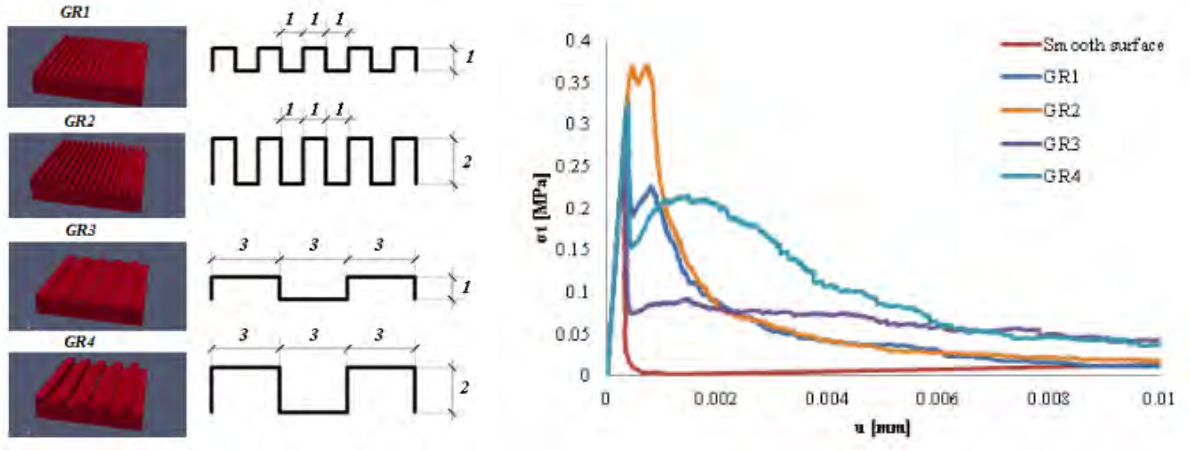

(a) (b)

Figure 3.21: Different profiles (a) used for direct tension test on concrete-concrete interface with accompanying stress-displacement curve (b), from [37].

To investigate the role of SHCC in the stress-crack opening curve a different study is used. In [38] a direct tension test is used to investigate the effect of different interface roughness between concrete and SHCC. Experimental testing was carried out on specimen with different roughness and profiles. Figures 3.23a, 3.23b and 3.23c show the stress-crack opening curve for a smooth interface, grooved interface and holed interface respectively. Although, the grooved profile matches the pattern of the profile used in this thesis best, the edges are slanted. Therefore, also the results of the holed interface are shown, which have vertical edges, but a larger contact area between the two materials. The lay-out of the holed and grooved interface are shown in Figure 3.22.

Figure 3.22: Left: holed interface, right: grooved interface, from [38].

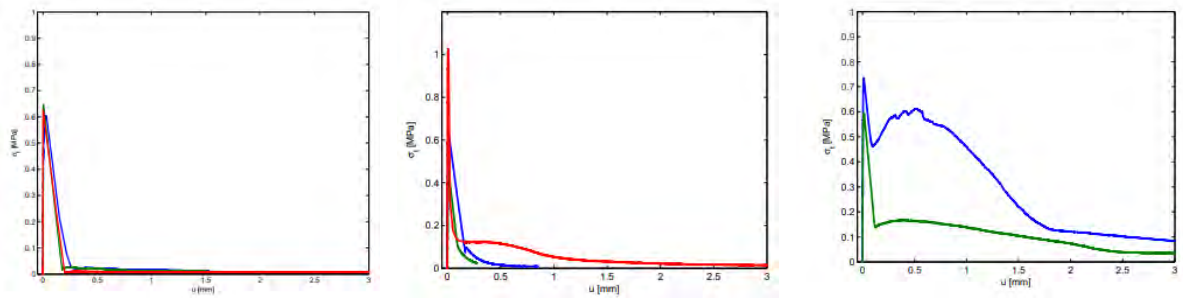

(a) (b) (c)

Figure 3.23: Stress-crack opening curves for smooth interface (a), grooved interface (b) and holed interface (c) for direct tension test on concrete-SHCC interface, from [38].

Comparing the stress-crack opening curves from the experiments to the stress-crack opening curves obtained in this thesis a similarity for the smooth interface is obtained. For the grooved interface, however, there is hardly a second peak visible. In the holed interface there is a distinct second peak present. In this case it is the vertical edges and increased contact area that cause the second peak. Also, in terms of fracture energy a better comparison is obtained with the drilled holes. It was found to shows significantly higher values compared to the smooth interface, while the grooved profile has similar fracture energy as the smooth interface. However, already for the smooth interface in this thesis the values are even a factor 10 lower compared to the fracture energy of the smooth interface in the experiments.

Lastly, the study carried out in [16] is used to compare the results. In this study the wedge splitting test was used to investigate different interface roughness for SHCC-HSC interfaces. In the study the concrete is with a smooth surface after which sand blasting is used to remove the concrete until aggregates are exposed. The roughness is defined as the measured depth of the surface. This type of roughness differs from a profiled interface, since a profile is explicitly cast and most of the time larger in size. In both cases an increase in interface contact area is obtained.

Figures 3.24a and 3.24b show the stress versus crack opening curve for the wedge splitting test with different roughness and on specimens with different dimensions respectively. From the roughness value it is seen that the roughness is smaller compared to the depth used in the profiles of this thesis. Still, a second peak is obtained. The second peak has a lower peak stress compared to the first peak, which is different from the results found in this thesis. But the wide tail of the peak is comparable. In the experiments it was observed that a high roughness led to an increase in post-peak hardening and fracture energy due to the activation of SHCC. With low roughness the SHCC was not activated. In the results of this thesis for both a profiled and smooth interface the fracture energy was found to increase with the activation of the adjacent materials. In Figure 3.24b a very low roughness results in a more brittle behaviour without a second peak. The fracture energy for this case is 5 N/m. In this thesis a smooth interface results in the same brittle behaviour for interface failure. The fracture energy was lower ranging from 0.175 to 1 for 30% to 70% interface tensile strength. This is lower, also considering the lower stress obtained in the experiments. Also, higher roughness values in the experiments increase the fracture energy with a factor 100, while in the simulations only a factor of 10 to 50 is obtained depending on the interface properties.

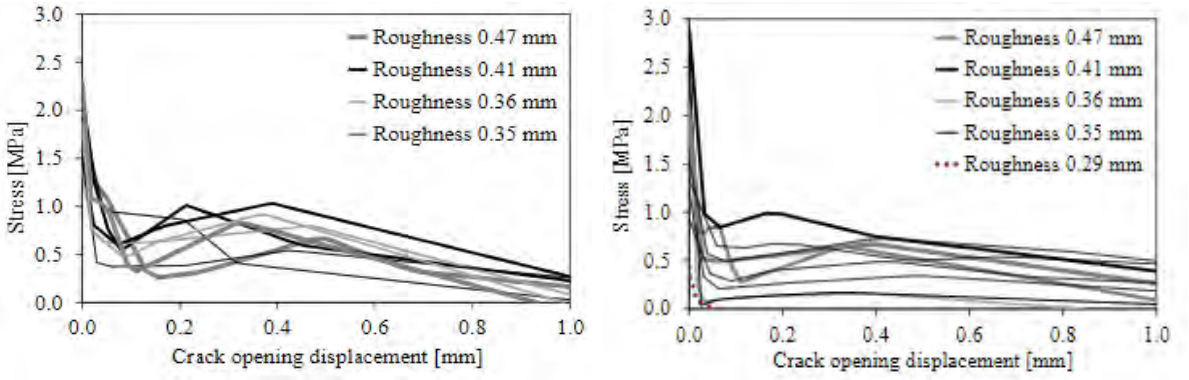

Figure 3.24: Stress-crack opening curve wedge splitting test on HSC-SHCC interface with different roughness for interface length of 60 mm (a) and 90 mm (b), from [16].

In this thesis fracture energy values are found to be lower compared to experimental findings. To indicate what causes this effect, a comparison between regular concrete is made. In [39] the fracture energy of regular concrete, with a lower stiffness compared to the concrete in this thesis, has a fracture energy of 56 N/m. For the direct tension test with a smooth interface and interface tensile strength of 100% of the concrete tensile strength a value of 34 N/m is obtained. In that case a crack in the concrete is present. Although, this value is already in the same order, it is still around a factor 3 lower as what is expected from this type of concrete and material properties. Although, the randomness in the lattice model should account for the fracture energy, the lattice model still has a more brittle behaviour compared to reality. It was seen from the direct tension test that an interface tensile strength of 90% already has localized cracking in the interface, resulting in a brittle behaviour. Due to the reduced strength in the interface, the cracks localize in the interface, while in regular

concrete the position of the crack is not known beforehand. In the lattice model the interface is modelled with only one row of elements. This one row might have a reduced effect of the randomness, decreasing the fracture energy. All in all, it can be concluded that the lattice model underestimates the fracture energy as a result of the more brittle behaviour of the model.

3.5. Direct shear test smooth interface

The results of the direct shear test for specimens with a smooth interface are discussed. In the direct shear tests both supports are fully restrained. At the bottom right support an imposed deformation is applied. The boundary conditions are shown in Figure 3.25. The boundary conditions have a large influence on the direct shear test as will be discussed at the result of altering the interface tensile strength. Different boundary conditions have been investigated. The results of sample 1 with 30% interface tensile strength and 100% interface stiffness are shown in Appendix B. The other samples used alongside with their input values for the interface properties are stated in Table 3.7.

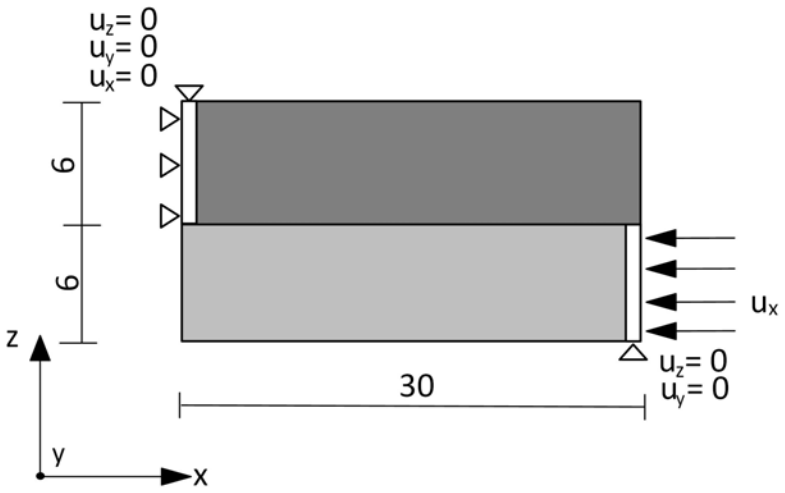

Figure 3.25: Test set-up and boundary conditions direct shear test with dimensions in millimetre.

For the direct shear tests the stress-strain curve and damaged model are investigated for different interface properties. The fracture energy will not be calculated and the stress-strain curve still includes the initial elastic deformation. The strain is calculated as the deformation of the right support divided by the width of the specimen. The displacement is negative, but the strain is set to positive values.

Table 3.7: Model input interface properties of samples used for interface stiffness in direct shear test on smooth interface.

Material	Sample number	Stiffness (MPa)	Tensile strength (MPa)	Compressive strength (MPa)
Concrete	all	32836	3.7	-70
Interface	1	100%	30%	-10*ft interface
Interface	2	50%	30%	-10*ft interface
Interface	3	20%	30%	-10*ft interface

3.5.1. Influence of interface stiffness

In Figure 3.26 the stress-strain curves for the samples 1-3 are shown. It can be seen that with an increase in stiffness the maximum stress increases. The maximum stress increases from 2.23 MPa to 2.54 MPa to 2.86 MPa from sample 1 to samples 2 and 3 respectively. The only difference in the shape of the curve can be seen in the orange curve of sample 1, where a small drop at the end of the first linear part is observed.

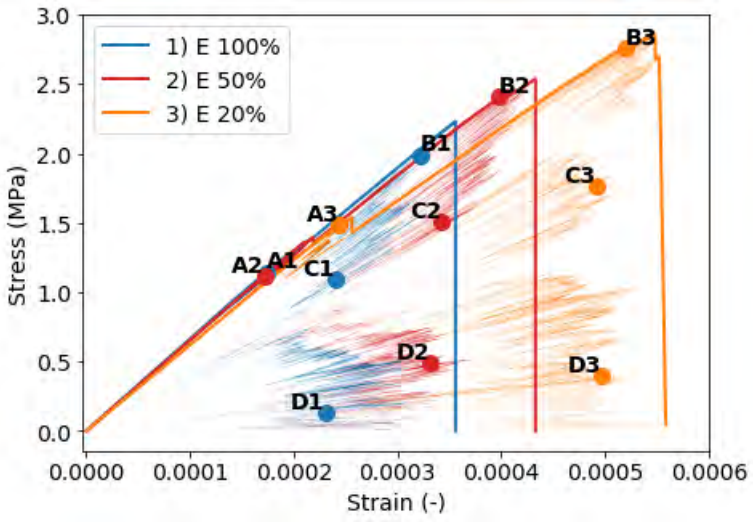

Figure 3.26: Stress-strain curve direct shear for sample 1-3 with a smooth interface and different interface stiffness.

To investigate where this increase in the load capacity and ductility comes from the damaged lattice is investigated. From the side view of the deformed damaged lattice for different loading stages on the stress-strain curve in Figure 3.27 it can be seen that with decreasing interface stiffness increasing amount of concrete and SHCC elements start to fail. The same can be observed from the top view of the damaged elements in Figure 3.28.

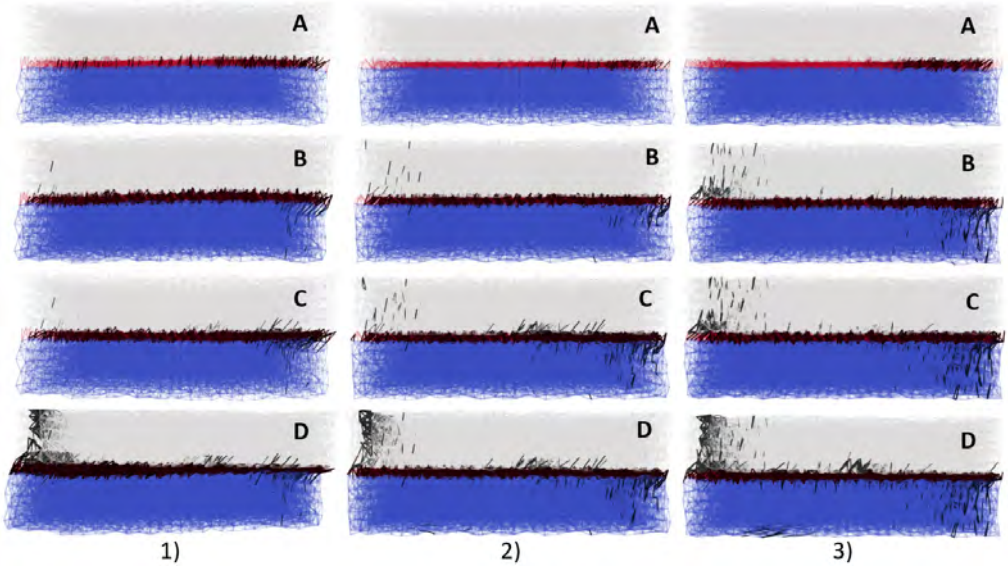

Figure 3.27: Side view of deformed damaged lattice of direct shear with smooth interface for samples 1-3 at different loading stages (A-D). Deformation scaling factor x200, x10, x10. Red indicates interface, blue SHCC, white concrete and black failed elements.

At point A of the different samples the minority of the failed elements are located in the interface. Only a few single elements in the SHCC are observed. From the damaged elements at point A it can be seen that the cracks move from right to left. On the right side the interface elements are oriented in such a way that tension is present in the elements, while on the left side the elements are in compression. As the crack propagates to the left more interface elements remain intact. These are elements that are loaded in compression. This contributes to the strength of the specimen as at the top of the curves (point B) these interface elements are not yet broken. However, the increase in strength between the different samples cannot be directly attributed to this mechanism, since it is the case for all three samples in the same manner. The increase in strength can be attributed to the SHCC being activated. At the top of the stress-strain curves multiple SHCC elements next to the bottom support have failed. This thus contributes to the increased load capacity as more SHCC

elements fail with lower interface stiffness. Only after the peak has been reached a crack in the concrete centre can be observed after which in the final stage also the concrete next to the support start to fail from rotating of the top layer. The failure of the concrete thus does not attribute to the strength. The increase in ductility comes from the fact that with a lower stiffness the deformability of the interface increases.

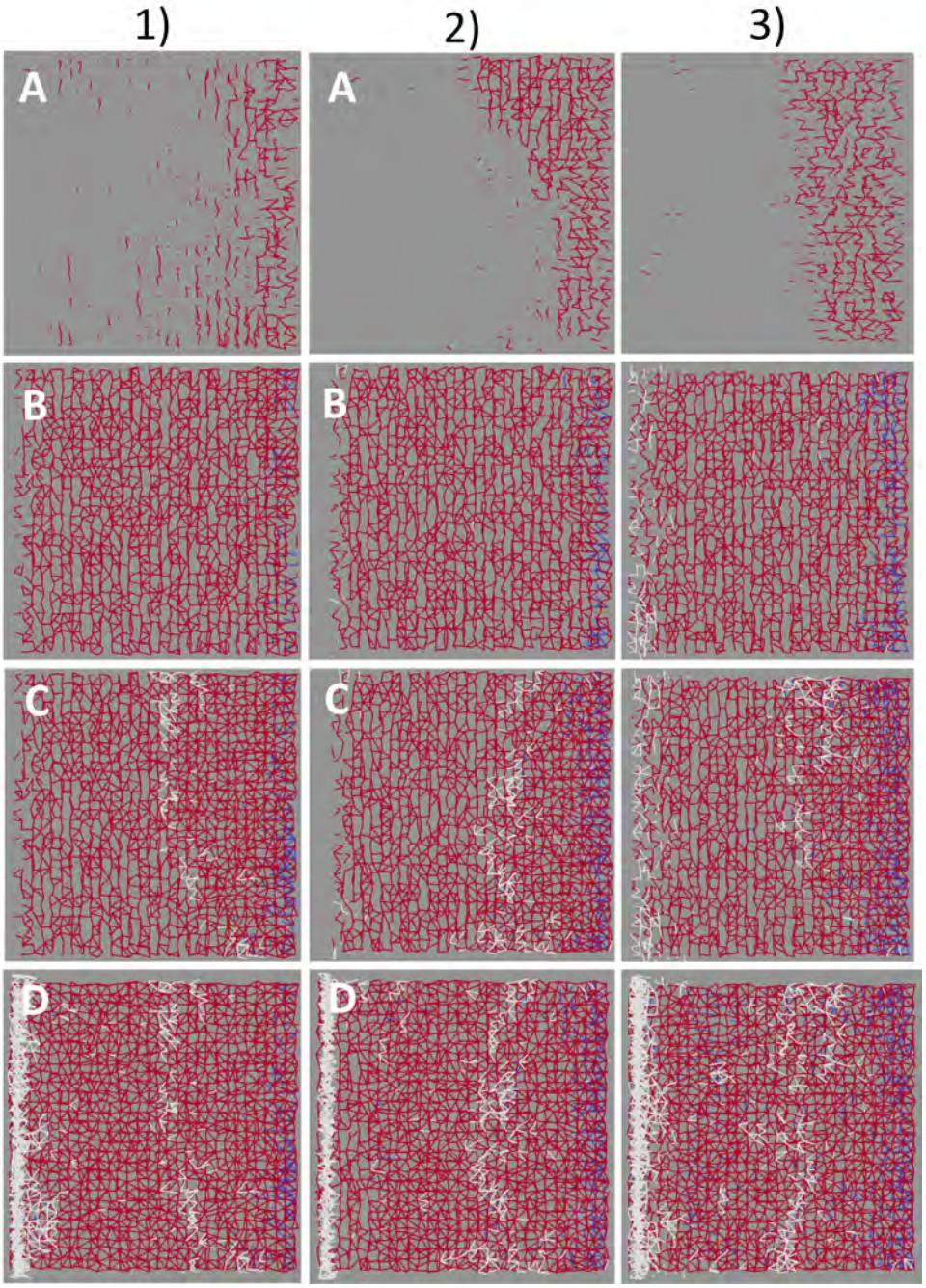

Figure 3.28: Top view damaged lattice of direct shear with smooth interface for samples 1-3 for different loading stages (A-D). Red indicates failed interface, blue failed SHCC and white failed concrete elements.

3.5.2. Influence of interface tensile strength

In Table 3.8 the input properties of the samples that are used to investigate the effect of changing the interface tensile stress with the direct shear test are stated. Figure 3.29 shows the envelope of the stress-strain curves for the accompanying samples. Samples 1, 4 and 11 are investigated more in depth. For these samples the stress-strain curve is shown in Figure 3.30.

Table 3.8: Model input interface properties of samples used for interface tensile strength in direct shear test on smooth interface.

Material	Sample number	Stiffness (MPa)	Tensile strength (MPa)	Compressive strength (MPa)
Concrete	all	32836	3.7	-70
Interface	5	100%	7.5%	-10*ft interface
Interface	4	100%	15%	-10*ft interface
Interface	1	100%	30%	-10*ft interface
Interface	11	100%	50%	-10*ft interface
Interface	13	100%	70%	-10*ft interface
Interface	14	100%	90%	-10*ft interface
Interface	12	100%	100%	-10*ft interface

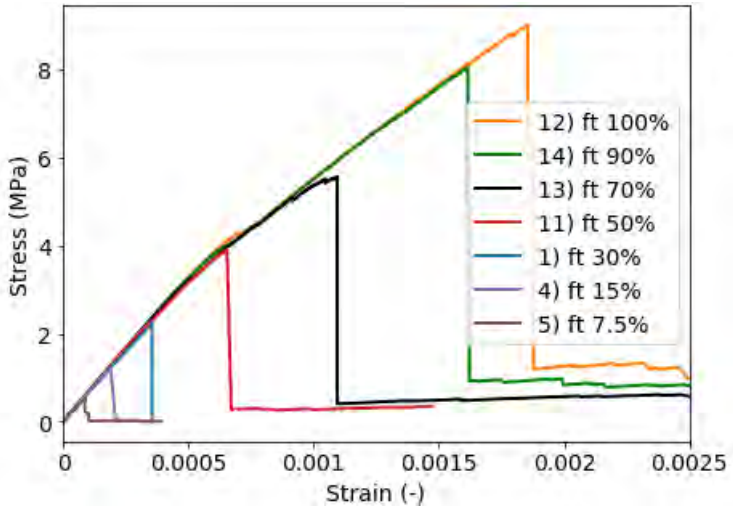

Figure 3.29: Stress-strain curve direct shear for smooth interface for samples with interface tensile strength ranging from 7.5% to 100%.

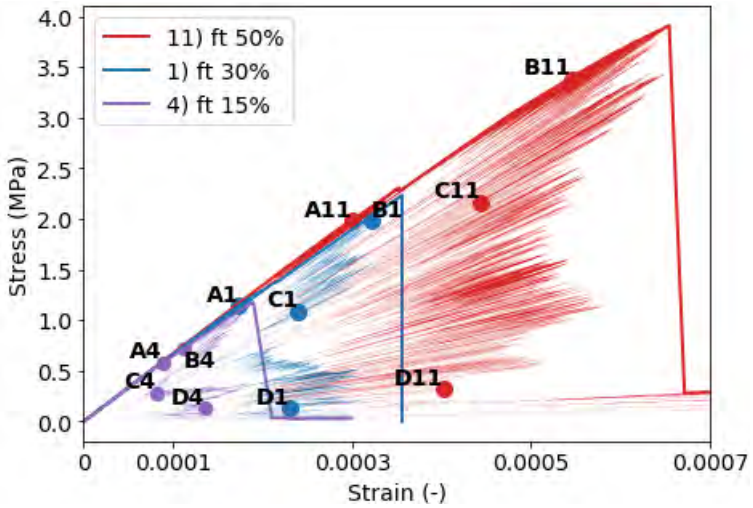

Figure 3.30: Stress-strain curve direct shear of samples, 1, 4 and 11 for smooth interface.

The lattice model output curves (the spikes) show a different pattern. However, this is often not looked at since the envelope is considered the stress-strain curve. Therefore, the focus is on the stress-strain behaviour. Between sample 4 and 1 the interface tensile strength is doubled. The maximum stress is also doubled, indicating a linear relationship between the interface tensile stress and maximum stress. Between sample 1 and 13 the interface tensile strength is also doubled, but the maximum stress is not doubled anymore. This means that the relation between the interface tensile strength and maximum stress is linear up to a certain threshold. The damaged lattice model is analysed to indicate what happens after this threshold that limits the increase in maximum stress.

The damaged lattice model is shown for different loading stages from a side view in Figure 3.31 and from a top view in Figure 3.32. From both views an increasing contribution in concrete damaged elements and damaged SHCC elements with increasing interface tensile strength is obtained. In the side view of sample 11 a crack through the concrete starts to get visible in point C.

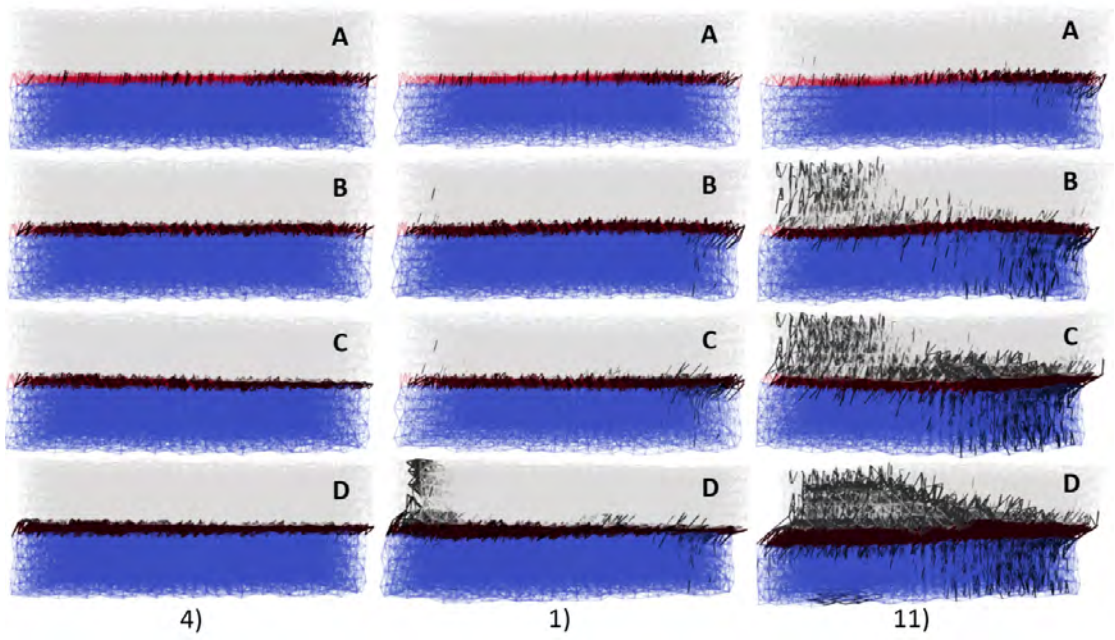

Figure 3.31: Side view deformed damaged lattice of direct shear with smooth interface for different loading stages (A-D) of samples 1, 4 and 11. Deformation scaling factor x200. Red indicates interface, blue SHCC, white concrete and black are failed elements.

In the first steps the interface elements start to fail. For sample 4 only interface elements fail and a fully interface failure is obtained. For sample 1 it was seen in the previous section that the failure of the SHCC and concrete elements contribute towards the strength. It can now be concluded comparing sample 1 and 4 that the increase in interface compressive strength was the cause of the failure of the SHCC and concrete.

If the interface tensile strength, and accordingly the interface compressive strength, is increased further more damaged elements are observed in the concrete and SHCC. In sample 11 the elements at the support start to break first. This still contributes to the increased strength, which is not the case for sample 1. In sample 1 the concrete elements fail due to rotation of the concrete top layer after most interface elements have debonded, but the remaining few element under compression are still pushing the concrete from the bottom. In sample 11 the concrete has not debonded yet. There are interface elements still intact spread over the interface. After the maximum strength is reached in sample 11 a line of broken concrete elements is seen. This crack is prevented from propagating due to the failure permission mode at the supports, which does not allow these elements to fail. In sample 4 the interface tensile strength, and thus also the interface compressive strength, is lower. This results in interface failure before the rotation damages the concrete layer. This indicates that the interface compressive strength is influencing the results in terms of cracking behaviour. However, the cracks next to the support in sample 1 only happen after the maximum stress has already been reached and the sample is close to failure.

Among the different boundary conditions testes for the direct shear test of sample 1 is a situation where an extra restraint in z-direction is included at the top right of the specimen. The rotation of the concrete layer is prevented due to this extra restraint. The deformed damaged lattice stated in Appendix B shows that

the cracks next to the support have been replaced by cracks at the bottom of the concrete layer. It could be argued, which situation provides the most accurate prediction. The maximum stress and strain for both cases are the same. Since in both cases the cracking happens when the specimen is close to failure, both cases are considered to provide insight into the load-capacity and ductility of the test method. But the influence on the cracking behaviour does indicate that a careful consideration of the boundary conditions is needed for this test. Also, over restraining the sample should be prevented.

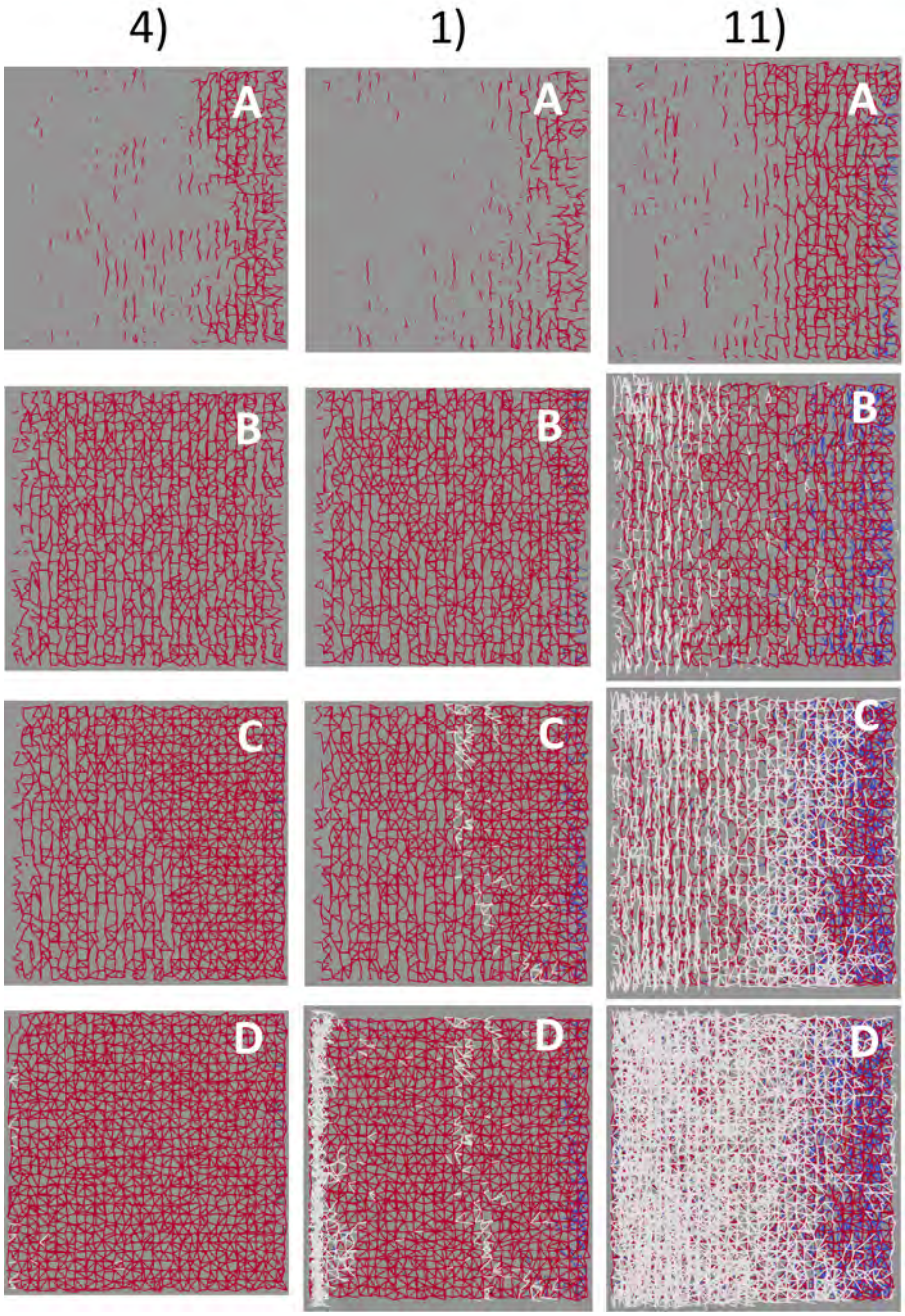

Figure 3.32: Top view of damaged lattice of direct shear with smooth interface for points A-D. Red indicates failed interface, blue failed SHCC and white failed concrete elements.

3.6. Direct shear test profiled interface

The last small-scale test discussed in this chapter is the direct shear test on a specimen with a profiled interface. The influence of the interface stiffness and interface tensile strength are discussed respectively.

3.6.1. Influence of interface stiffness

Table 3.9 states the input values of the material properties for the samples 1-3 for investigating the effect of the interface stiffness. For these samples the stress-strain curve is shown in Figure 3.33. The first thing to notice is the increase in strength for a decrease in interface stiffness. Alongside this trend it is also seen that the shape of the curve differs slightly. A low interface stiffness shows a lower slope towards the peak of the curve. After the peak the strain does not increase a lot compared to sample 1 with a high interface stiffness. Sample 1 shows a sharp decrease after the peak after which the strain increases in three sharp steps. A closer look is taken at the failure mechanism with comparing the damaged lattice.

Table 3.9: Model input interface properties of samples used for interface stiffness in direct shear test on profiled interface.

Material	Sample number	Stiffness (MPa)	Tensile strength (MPa)	Compressive strength (MPa)
Concrete	all	32836	3.7	-70
Interface	1	100%	30%	-10*ft interface
Interface	2	50%	30%	-10*ft interface
Interface	3	20%	30%	-10*ft interface

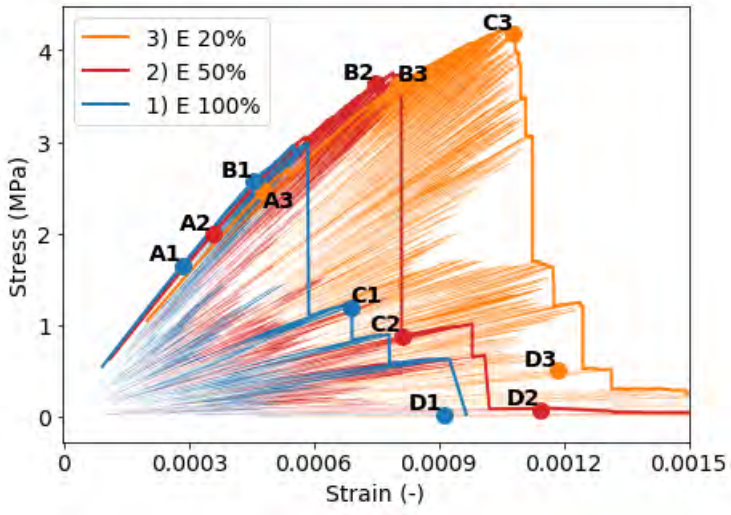

Figure 3.33: Stress-strain curve direct shear of samples 1-3 for a profiled interface.

Figure 3.34 shows the deformed damaged lattice of the direct shear test of samples 1-3 with a profiled interface. For sample 1 it can already be observed that more elements in the SHCC and concrete start to fail compared to the smooth interface. At point B of the stress-strain curve the peak has not been reach, but elements have failed in the concrete and SHCC. This indicates the contribution of the adjacent materials to the strength of the specimen. With decreasing interface stiffness more and more elements start to fail in the SHCC and concrete as can be observed in the damaged lattice of samples 2 and 3. For Sample 3, point C is positioned at the top of the stress-strain curve. In the corresponding damaged lattice model it can be observed that a region of damaged concrete and SHCC elements have failed and some interface elements are still intact. For sample 2 the interface has eventually failed with scatter in the adjacent materials of broken elements. For sample 3 a crack in the concrete can also be observed. The supports are, however, prevented from failure, which on its turn prevents the crack from fully penetrating. This might be why the crack does not cause significant deformation in the sample.

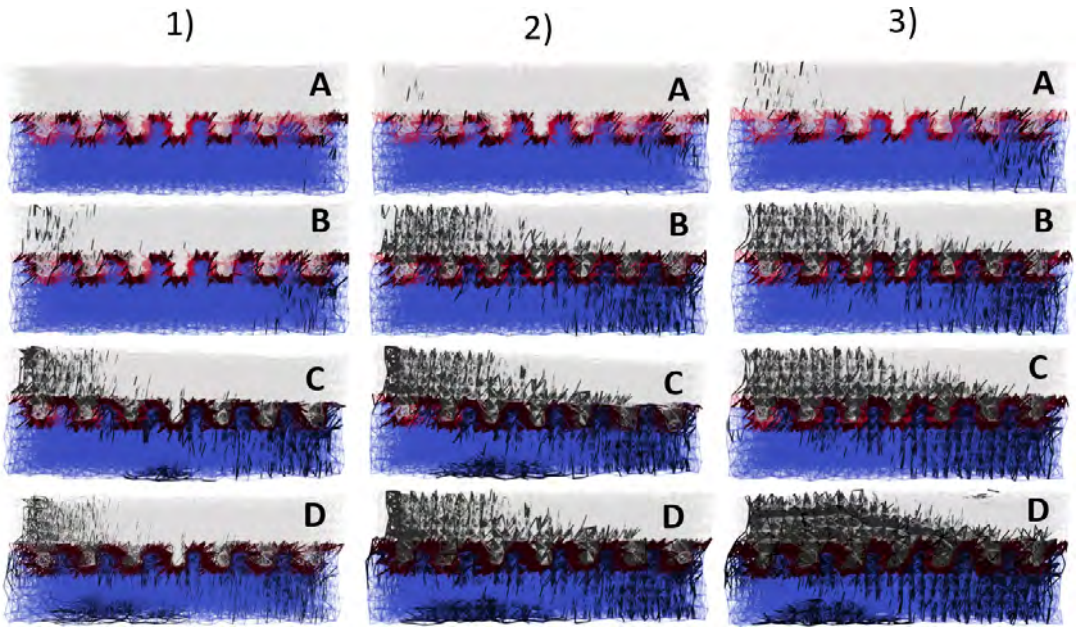

Figure 3.34: Deformed damaged lattice of the direct shear test with a profiled interface for different loading stages (A-D) of samples 1-3. Deformation scaling factor is x20. Red indicates the interface, blue SHCC, white concrete and black the failed elements.

3.6.2. Influence of interface tensile strength

Table 3.10 states the sample properties to investigate the influence of the interface tensile strength. For all these samples the envelopes of the stress-strain curve are shown in Figure 3.35.

Table 3.10: Model input interface properties of samples used for interface tensile strength in direct shear test on profiled interface.

Material	Sample number	Stiffness (MPa)	Tensile strength (MPa)	Compressive strength (MPa)
Concrete	all	32836	3.7	-70
Interface	5	100%	7.5%	-10*ft interface
Interface	4	100%	15%	-10*ft interface
Interface	1	100%	30%	-10*ft interface
Interface	11	100%	50%	-10*ft interface
Interface	13	100%	70%	-10*ft interface
Interface	14	100%	90%	-10*ft interface
Interface	12	100%	100%	-10*ft interface

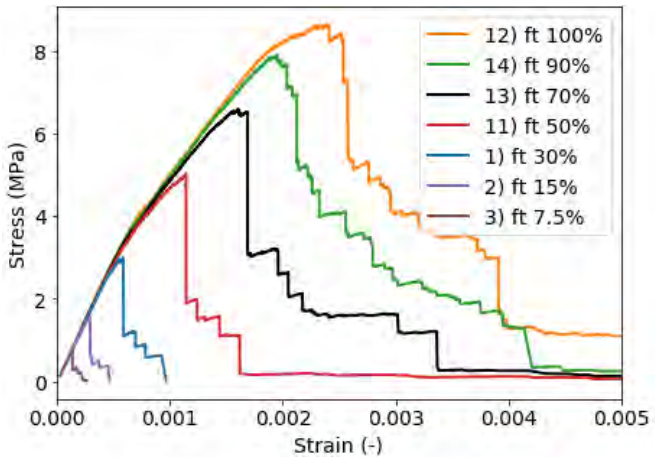

Figure 3.35: Stress-strain curve direct shear with profiled interface for different interface tensile strength.

From this graph a slight bend can be observed in the first part of the curves when the interface stiffness increases. Next to that, the tail of the stress strain curve shows increasing softening with increased interface tensile strength. This softening was not obtained for the direct shear test carried out on a smooth interface. The samples 1, 4 and 11 will be considered more closely. The stress-strain curves of these samples are repeated in Figure 3.36. From this figure the decrease in slope of the curve of sample 11 is clearly visible. What leads to this decrease in slope will be discussed with analysis the damaged model in Figure 3.37.

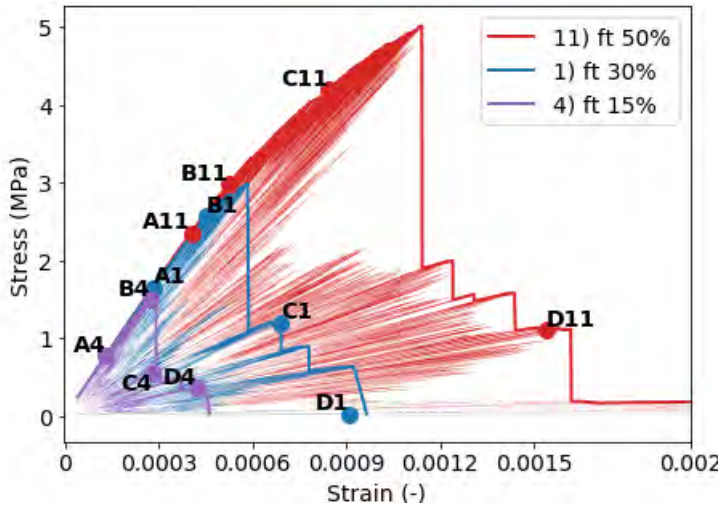

Figure 3.36: Stress-strain curve direct shear with profiled interface for samples 1, 4 and 11 with different interface tensile strength.

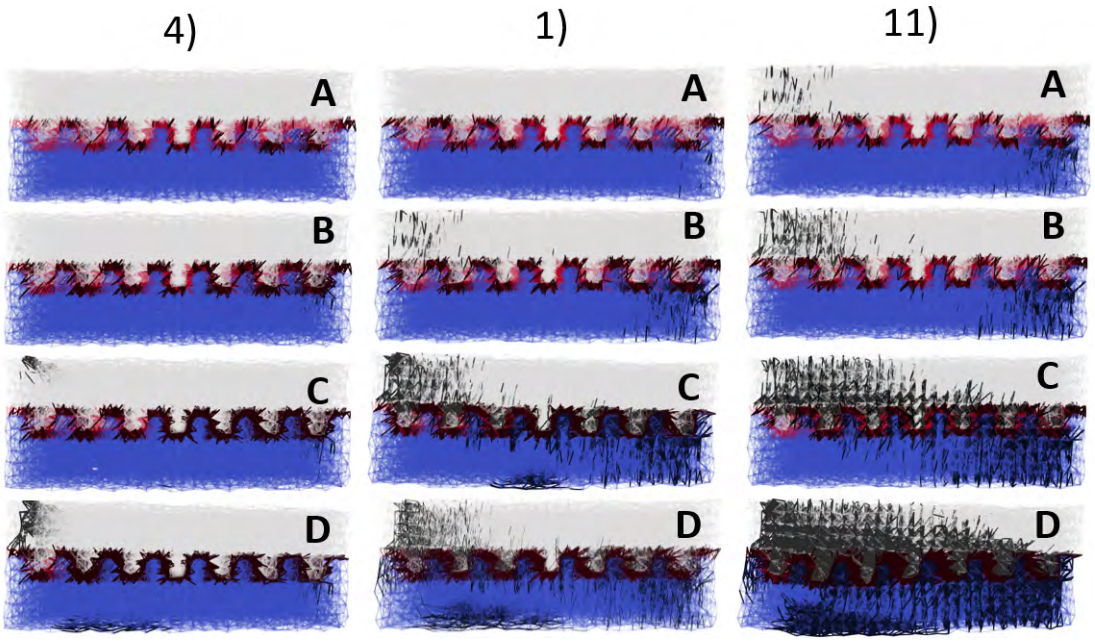

Figure 3.37: Deformed damaged lattice of direct shear with profiled interface for different loading stages (A-D) of samples 4, 1 and 11. Deformation scaling factor x20. Red indicates interface elements, blue SHCC, white concrete and black are failed elements.

In point A of samples 1 and 4 the interface elements are failing first. For sample 11 already elements in the concrete and SHCC next to the support start to fail. This happens at point B, which is still before the peak stress. This means that the elements in the concrete and SHCC that are activated contribute to the strength of the specimen. For sample 4 in point B the elements are still breaking in the interface. The peak stress is thus mainly determined by the interface tensile strength. For sample 11 point C is still in the increasing part of the curve, but the slope has reduced. It is seen from the damaged lattice that the elements fail in a slant line between the supports. There is, however, no crack visible as what was the case with decreasing stiffness. An

increase in interface tensile strength will increase the activation of the adjacent materials. This mechanism increases the strength, but reduces the strength increase.

3.6.3. Influence of profiled interface

Comparing the results between the direct shear test on a smooth and profiled interface the effect of adding a profile in the interface can be discussed. The complete data of all samples stated in Appendix A is used for the comparison in a general trend. The maximum stress of all samples is plotted against the interface properties in Figures 3.38a and 3.38b. The same data is used in both figures, but the axis are reversed to show the effect of interface tensile strength and interface stiffness respectively.

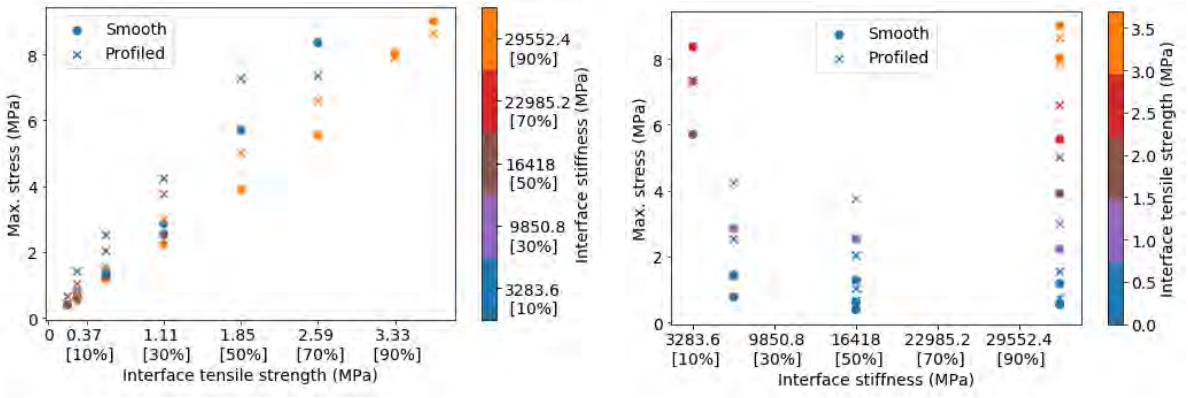

(a) (b)

Figure 3.38: Scatter plot of maximum stress vs. interface tensile strength (a) and stiffness (b) for all samples under direct shear of both smooth and profiled interfaces.

Comparing the results of the smooth and profiled direct shear test from Figure 3.38a it can be seen that with increasing interface tensile strength the effect of adding a profile increases. The maximum stress increases more rapidly for the profiled interface compared to the smooth interface. However, this difference vanishes after a certain threshold of interface tensile strength, after which the results are close together. At around 50% of interface tensile strength the maximum increase of stress for applying a profile is reached. For very low and very high interface tensile strength the effect of adding a profile is limited. In the intermediate range adding a profile is beneficial. From the damaged lattice models it could be seen that for lower interface tensile strength the adjacent materials were activated sooner for a profiled interface compared to the smooth interface. The activation of the adjacent materials leads to an increase in load capacity. However, with increasing activation of the adjacent materials this increase reduces.

For indicating the effect of the profiled interface on the influence of the interface stiffness the purple dots in Figure 3.38b can best be investigated. It is seen that for both a smooth and a profiled interface a decrease in interface stiffness leads to an increase in stress. For the profiled interface the peak stress is always higher. With decreasing interface stiffness this difference increases, as a result of the profiled interface reaching higher strength faster. For both the smooth and the profiled interface a crack was formed in the concrete with lower interface stiffness. The main difference in the damaged lattice between the two cases was the number of elements of the adjacent materials that was activated. In case of a profiled interface more elements of the adjacent materials are activated.

3.6.4. Comparison with literature

A comparison is made between results from literature to indicate the correctness of the results and found trends. First a comparison is made with the results of Luković [37] as was done with the direct tension test. The direct shear test results are shown for different interface profiles in Figure 3.39a and 3.39b. For the smooth curve a similar shape is obtained. Comparing the profiles with the same height-to-width ratio of the notches as used in this thesis, profiles 1 and 4, the same softening can be obtained. The use of a profile will thus result in a more ductile behaviour compared to the brittle smooth interface.

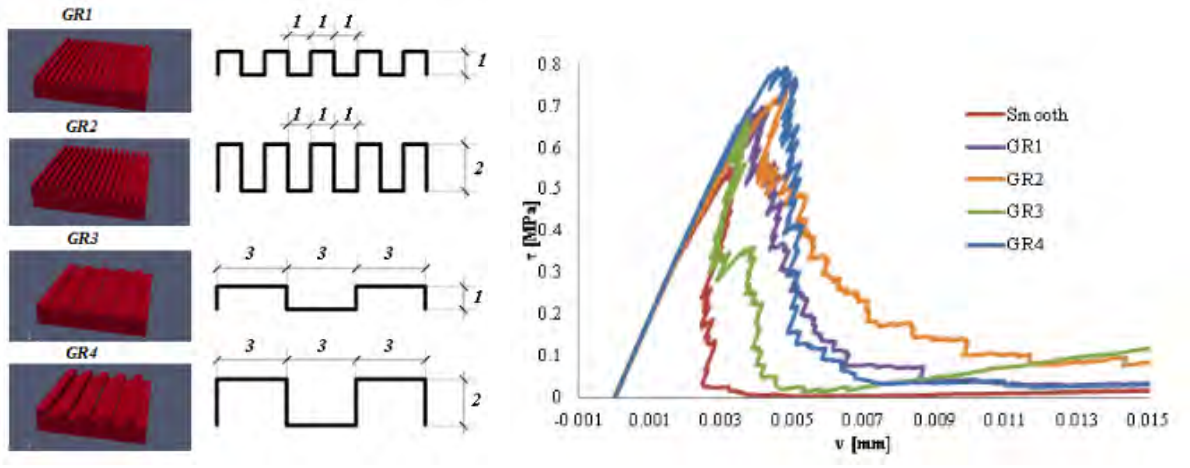

(a) (b)

Figure 3.39: Geometry of different profiles used for direct shear test (a) and accompanying stress-displacement curve (b), from [37].

When comparing the results to experimental testing from Stander [38] a difference between the results can be observed. Three interface roughness are investigated of which scraped, holed and grooved interface. The geometry of the grooved and holed interface were shown in Figure 3.22. The stress-strain curves for the smooth, holed and grooved interface are shown in Figures 3.40a, 3.40b and 3.40c respectively. The first thing to notice is the softening in the curve of the smooth interface. In this thesis and in the study of Luković [37] a more brittle behaviour was obtained. Luković states that this is because of the compression members becoming dominant. This was also seen in this thesis in the damaged lattice, where interface elements remain intact or failing last if they were loaded in compression. In the study of Luković a fully interface failure is obtained. Here in case of very low interface tensile strength, a fully interface failure is seen with a better softening. Still the softening is minor compared to the literature.

For both the grooved and holed interface increased softening is obtained in [38]. This behaviour is also found in this thesis. This indicates that a profiled interface causes increases softening. The maximum stress is, however, not increased in the experimental results, while an increase in stress was obtained in this thesis for most cases. Only for very low interface tensile strength or very high interface tensile strength the increase was negligible. This means that either the experiments had a very weak of very high interface strength or that the activation of the adjacent materials in this thesis are overestimated. Since no damaged images in the experiments of the shear results are shown for the profiled cases, this conclusion cannot be supported.

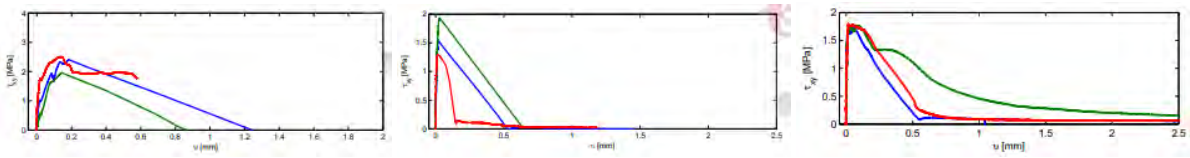

(a) (b) (c)

Figure 3.40: Stress-strain curve for smooth (a), holed (b) and grooved (c) interface under direct shear, from [38].

3.7. Conclusion

A conclusion will be given about the effect of the interface tensile strength, interface stiffness and adding a profile to the interface on the behaviour in small-scale tests. Also, the suitability of the small-scale tests will be discussed.

3.7.1. Influence of interface tensile strength

An increase in interface tensile strength leads in all cases to an increase in load capacity. The relation between the load capacity and the interface tensile strength could be defined as linear in most cases if interface failure occurs. For the direct tension test with a profiled interface this accounts for the first peak and for very low interface tensile strength, where interface failure occurs. For all tests count that after a certain threshold, the

adjacent materials are activated and the increase in load capacity is decreased. With the activation of the adjacent materials, the strength is still increased in all cases, but the effect of increasing the interface tensile strength is limited. This is because now the adjacent materials start to play a role in the failure mechanism and become governing for the peak stress.

For the direct tension test the fracture energy is measured. In case of a smooth interface the fracture energy showed a strong dependence on the interface tensile strength. The fracture energy increased almost two times if the interface tensile strength was doubled. In the profiled interface the increase in fracture energy with an increase in interface tensile strength was limited. In the profiled interface the increase in interface tensile strength showed limited influence on the softening part of the curve, since the second peak was mainly influenced by the activation of the adjacent materials. This also limits the effect of the interface tensile strength on the load capacity in most cases where the second peak was governing.

For the direct shear test with as smooth interface an increase in interface tensile strength reduced the softening when the adjacent members became activated. In the damaged lattice of the smooth and profiled test now a crack in the concrete was observed. For the profiled interface the tensile strength was found to influence the load capacity more compared to the smooth interface, expect for very high values, where the strength of the interface was too high and the adjacent materials were governing for the strength of the specimen.

3.7.2. Influence of interface stiffness

In general, a decrease in interface stiffness leads to an increase in the peak stress. This effect was, however, less strong compared to the increase in interface tensile strength. Also, for the direct tension test on a smooth interface the increase in strength was very limited. But, the effect on the softening of the curve was significant. An increase in interface stiffness leads to a more localized crack propagation. A lower interface stiffness showed scattered elements across the interface. Along with this increased softening an increase in fracture energy was obtained. For the profiled interface the effect of the increased interface stiffness was limited. The fracture energy increased slightly with a decreasing interface stiffness. The same strength was observed with the peak stress, which was the cause of the second peak. The first peak was influences most, with an increasing stress with decreasing interface stiffness.

For the direct shear test with a smooth interface the decreased interface stiffness leads to an increased activation of the adjacent materials. An increased contribution to the strength was found compared to the direct tension test. In case of the profiled interface an increased softening was obtained for lower interface stiffness. The softening came from the contribution of the adjacent materials. Also, for the shear tests the influence of the interface stiffness was less strong compared to the effect of the interface tensile strength.

3.7.3. Effect of a profiled interface

The effect of roughness is in general an increase of load capacity and ductility. In more cases of the direct tension test the concrete is involved in the failure mechanism, showing a horizontal crack at the top of the interface profile rather than following the interface. In tension it is seen that the roughness leads to a decrease in influence of the interface tensile strength, since the tensile strength only influenced the first peak. Only in case of a very low interface tensile strength, the load capacity was influenced. With very high interface properties the adjacent materials would govern the behaviour, limiting the effect of the profile.

For the direct shear test it was found that the profile increased the activation of the surrounding materials from already low interface properties. This leads to an increase in peak stress. Only for very low interface properties, where the failure would take place in the interface, the profile showed limited effect and also for very high interface properties the effect is limited. In the latter case, the adjacent materials were activated influencing the behaviour of the specimens. Looking at the effect of the stiffness a low stiffness resulted in higher stress for a profiled interface, compared to a smooth interface. This can again be attributed to the surrounding elements being activated.

In general, the profiled interface causes a more monolithic behaviour compared to a smooth interface. With increasing interface properties the adjacent materials become governing, reducing the effect of the interface.

3.7.4. Suitability of the test method

In this chapter the direct tension and direct shear test are used to investigate the effect of different interface properties on the interface and structural behaviour. This was investigated with the lattice model.

With the range of interface properties used both interface and partial failure with the adjacent materials were obtained. This means that the test method is suitable to obtain different failure mechanisms. The effect of changing the interface properties on the interface individually and on the complete specimen can be investigated. Trends were found on the effect of the interface properties and the addition of a profile on the interface and global behaviour.

With regard to the direct tension method, the results in terms of stress-crack opening were comparable to results found in literature, especially for the smooth interface. However, the fracture energy was underestimated. For the profiled interface the results showed a second peak in the stress-crack opening curve. This peak is obtained in literature, but is often lower compared to the first peak. This could be due to the model or due to the assigned interface properties. Also, it was seen from literature that the shape of the profile effects the shape of the second peak in both modelling and experiments.

For the direct shear method the smooth interface lacked softening of the stress-strain curve. This was the cause of interface elements loaded under compression. The ratio between the tensile strength and compressive strength was already lowered in this thesis compared to the actual ratio found in concrete. To calibrate the model the ratio was altered in this thesis to find a shear stress of two times the tensile strength for sample 1 (30% interface tensile strength and 100% stiffness). This is obtained with a ratio of 10, however, in the direct shear test, elements are breaking next to the support. This ratio and the applicability of the lattice model on the direct shear test is arguable. The effect of the different interface properties on the behaviour can still be investigated. However, with the increase in interface tensile strength, the interface compressive strength is increased as well and affects the behaviour. Also, the addition of a profile in the interface provided results comparable to experiments. This effect is, therefore, found suitable to investigate with the direct shear test and the lattice model.

The goal of this chapter was, however, not to calibrate the model to the actual behaviour found in literature. Although the found results might differ from literature on some aspects, the effect of the different interface properties and the addition of the profile can still be investigated. The found trends were comparable to literature.

4

Notched-beam test

In this chapter the model set-up of the notched-beam test with different interface preparations is described. A smooth interface and a profiled interface are modelled according to the experimental testing of Harrass [8]. A data set is generated from the simulation results using the information at the point of failure of the beams. The effect of the interface properties on the structural behaviour will be described, focusing on failure load, displacement, interface opening, joint opening, crack pattern and failure mode. A comparison with the results of [8] will be made to relate the modelling results to experimental results. A classification method is proposed to categorize the data based on the different failure modes. Within the different classes the data is discussed more in depth. Lastly, the suitability of the notched-beam test to investigate the effect of the interface behaviour is discussed.

4.1. Set-up of the model

Two notched beams are modelled, based on the experiments of Harrass [8]. A four-point bending set-up is used with a notch in the middle of the SHCC layer. A force-controlled analysis will be carried out. The test set-up of the experiments is shown in Figures 4.1 and 4.2 for smooth and profiled interface respectively. In the simulations the beam between the supports is modelled. In the simulations the beams have a length of 1700 mm and equal height and width as the experiments of 200 mm 150 mm respectively. Two beams were modelled: smooth interface and profiled interface. The beam with an epoxy resin interface from the experiments is not modelled explicitly. The test set-up of this beam is the same as for the smooth interface. The effect of the epoxy resin will be modelled by adjusting the interface properties of the beam with a smooth interface. The results of the experiments of both the smooth interface (reference beam) and epoxy resin interface will help compare the outcome of the simulations to the different interface preparations of the experiments.

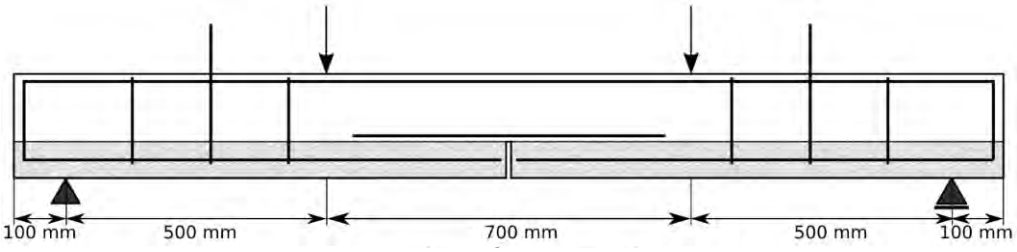

Figure 4.1: Experimental test set-up for smooth interface from [8].

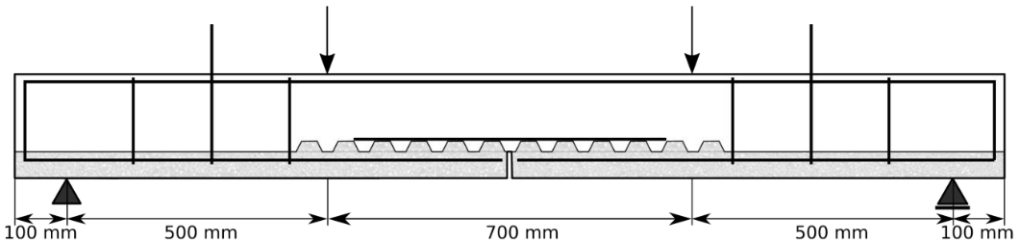

Figure 4.2: Experimental test set-up with profiled interface from [8].

The profiled interface will be modelled explicitly of which again the interface properties will be altered. Due to a profiled interface for macro-roughness, the SHCC layer will have a lower height over the length of the beam, with the profile on top in the middle section of the beam. Exact dimensions of the lay-out are not given in the thesis of Harrass [8]. But it is stated that the coupling reinforcement is on top of the profiled SHCC layer. It can also be seen that the SHCC layer is reduced in height compared to the reference beam with smooth interface and also the notch is reduced in height. The dimensions of the profile used in the experiments is shown in Figure 4.3a. In the model the slope cannot be modelled with the course mesh of 10 mm. Therefore, the profile will be modelled with straight edges leading to the dimensions shown in Figure 4.3b. With the top of the profile now being situated right under the coupling reinforcement, the height of the SHCC layer will be reduced to 60 mm.

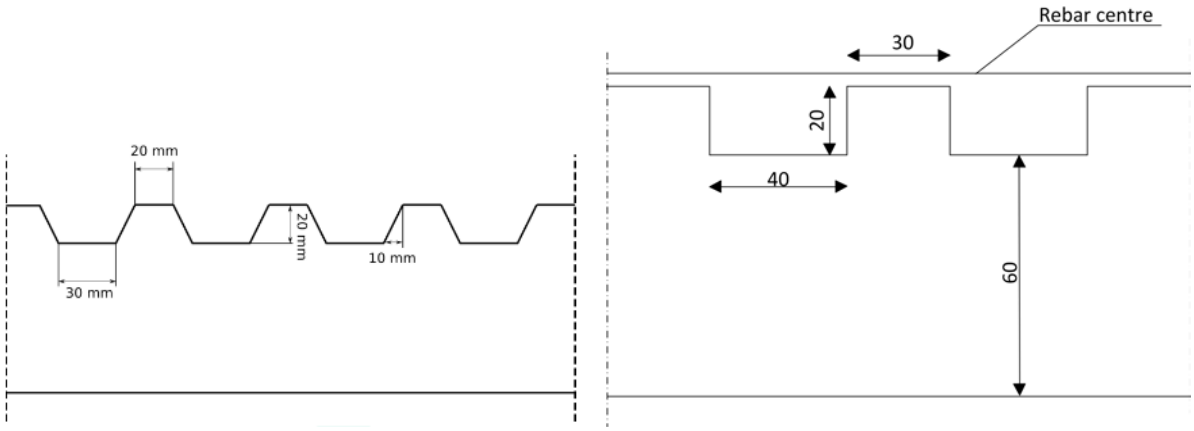

Figure 4.3: Dimensions profiled interface in experiments, from [8] (a) and in simulations (b).

All material properties are the same as used in the small-scale test, including the lattice element radius. This also means that the ratio between the input values for the tension and compression strength of the interface remains 10. Although now both tension and shear are present in the interface as described earlier in Section 2.3.3 and this ratio could be different in reality, the ratio remains unaltered for the notched beam tests. Determining the ratio for the notched beam test would require the knowledge on the exact stress state in the interface, which is not known. With the ratio of 10 the behaviour from the small-scale test can be used as a foundation for discussing the effects shown on the larger scale notched-beam test.

The rebars will be modelled with the same radius as used in the experiments, which is in all cases 4 mm. The material properties of regular reinforcement steel are used. Two segments are needed to describe the behaviour. The input values for the steel rebars are shown in Table 4.1, alongside with the segmentation on the stress-strain curve in Figure 4.4. The bond between the concrete/SHCC and the reinforcement is defined as proposed in [41].

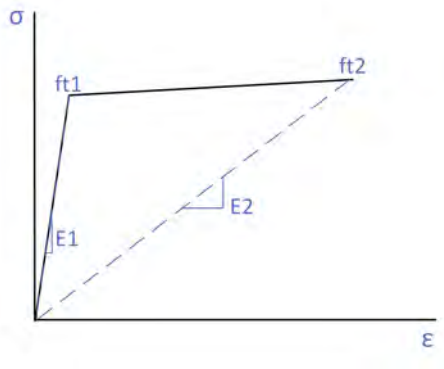

Figure 4.4: Segmentation of steel rebar material behaviour.

Table 4.1: Material properties steel rebar model input.

Segment	E-modulus (MPa)	Tensile strength (MPa)	Compression strength (MPa)
1	200000	500	-500
2	12000	550	-550

In the model inspection points are defined from which the deformation of the nodes is collected. The inspection points in the analysis are at the same position as the LVDT sensors (Linear Variable Differential Transformer) from the experiments of [8], which is shown in Figures 4.5 and 4.6. In the experiments one LVDT covers two points. This means that for one LVDT two inspection points are defined in the model.

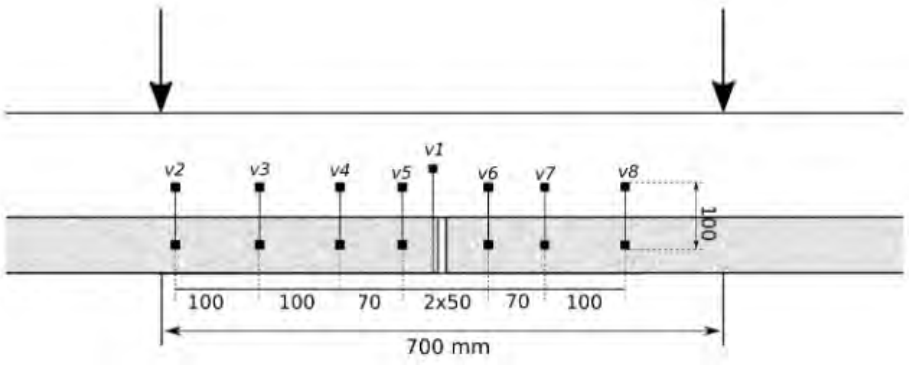

Figure 4.5: LVDT positions of experiments on the side, from [8].

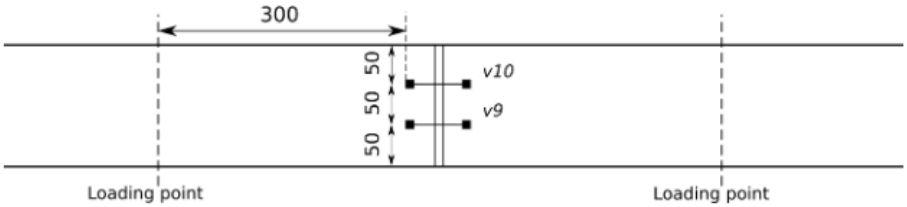

Figure 4.6: LVDT positions of experiments on the bottom, from [8].

For the beam deformation LVDT 1 is used, which is represented in the simulations with one single inspection point in the centre of the beam. The centre of the beam is located in the concrete. The joint opening is the opening of the notch, this is taken as the average of LVDT 9 and 10. Each LVDT is the difference between two inspection points on the same positions of the LVDT. For the interface opening the maximum of LVDT 5 or 6 is taken. In most cases one side will open and this side will be the side where the failure mechanism manifests. Therefore, only the maximum of the LVDT 5 or 6 is used.

4.2. Generating data set

From the simulations different data is gathered. The data is used to investigate the effect of the interface properties on the beam behaviour. In the next chapter the data is used to perform the regression analysis. The data sets containing the input and output information from the simulations can be found in Appendix C. Each beam simulation with different interface properties is numbered. A specific sample is referred to with a number, which corresponds to the sample numbers found in the data set. In the first collection of data there were 59 beam samples with the smooth surface and for the profiled surface 66 samples. These samples were used for classification and a first observation of the results. For the regression analysis extra data was added to provide a better fit of the model. This extra data is used in this chapter to compare the results with experiments and to investigate the effect of the interface properties.

For the regression analysis the interface properties are needed as input together with the beam behaviour as output. The material properties are an input of the model and will be known before the simulation is carried out. To gather information about the beam behaviour, it should first be defined when a simulation has reached failure and can be aborted. The simulation results at this point of failure will be used for determining the behaviour output of the simulation. Two criteria are set to define the point of failure. The first criterion to define the point of failure is based on a drop in the load-displacement envelope. The point of failure is the step after which a drop in force occurs in the envelope. The drop must be at least 25%. Meaning the step at the bottom of the drop has a load of less than 75% of the previous step on the envelope. This first case is seen in the case of beam 49 with a smooth interface of which the load-displacement curve is shown in Figure 4.7. In the load-displacement curve the point of failure is indicated together with point A. Point A indicates the point on the envelope closest to the point of failure of which the simulation provides a damaged model. This damaged model is shown in Figure 4.8.

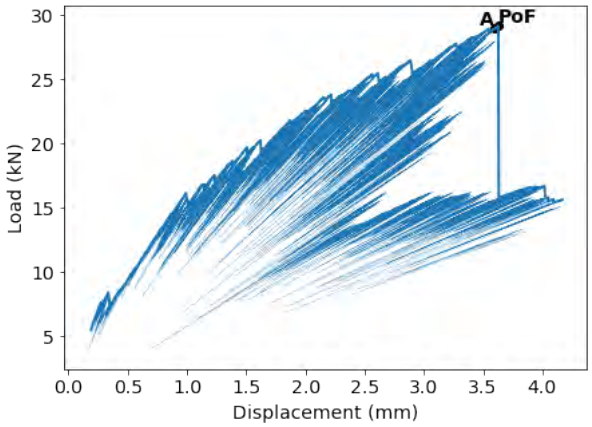

Figure 4.7: Load-displacement curve of beam sample 49 indicating point of failure (PoF) and damaged lattice output (A).

Figure 4.8: Damaged lattice model beam sample 49 showing partial failure. Deformation scaling factor x30. Red indicating intact elements, blue failed elements.

In some cases it requires a long computational time to obtain the drop in the envelope. This is because after the point of failure in most cases the displacement per step decreases in the analysis. Therefore, a second criterion is set to limit the computational time. This criterion stops the analysis if the last load value of the simulation is less than 10% of the last load value on the envelope. This criterion counts for the simulation of beam 17 with of smooth interface. The load-displacement curve of this simulation is shown in Figure 4.9. In the load-displacement curve the point of failure is indicated and point A of which the simulation provides the damaged model. From this point A the accompanying damaged model is shown in Figure 4.10.

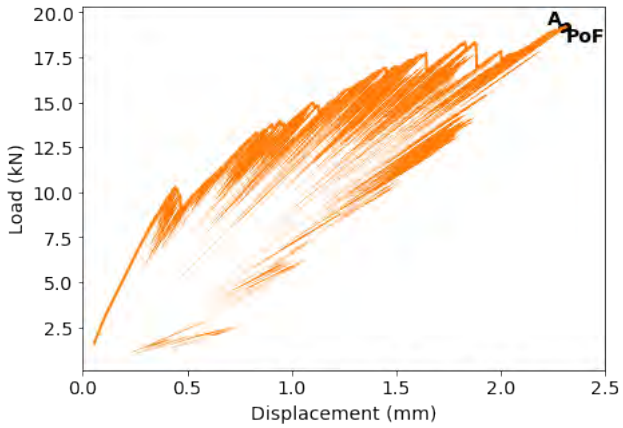

Figure 4.9: Load-displacement curve of beam sample 17 indicating point of failure (PoF) and damaged lattice output (A).

Figure 4.10: Damaged lattice model beam sample 17 showing interface failure. Deformation scaling factor x30. Red indicating intact elements, blue failed elements.

It can happen that a point of failure is set incorrectly. This can happen because for example the envelope drops in load at an earlier stage with 24% instead of with 25% of the criterion. This means that some errors are present in determining the point of failure. These can be altered manually or can be accepted.

For the cases with failure in concrete the point of failure is often more difficult to determine. These cases are not considered in the regression analysis, because the behaviour is governed by the concrete and not the interface properties. But the data of these simulations is still required to allow for classification. Therefore, the simulations where concrete failure is governing are aborted if the displacement has reached beyond 4 mm. Figure 4.11 shows the load-displacement curve of beam 34 with a smooth interface, in which a point of failure is difficult to determine and concrete failure is the governing failure mechanism. In the load-displacement curve point A is indicated of which the damaged lattice model is shown in Figure 4.12.

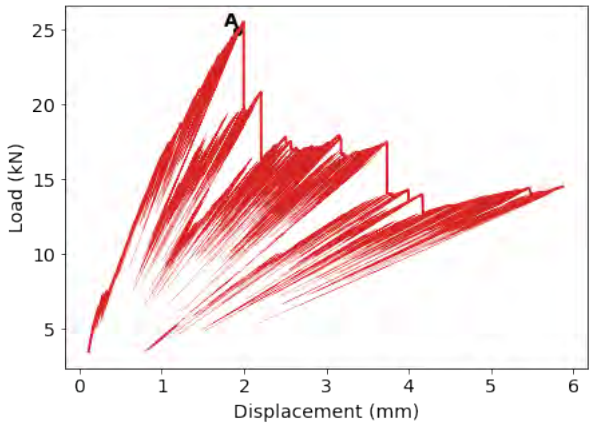

Figure 4.11: Load-displacement curve of beam sample 34 indicating damaged lattice output (A).

Figure 4.12: Damaged lattice output beam sample 34 showing concrete failure. Deformation scaling factor x30. Red indicating intact elements, blue failed elements.

At the point of failure, four values are retrieved from the simulation output. These are: the load, deformation, joint opening and interface opening. The deformation, joint opening and interface opening are defined using data from the inspection points as discussed earlier.

The Figures 4.7 to 4.12 above show the results for the beam simulations with a smooth interface. The beam simulations with a profiled interface can be divided into the same three failure modes. The figures below show for each failure mode a beam simulation output for the beams with a profiled interface. For each case the load-displacement curve is shown and the damaged lattice at the point closest to the point of failure. A brief comparison is given between the failure patterns of a smooth and profiled interface. It should be noted that these are just one example for each failure mode and the interface properties are not the same for both interface geometries.

Figures 4.13 and 4.14 show interface failure of a profiled interface. The damaged elements are located around the interface and even delamination can be seen outside the loading region. Vertical cracks move into the concrete. The same was found for interface failure in the smooth interface. Both the smooth and profiled interface show a sharp drop in load after the point of failure, indicating brittle failure.

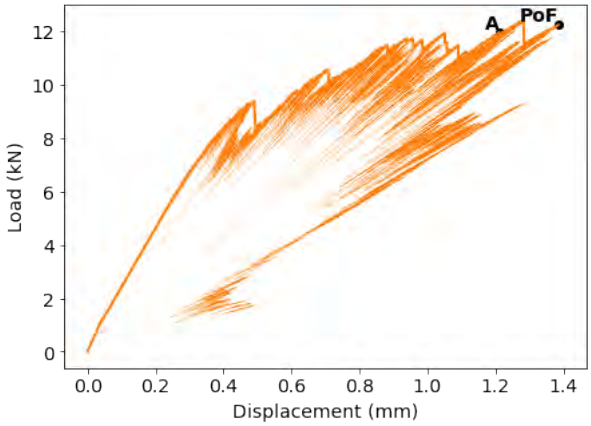

Figure 4.13: Load-displacement curve of beam sample 24 indicating point of failure (PoF) and damaged lattice output (A).

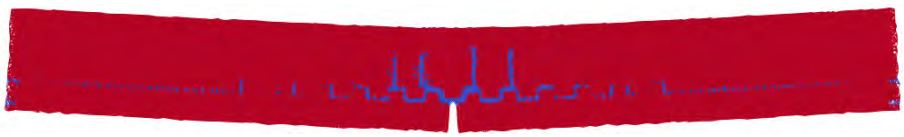

Figure 4.14: Damaged lattice output beam sample 24 showing interface failure. Deformation scaling factor x30. Red indicating intact elements, blue failed elements.

Figures 4.15 and 4.16 show the result for partial failure. With the partial failure damaged elements follow the profile less creating more connecting cracks on top of the profile through the concrete. In case of a smooth interface the connecting cracks cannot occur. In that case the vertical cracks through the concrete show additional cracks forming a triangle at the base of the vertical crack.

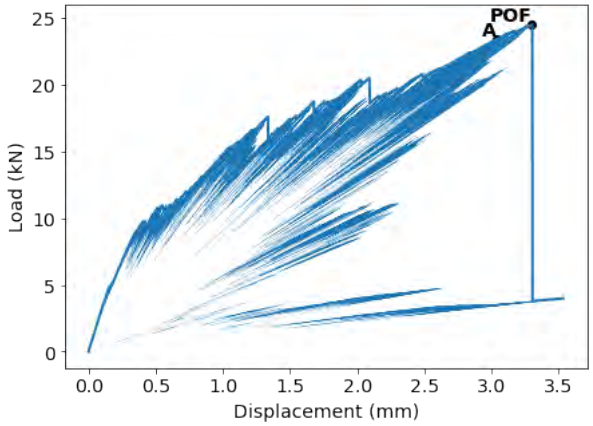

Figure 4.15: Load-displacement curve of beam sample 32 indicating point of failure (PoF) and damaged lattice output (A).

Figure 4.16: Damaged lattice output beam sample 32 showing partial failure. Deformation scaling factor x30. Red indicating intact elements, blue failed elements.

Figures 4.17 and 4.18 show the load-displacement curve and deformed damaged lattice of a beam with concrete failure. A vertical crack forms upward from the notch and moves sideways. On the right side move failed elements can be seen in the concrete on top of the profile. In case of the smooth interface only a vertical crack was seen with symmetry at the top. In general the concrete failure of the smooth interface showed less damaged around the interface compared to the profiled interface.

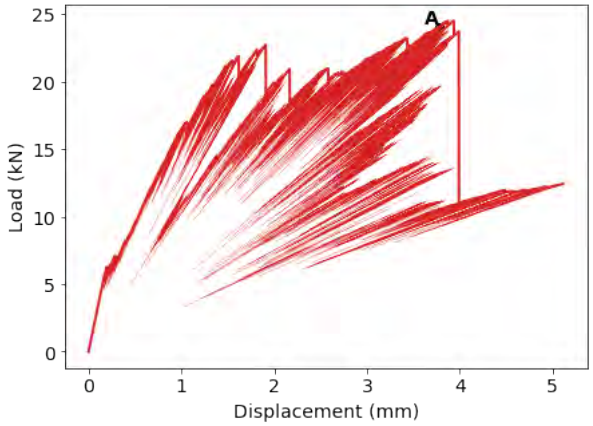

Figure 4.17: Load-displacement curve of beam sample 65 indicating damaged lattice output (A).

Figure 4.18: Deformed damaged lattice output beam sample 65 showing concrete failure. Deformation scaling factor x30. Red indicating intact elements, blue failed elements.

4.2.1. Simulation results

With the information at the point of failure of all curves a data set is created. This data set is presented in Appendix C. The complete data set will be shown to describe the effect of the interface properties on the interface and structural behaviour. Also, with this data the results closest to the experiments are indicated and compared to simulations. General trends are indicated. After the data is classified, the results will be investigated in depth.

Simulation results smooth interface

In Figures 4.19a to 4.19d the results for the smooth beams are shown in a scatter plot. The load, displacement, interface opening and joint opening at failure are plotted against the interface properties. The experimental results at point of failure for these output features are indicated with black lines for the epoxy resin and smooth interface case. Beams showing concrete failure often do not have a point of failure. Also, in concrete failure the interface is not governing. Therefore, the data for failure in concrete is left out.

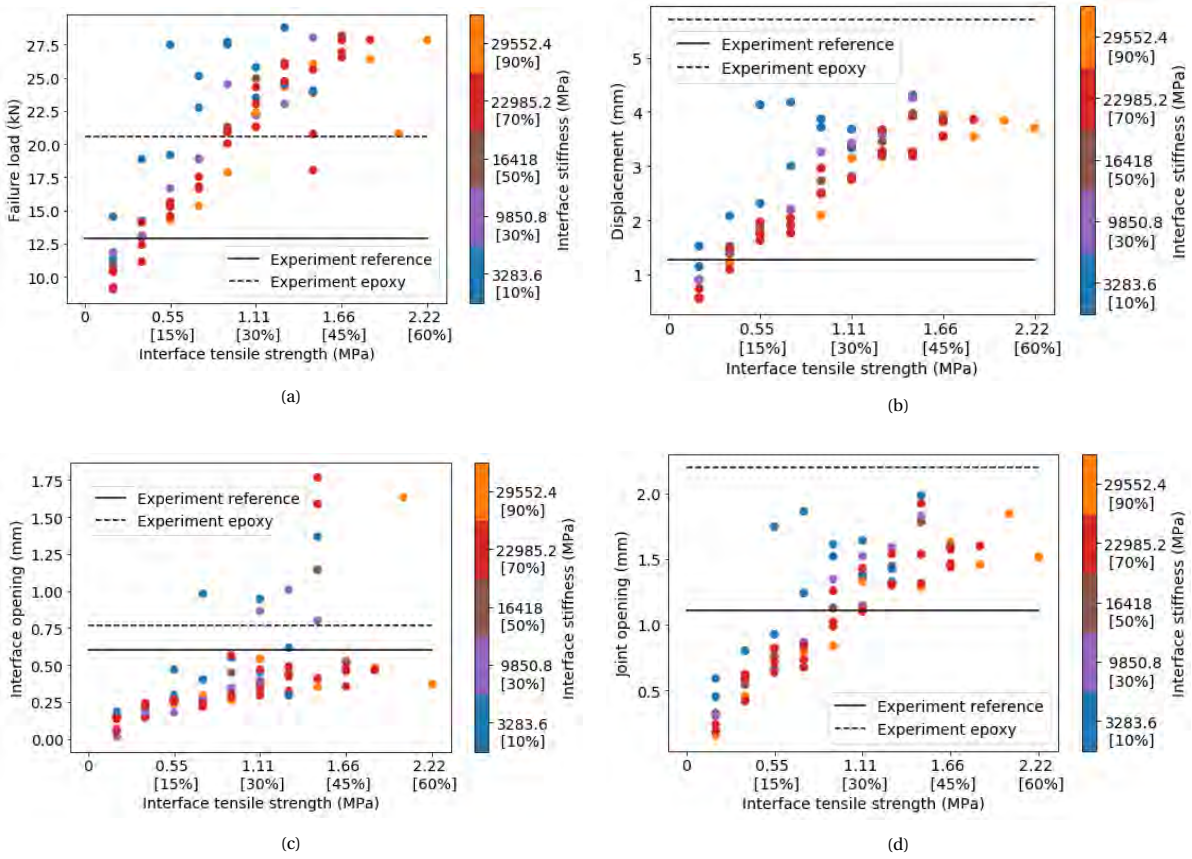

Figure 4.19: Simulation result smooth interface load (a), displacement (b), interface opening (c) and joint opening (d) at failure vs. interface tensile strength and stiffness.

The same relation between the interface properties and the different output values can be observed in all cases. An increase in interface tensile strength and a decrease in interface stiffness leads to an increase in the obtained simulation output variables. In the small-scale test the same was obtained for the maximum stress. For the interface opening this relation is less strong compared to the other output values. Also, more points outside the main cluster can be observed. This is because around failure the interface opening starts to open more rapidly in the simulations. The interface opening will, because of this, be more prone to deviations and scatter from the main cluster. The opening of the interface is a local behaviour, while the load and displacement are global behaviours. Locally more deviations in measuring and in behaviour are present. In Figure 4.19a three dots can be observed on the right side of the cluster with a considerably lower failure load than expected from the trend. Two of them cross the black line and the third is situated below these dots. This could be an example in which a wrong point of failure is assigned with the given criteria.

The values at the point of failure of the experiments are indicated with the black lines. Lines are used, since the interface properties are unknown. Both the experimental results for the reference beam and the beam with an epoxy layer at the interface are indicated. The reference beam is the same as the beams with a smooth interface as modelled in this thesis. This data is used to compare the simulations with the experiments after the results of the profiled interface are discussed.

Simulation results profiled interface

The same output is plotted against the interface properties for a profiled interface. Figures 4.20a to 4.20d show the results. The experimental results are shown with the solid black line.

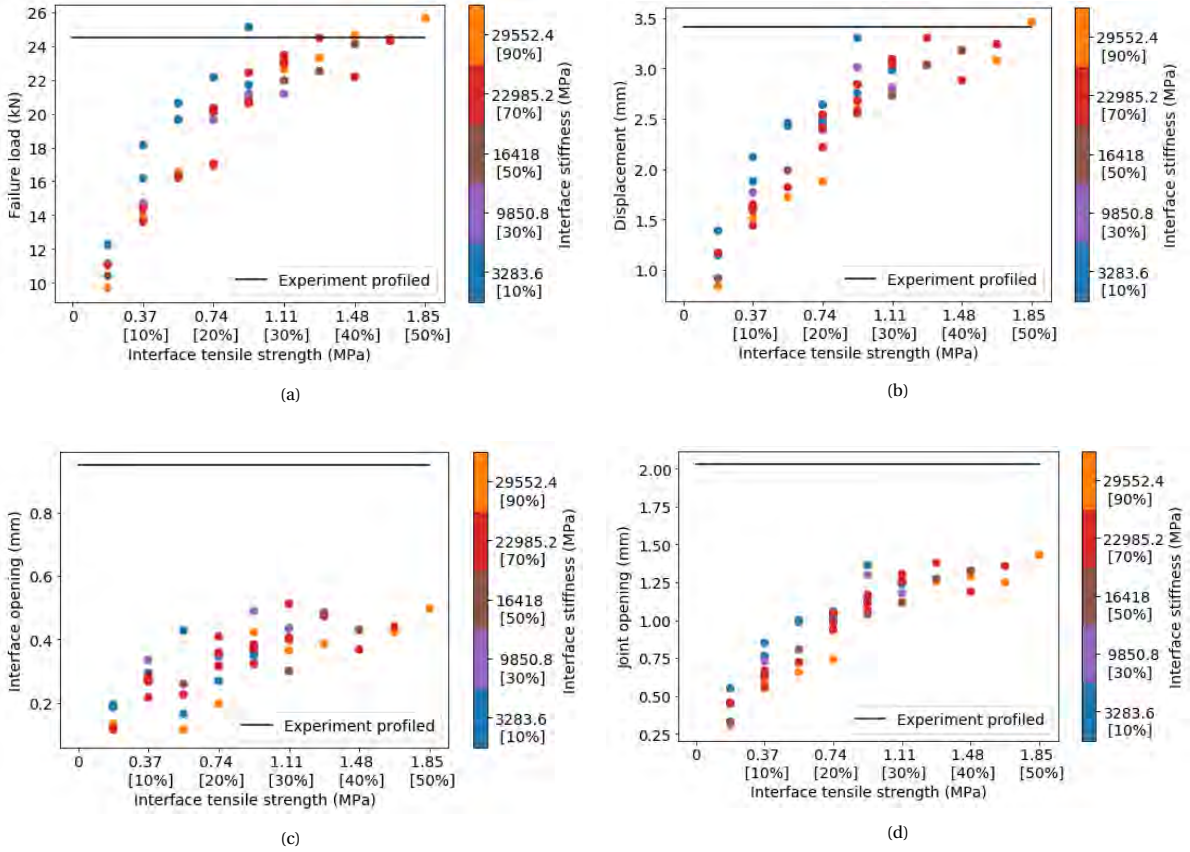

Figure 4.20: Simulation results profiled interface load (a), displacement (b), interface opening (c) and joint opening (d) at failure vs. interface tensile strength and stiffness.

Especially in the plot of Figure 4.20c it is difficult to define a trend. For the interface opening the blue dots, indicating a low interface stiffness, are situated in between the other coloured dots. This is again because of the behaviour being influenced too much by local aspects. For the failure load and displacement the blue dots are situated on top of the cluster.

The relation that can be observed between the different interface properties and output values is the same as with the smooth beams. Compared to the smooth beams, only the joint opening seems to have lower values with a profiled interface. For the other features the values are similar between the smooth and profiled interface. But the experimental results, indicated by the solid black line, shows higher failure load and displacement for the profiled interface compared to the smooth interface. The experimental values for the profiled interface are on the top of the cluster for the load and displacement. The interface and joint opening are much higher in the experiments. These values are not obtained in the simulations. The results of the simulations and the experiments are compared in depth in the next section.

4.2.2. Comparison with experiments

The suitability of the lattice model to simulate the notch-beam test is discussed by comparing the results between simulations and experiment. This is done using the data set and looking for similarity in failure load

and displacement. If agreement is found in load and displacement the crack propagation is compared as well. With this comparison a link between the interface properties in the simulation and the experimental results can be established.

Reference case smooth interface

In the reference case of the experiments there is close agreement with a case from the simulations. From the results in Figures 4.19a and 4.19b it is seen that multiple dots are crossed by the black lines. This indicates that there is no unique solution. Of the results the orange dot (sample 3) has the closest displacement to the experiments. In the load graph the dot is not visible, because it is covered with other data points of lower interface stiffness. The orange dot represents an interface tensile strength of 0.37 MPa, which is 10% of the concrete strength, and an interface stiffness equal to concrete of 32836 MPa. The interface and joint opening of the simulations with these interface properties do not match the experimental results.

Sample 3 is compared in depth to the experimental results. Figure 4.21 shows the load-displacement curves of both cases. It can be seen that the curves are close. Except for the structural behaviour, the crack pattern is also of interest. Figure 4.22a shows the cracks obtained in experiments for the reference case using digital image correlation (DIC). Different steps are shown with the accompanying points on the load-displacement curve shown in Figure 4.21. Figure 4.22b shows the crack width output of the corresponding beam from the simulations, sample 3. The cracks first start in the interface. On the side where failure occurs, three cracks can be seen in the concrete. The fourth crack causes failure in the experiments and the same happens in the simulation. Looking at the crack pattern and spacing it can be concluded that the behaviour of the simulations and experiments are equal.

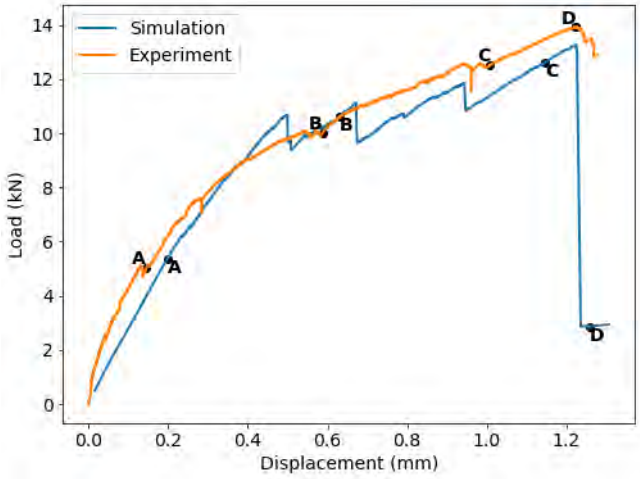

Figure 4.21: Load-displacement curve of smooth interface for experiment and simulation sample 3.

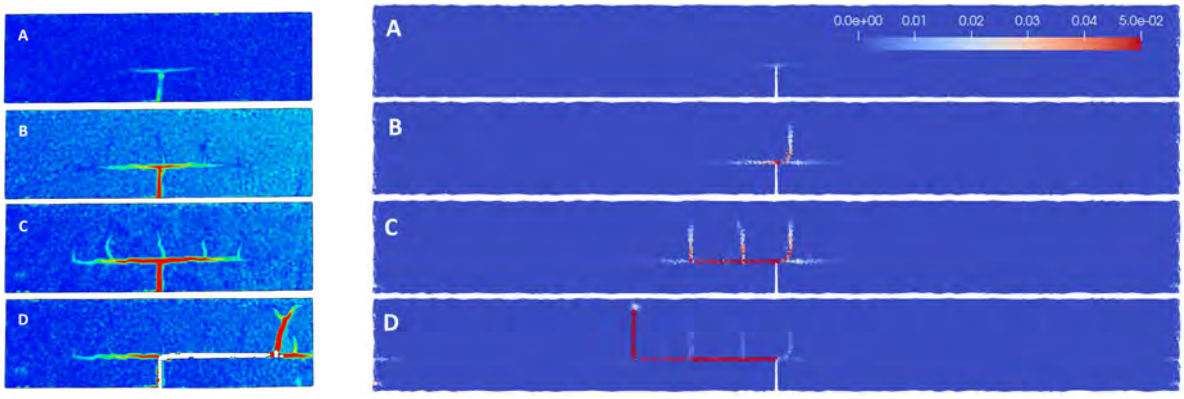

(a) (b)

Figure 4.22: Crack width for smooth interface of experiments using DIC, from [8] (a) and simulation sample 3 (b) for different loading stages (A-D).

Epoxy-resin interface

The beam with an epoxy layer is simulated by altering the interface properties of the smooth interface. In case of the displacement (Figure 4.19b) and the joint opening (Figure 4.19d) the epoxy layer has higher values in the experiments compared to the simulations. In case of the interface opening the experimental results also lay on top of the main cluster. The failure load in the experiment is around the average of the simulation results (Figure 4.19a). However, these cases do not show agreement in crack propagation. The crack pattern is checked for the beams with a smooth interface that have the maximum displacement, since the epoxy-resin results in higher ductility. Sample 78 shows the highest displacement. The load-displacement curve of this sample and the experimental results are shown in Figure 4.23. From this graph it can be seen that the load is overestimated, but the initial stiffness is the same.

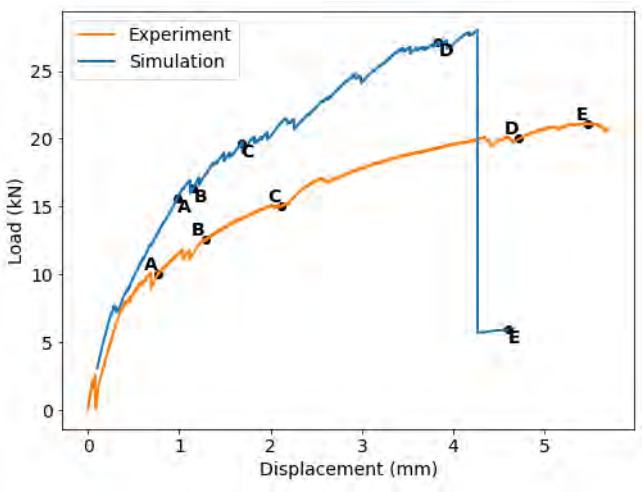

Figure 4.23: Load-displacement curve of epoxy-resin interface of experiment and simulation sample 78.

Figures 4.24a and 4.24b show the crack pattern for different loading stages for experiments and simulations respectively. It can be seen that the crack spacing is smaller in the lattice model compared to the experiments. However, the crack formation is similar. The first crack appears close to the notch. When the cracks propagate the cracks move to the concrete. The results are comparable, although not the same.

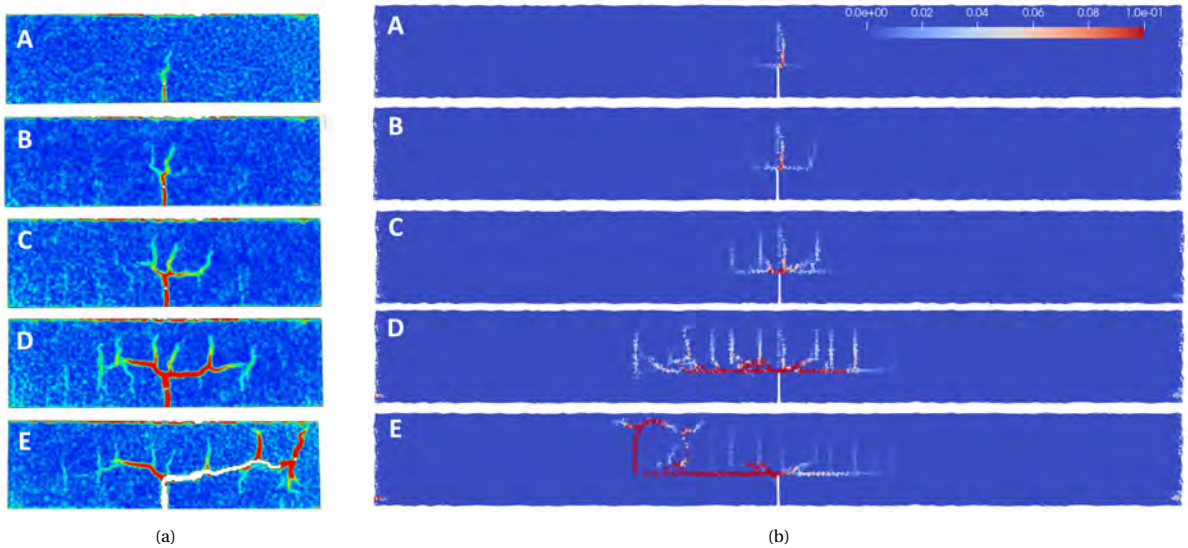

(a) (b)

Figure 4.24: Crack width for epoxy resin interface of experiments using DIC, from [8] (a) and simulation sample 78 (b) for different loading stages (A-D).

The reason why the load is overestimated in the simulations is because of the modelling of the SHCC. In [2] the SHCC was modelled and found to be overestimating the stiffness. For this to influence the results in the lattice model the SHCC should fail. To check this a zoom in on the loading of the final step is made with a different scale for the crack width range to observe the failed SHCC elements. This close-up is shown in Figure 4.25. More SHCC elements are coloured to white or even red, indicating crack widths in SHCC. Most SHCC elements are failed right below the interface. This indicates that these SHCC elements were part of the crack formation. Together with the modelling of the SHCC overestimating the stiffness this indicates why the load-displacement curve shows less ductility and higher failure load.

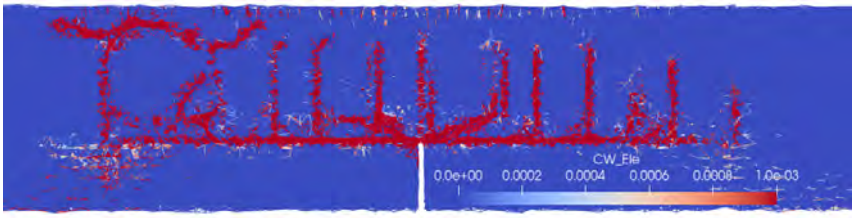

Figure 4.25: Close-up of loading region at failure showing crack width.

Profiled interface

Lastly, the results are compared for the beam with a profiled interface. For the interface and joint opening in Figures 4.20c and 4.20d, it can be observed that the experimental value is much higher compared to the simulation results. In case of the failure load and displacement (see Figures 4.20a and 4.20b) the top of the graph shares several points with the simulation results. A blue dot with a low interface stiffness and 25% interface tensile strength shows good agreement, but also a higher interface stiffness and tensile strength show two more dots close to the experimental results. The best fit has an interface tensile strength of 1.3 MPa, around 35% of concrete, and an interface stiffness of around 23000 MPa, 70% of concrete. This is sample 32. This is a good example of multiple interface properties resulting in somewhat the same structural behaviour in terms of failure load and displacement. There is no unique solution.

Figure 4.26 shows the load-displacement curves of both the experiment and the simulation of beam 32. It can be seen that next to the output values the shapes of the load-displacement graph are also close. This indicates good agreement already. Additionally, the crack propagation can be compared using Figure 4.27a and 4.27b.

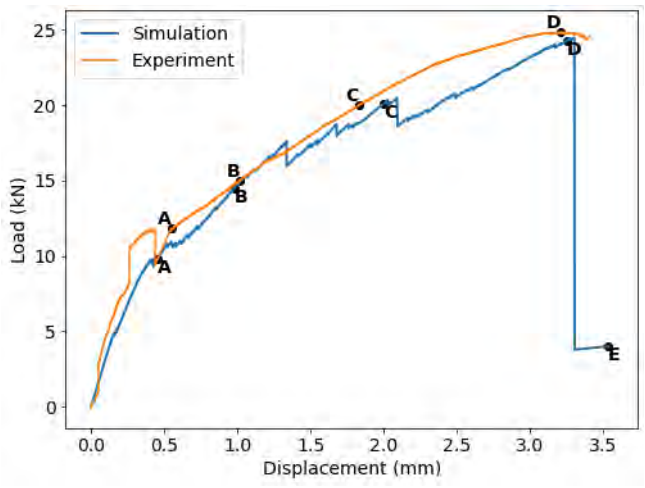

Figure 4.26: Load-displacement curve of profiled interface of experiment and simulation sample 32.

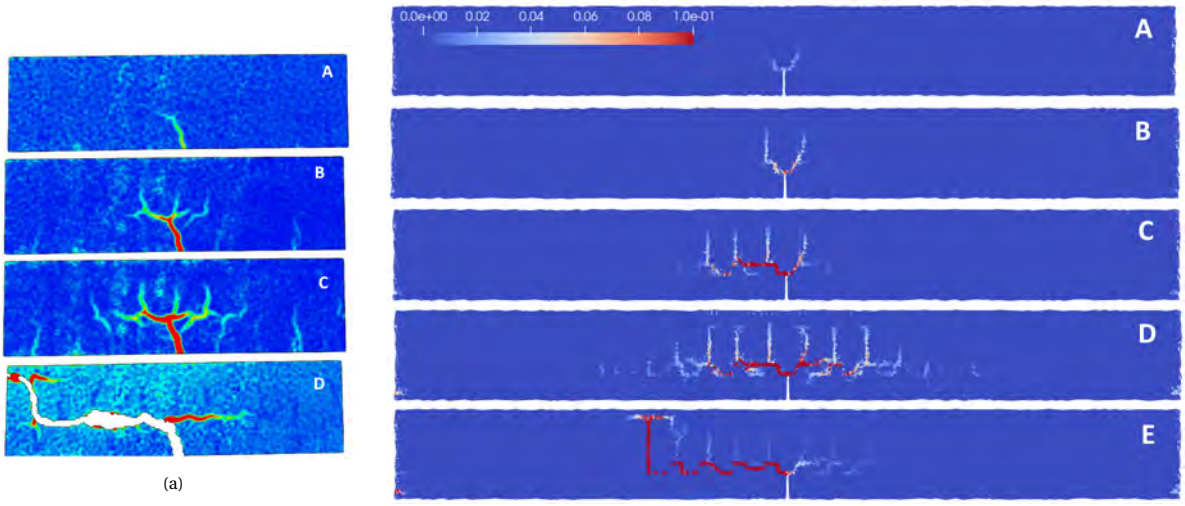

(a) (b)

Figure 4.27: Crack width for profiled interface of experiments using DIC, from [8] (a) and simulation sample 32 (b) for different loading stages (A-E).

In both the experiment and the lattice model cracks are formed. In the final step showing failure in Figure 4.27a a crack is shown on top of the concrete. In the beginning cracks are scattered around the profile. The crack moves to and ends with a vertical crack in the concrete. In the crack width propagation of beam 32 in Figure 4.27b the same is seen with a connecting crack on top of the first two profiles, following the profile afterwards and ending with a vertical crack through the concrete. Also, in this case the crack behaviour can thus be considered similar.

The interface properties for the profiled interface are different compared to the smooth interface. In the experiments there is no difference in interface preparation. It would, therefore, be expected that the same interface properties would lead to the correct crack propagation for each interface geometry. In the next section it is seen if there are simulations where this counts for.

Same interface properties smooth and profiled interface

In the simulated beams results it is investigated if there is a combination of interface properties that leads the crack pattern comparable to the experiments for both smooth and profiled interface. For interface properties of sample 21 with 10% interface tensile strength and 10% interface stiffness an agreement in crack propagation with experiments was found for both interface geometries. The load-displacement curves and crack width propagation are shown for the smooth interface in Figures 4.28 and 4.29 respectively. For the profiled interface these results are shown in Figures 4.30 and 4.31.

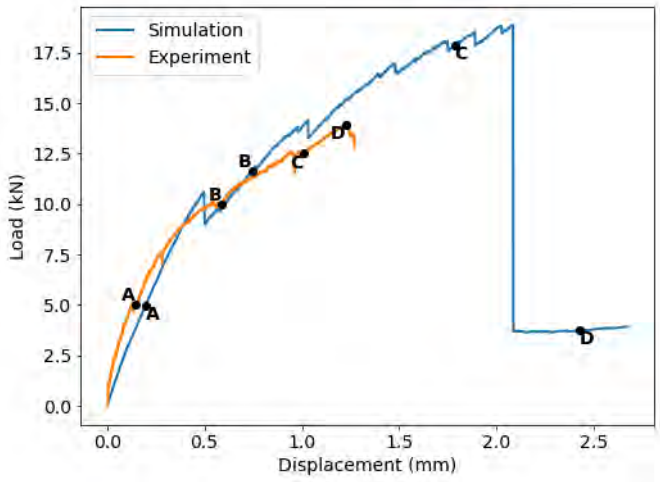

Figure 4.28: Load-displacement curve of smooth interface for experiments and simulation sample 21.

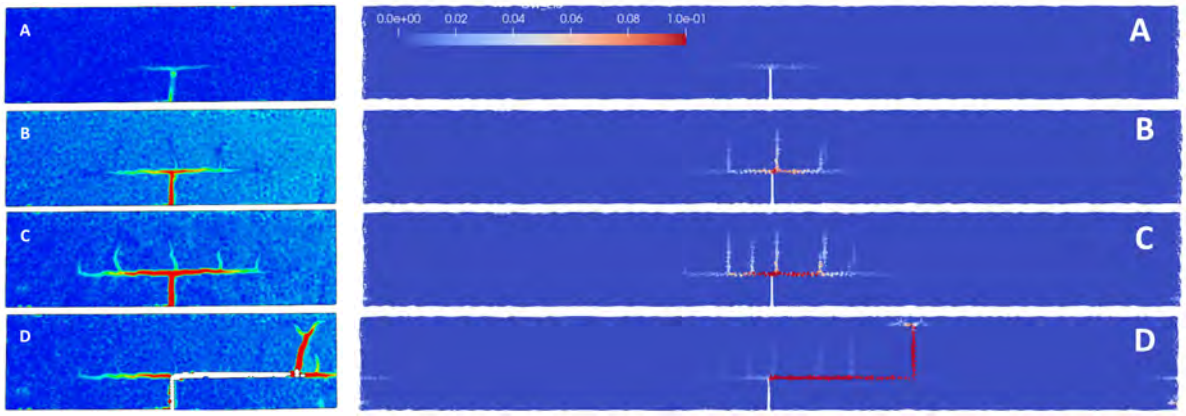

(a) (b)

Figure 4.29: Crack width for smooth interface of experiments using DIC, from [8] (a) and simulation sample 21 (b) for different loading stages (A-D).

It can be immediately observed that the load-displacement behaviour is not comparable. The simulation shows a larger load and displacement compared to the experiments. The load-displacement is of minor importance, because the goal is a comparison in crack propagation and failure mode. It can be seen that the crack propagation is similar to the experiments. The cracks start in the interface. Vertical cracks start to occur with equal crack spacing as seen in the experiments. In both cases at failure eventually a crack in the interface that ends in a vertical crack in the concrete is shown. The crack propagation is comparable.

The same comparison is made for the profiled interface for the beam with the same interface properties. The result of the beam with the same interface properties but a profiled interface is shown in Figures 4.30 and 4.31.

For the profiled interface the sample with the same interface properties now shows lower load and displacement values compared to the experiments. Around the same load capacity and displacement is obtained for the smooth and profiled interface. This indicated that the same interface properties can lead to different failure modes. But the addition of a profile does not lead to an increase in load capacity or ductility. However, the crack propagation is again of interest for this comparison. The steps A-D show good comparison between the experiments and the simulations. The cracks start at the notch, moving to through the interface. Next, vertical cracks are formed upward. The cracks continue from the interface through the concrete, connecting the top of the profiles. However, in the final step the cracks seem to have followed the interface only with a vertical crack through the concrete. The connecting cracks are still present, but are minor compared to the final vertical crack.

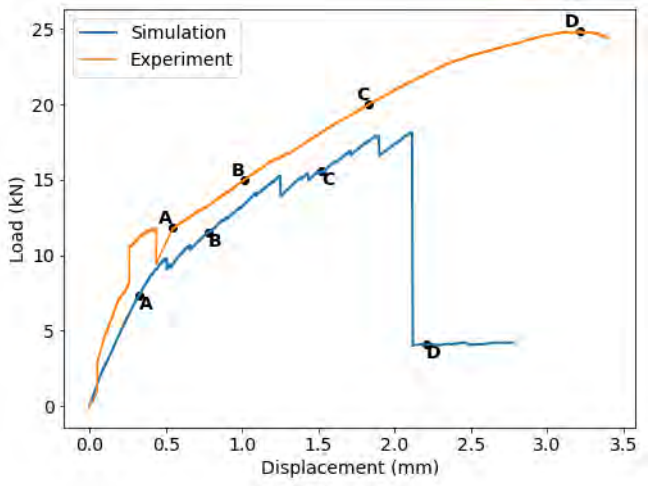

Figure 4.30: Load-displacement curve of profiled interface for experiments and simulation sample 21.

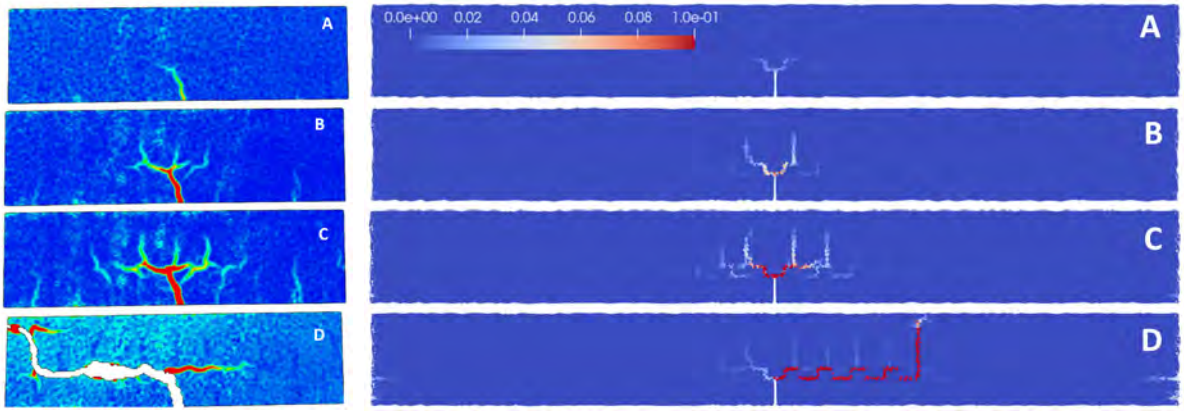

(a) (b)

Figure 4.31: Crack width for profiled interface of experiments using DIC, from [8] (a) and simulation sample 21 (b) for different loading stages (A-D).

The example shown indicates that there is a combination of interface properties that leads to the corresponding crack behaviour in experiments for smooth and profiled interface. The load-displacement is in those cases not comparable. The results can indicate two things. One is that the interface properties differ in reality in case of adding a profile. The other option is that the model cannot fully capture the real-life behaviour. Both options do not indicate that the model cannot be used for the purpose of this thesis. The model results will allow for investigating the effect of the interface properties on the structural behaviour of the notched-beam test.

4.3. Classification by failure mode

In this section the gathered data will be classified based on the failure mode of the simulations. This is needed to carry out the regression analysis within each class. The regression analysis will provide the best fit if the results from the same failure mode are used for the regression. If all data will be put together, the regression will try to fit for all different failure mechanisms. The effect of the interface properties within each failure mode can be investigated. Therefore, the boundaries between the failure mechanisms will be determined before the regression analysis is carried out. Three failure modes can be distinguished: interface failure, concrete failure and partial failure. In case of partial failure, both interface and concrete are part of the failing mechanism. Three methods are used to assign the failure modes to each sample. One supervised classification method is used and two unsupervised classification methods: k-means and time series. The most suitable method shows the least amount of misclassification. The three methods will be discussed and explained for the beams with a smooth interface first. After this the methods will be used for the beams with a profiled interface. Lastly, the applicability of the methods is discussed.

4.3.1. Method I: supervised classification

Each simulation will return information about the damaged elements. The damaged elements within the loading region will be counted per material until the point of failure and will be divided by the total number of elements per material in the same loading region. With these ratios the beams will be put into categories of failure modes. Next to these ratios the damaged lattice model is checked. From the damaged model output a note is made about what visually the failure mode is. A manual classification is made by sorting the data based on the ratios for different element tags. Eventually sorting the data based on the coupling rebar bond was found to suit the data most. The lowest ratios of damaged coupling ratio bond indicate an interface failure. The boundary between interface failure and partial failure and the boundary for partial and concrete failure is set by checking the visual output of the model. The boundary is set if the visual output of the model with the damaged elements between two simulations shows a different failure mode. In this method misclassification can be present if the boundary is set incorrectly. This can happen if the model is visually interpreted incorrectly or the sorting does not show a distinct difference between the different failure modes. Because the total number of damaged elements is used one more uncertainty arises. The point of failure indicates the end point of the simulation and thus the point until where the damaged elements are counted. A mistake in point of failure will influence the total number of damaged elements.

Results

Figure 4.32 shows the results of the supervised classification method for the beams with a smooth interface. On the axes the interface properties are stated. In addition, the sample numbers are indicated. The data was sorted based on the ratio of damaged coupling rebar bond to the total number of coupling rebar bond elements. Each colours represents a class.

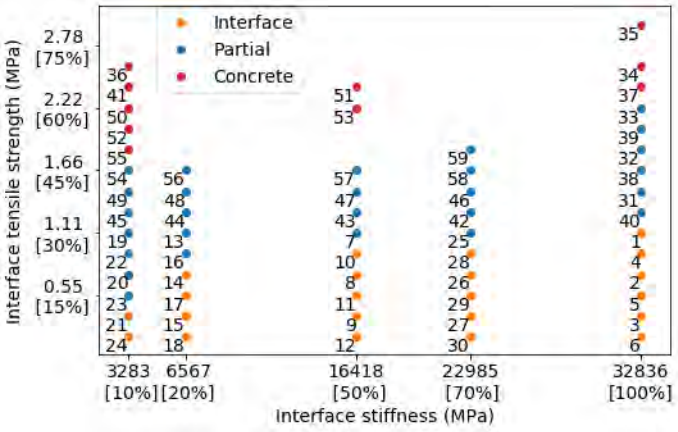

Figure 4.32: Results of supervised classification method for beams with a smooth interface. Numbers indicating sample number.

The beams are clustered well, meaning that the beams are grouped nicely. The colours are well separated. The only uncertainty is if the boundaries are correct.

Figure 4.33 shows the results of the supervised classification method for the beams with a profiled interface. The data was also sorted based on the ratio of damaged coupling rebar bond to the total number of coupling rebar bond elements.

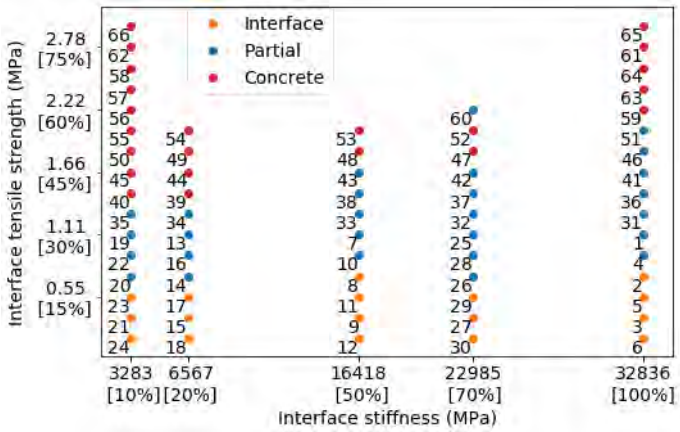

Figure 4.33: Results of supervised classification method for beams with a profiled interface. Numbers indicating sample number.

The beams are clustered less accurately with this method compared to the beams with a smooth interface. Beam 60 is for example coloured blue, while the dot is situated in the red area. Beam 60 was in the sorted data not next to the boundary, meaning the misclassification comes from setting the boundary incorrectly. The problem with the data is that a snapshot is taken at the point of failure and is difficult to classify. Also, beam 8 seems to be out of the trend. Looking at the sorting, it was seen that this beam was on the boundary between the interface and partial failure. The beams on the boundary between partial failure and concrete failure were also more difficult to visually interpret, since the visual output shows small differences for the boundary cases. This indicates that the unsupervised method is less suitable for this case.

4.3.2. Method II: unsupervised classification using k-means

The first unsupervised clustering method is carried out using the Python package sklearn. Clustering is possible, since the number of clusters the data needs to be divided in, is known. The three failure modes represent one cluster each. The clustering method is k-means. In the Python function used, the Lloyd algorithm [42] is set by default, which will be used here to explain the process of k-means algorithm. In the k-means algorithm the data is clustered in the previous set number of clusters. The goal of the algorithm is to minimize the sum of distances from the cluster centre to the data points. The algorithm is as followed:

- K cluster centres are chosen $C = \{c_1, c_2, ...c_k\}$.
- Each data point is assigned to the cluster which is closest in distance.
- Set the new cluster centre to be the centre of mass of all points assigned to that cluster $c_i = \frac{1}{|C_i|} \sum_{x \in C_i} x$.
- Iterations stop if the clusters no longer change.

The position of the cluster centres is searched for in the algorithm. The algorithm starts with choosing k cluster centres. In the Python package this is done using the k-means++ method as described in [43]. In this algorithm the first cluster centre is taken randomly from the data set. The next centre is chosen, but in this case the probability function from Equation 4.1 is added. This indicates that data points with a large distance from the present centres have a higher probability of becoming a centre. After all centres have been defined with this algorithm the standard algorithm is continued with.

$$p = \frac{D(x)^2}{\sum_{x \in X} D(x)^2} \tag{4.1}$$

With $D(x)$ the shortest distance from a data point to the closest centre that is already present.

Here, three dimensions were chosen to carry out the cluster algorithm described above. The deformation, the ratio of damaged interface elements and the ratio of damaged coupling rebar bond elements.

Results

In Figure 4.34 the result of the k-means classification is shown for the beams with a smooth interface. On the axis the interface properties are stated. The clustering was carried out using the displacement, total damaged interface ratio and total damaged coupling rebar bond ratio at the point of failure.

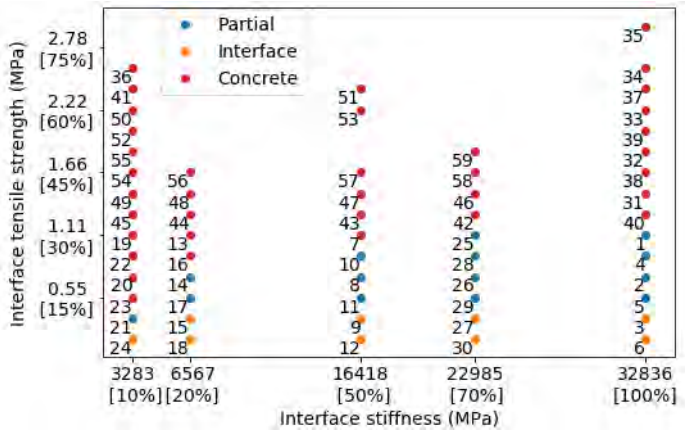

Figure 4.34: Results of unsupervised classification method k-means for beams with a smooth interface. Numbers indicating sample number.

From the results it can be seen that different failure modes are clustered well, since the different colours are grouped. The concrete cluster is, however, the largest and does contain beams that do not have concrete as a governing failure mechanism. Also, beam 21 is for example categorized as partial failure in this method. This beam shows interface failure in the final damaged model of the simulation after failure. This means that the boundaries of the cluster are most likely incorrect and the method cannot be considered as accurate.

Figure 4.35 shows the result of the k-means classification for the beams with a profiled interface. The results are shown using the sample information. The clustering was carried out using the deformation, total damaged interface ratio and total damaged coupling rebar bond ratio at the point of failure.

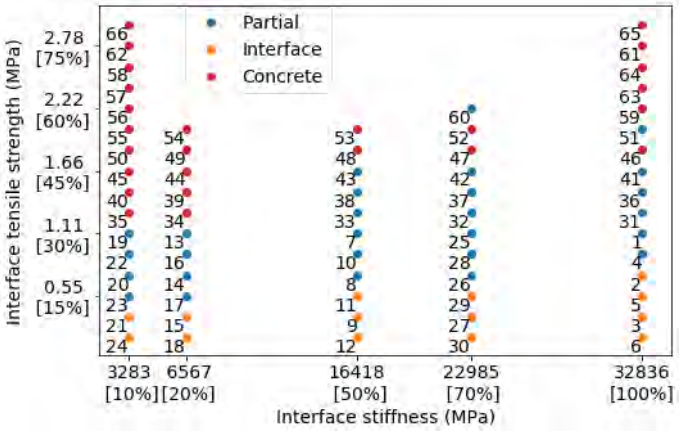

Figure 4.35: Results of unsupervised classification method k-means for beams with a profiled interface. Numbers indicating sample number.

The clustering shows incorrect clustering of beam 60 and 51. Beam 60 was also misclassified using the supervised sorting. This means that the data implies a classification in partial failure. This is because the failure of this sample happens at a lower displacement compared to sample with similar interface input values. The reduced capacity also leads to a lower number of failed elements at the point of failure than expected for the interface properties.

4.3.3. Method III: unsupervised classification using time series

In the second unsupervised classification method time series is used. In this method the development of the damaged element per material over time is used. Instead of time, displacement is used. For each beam simulation this data is collected. In time series normally equal time steps are present in the data. Here the information from the points on the envelope of the load-displacement curves are used. This means that for each beam the total number of data points is different and thus the length of each beam data differs from the other beams. The Python package tslearn [44] is used to apply k-means time series clustering using dynamic time warping. This method consists of two phases:

- Dynamic time warping to find similarity in shape.
- Finding cluster centroids by using dynamic time warping barycentre averaging (DBA).

Because each beam data has a different length, dynamic time warping is used as the similarity measure between time series. At the end of this process time series with similar shape are clustered. In dynamic time warping the warping path is minimized. In formula form this is as follows:

$$D = min \sqrt{\sum_{k=1}^{K} d_{wk}} \tag{4.2}$$

With K the length of the warping path and d_{wk} is the distance of the k^{th} element of the warping path. This distance is the square of the distance between the data points which form the element of the warping path.

For each data point in the times series the distance to the closest points of the other time series data set is calculated. This process is indicated in Figure 4.36. The warping path minimizes the sum of the total warping distance by choosing which points connect to obtain the lowest total warping distance. It could be possible that multiple warping paths are obtained if there are multiple paths that have the same warping length.

By determining the distance between data points it can be the case that in a time series two points are closest to one point of the other time series data. This is allowed in the dynamic time warping method. This happens in Figure 4.36 at the beginning and at the end of the time series. In this method all points need to

have at least one connecting point with the other time series. The data points forming the distance of the warping path is thus the minimum distance and does not need to have the same index of the data. This allows the time series data sets to have different length.

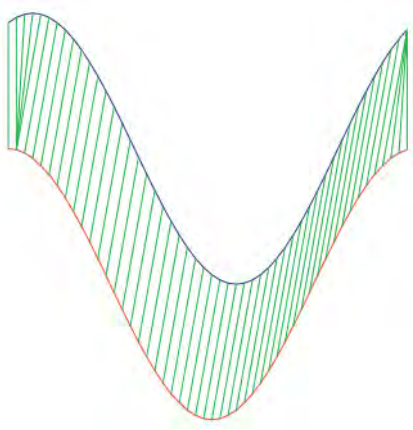

Figure 4.36: DTW between two time series, retrieved from [45].

The second part of the method is an iterative process to find the cluster centres. The cluster centre is a time series as well. The cluster centre is calculated by averaging all the members. The method used in the tslearn package is DTW barycentre averaging (DBA). In this method the averaging of the time series leads to minimized warping paths between the average and the individual time series [45]. The data points of the individual time series contribute to the average. With dynamic time warping it was seen that one data point of one time series can be connected to multiple data points of the other time series. Due to this it is possible that multiple data points of one time series contribute to one point on the averaged time series. When multiple points are involved, the average is determined by defining the centre of mass, also called the barycentre. This part coincides with the k-means algorithm. Since the centre of mass differs and leads to different warping paths each time, an iterative process is needed to find the average with the minimum warping path to the individual time series. This process is indicated in Figure 4.37.

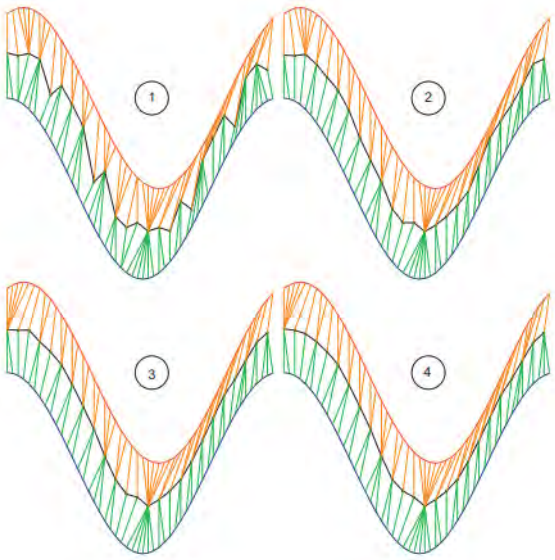

Figure 4.37: DBA iteration process between two time series, retrieved from [45].

For the smooth beams the ratio of the coupling rebar bond and the interface over the displacement are used. In Figure 4.38a the coupling rebar bond ratio over displacement is shown for all beams with a smooth inter-

face. All data together does not provide insight in how to classify the data. But in the figure next to it, the plot is shown using the supervised classification results. Now it is visible that beams with interface failure reach lower damaged coupling ratios compared to beams failing in concrete or partially in concrete and at a lower displacement. For partial and concrete failure the final values are overlapping, making it difficult to separate the data based on this criterion. This indicates that it is difficult to set the boundary correctly in the supervised and k-means method.

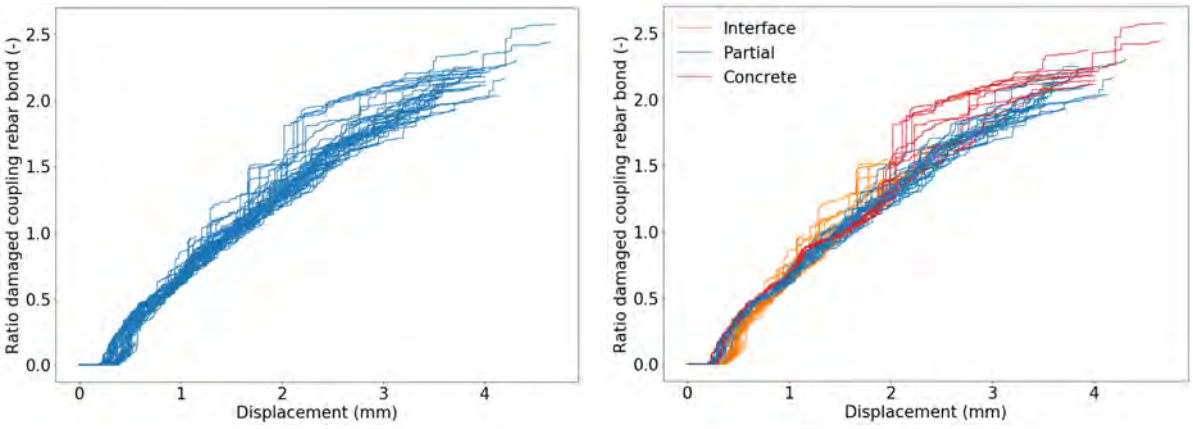

(a) (b)

Figure 4.38: Ratio damaged coupling rebar bond vs. displacement for unclassified (a) and classified (b) beams with smooth interface.

Figures 4.39a and 4.39b show the ratio of damaged interface elements over the displacement for all beams without and with using the supervised classification results respectively. From this graph it can be seen that the data of the beams is more spread out, which might make it easier to distinguish the different beam information. However, from the supervised classification it can be seen that the boundaries are not yet clear, which could indicate that the supervised classification is not completely accurate and improvements can be made, or that multiple aspects play a role in determining the failure mode. Since one time series does not distinguish the failure modes, multiple data is used.

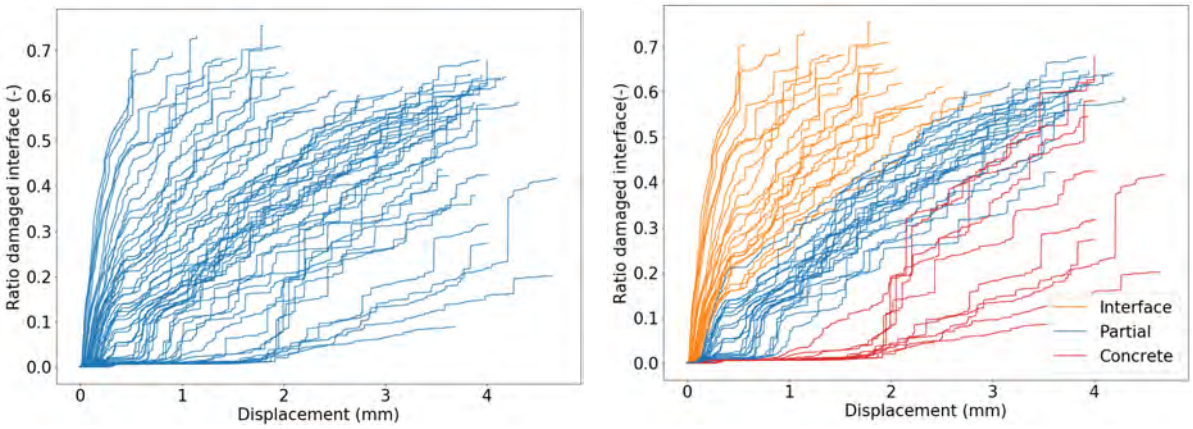

(a) (b)

Figure 4.39: Ratio damaged interface vs. displacement for unclassified (a) and classified (b) beams with smooth interface.

The same time series are used for clustering the beams with a profiled interface. Figures 4.40a and 4.40b show the time series with the ratio of damaged interface elements over the displacement and the ratio of damaged coupling rebar bond elements over the displacement respectively. The classification used is from sorting data with the supervised classification method. In both cases overlapping clusters are found, therefore, both series are used.

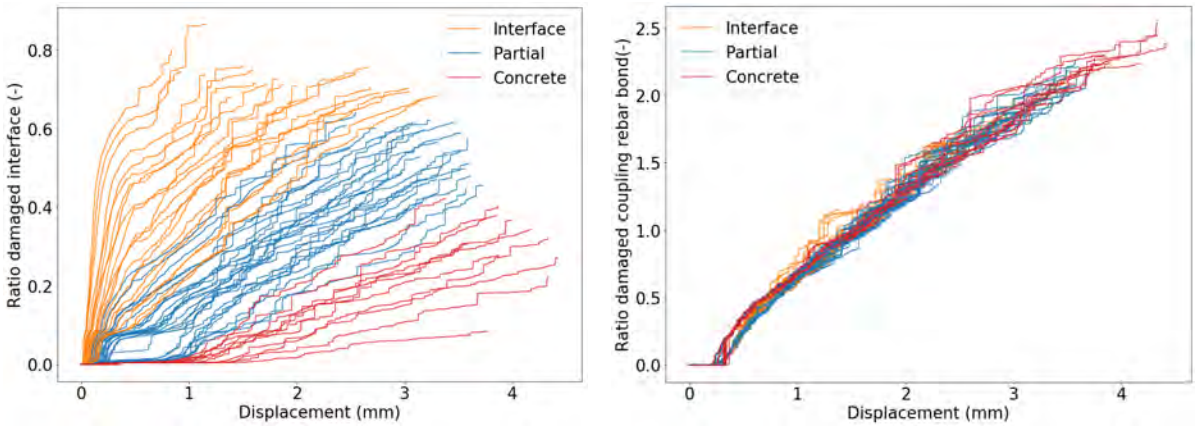

(a) (b)

Figure 4.40: Ratio damaged interface elements (a) and ratio damaged coupling rebar bond elements (b) vs. displacement for beams with profiled interface.

The data needs to be post-processed differently. The time series data needs to be arranged in three dimensional matrices for each beam to use the tslearn package in Python for clustering time series. More dimensions can be added, however, more dimensions require more computational time. Because of this reason the dimensions are limited to three. It can be checked by using different dimensions if the same clustering is obtained. After arranging the data the clustering method can be carried out. In the next sections the results are shown and discussed.

Results

The classification was carried out using the time series for the interface and coupling rebar bond with time being the displacement. Carrying out the time series clustering, a few things were noticed. Each time the outcome was slightly different in terms of number of iterations needed. Also, the classification of samples on the cluster boundaries changed. In case of the beams with a smooth interface the beams with sample number 1, 45 and 49 were classified differently in each case. These are at the boundary between failure modes. Therefore, it is recommended to check these samples manually.

A check was carried out by using the concrete time series instead of the coupling rebar bond data. In that case also beam with sample number 10 was sometimes classified differently. The final classification based on the time series clustering is shown in Figure 4.41 for a smooth interface. For a profiled interface the results are shown in Figure 4.42.

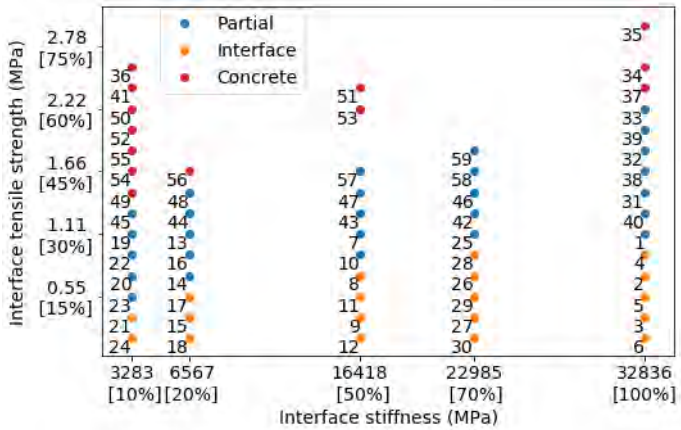

Figure 4.41: Results of unsupervised classification method time series clustering for beams with a smooth interface. Numbers indicating sample number.

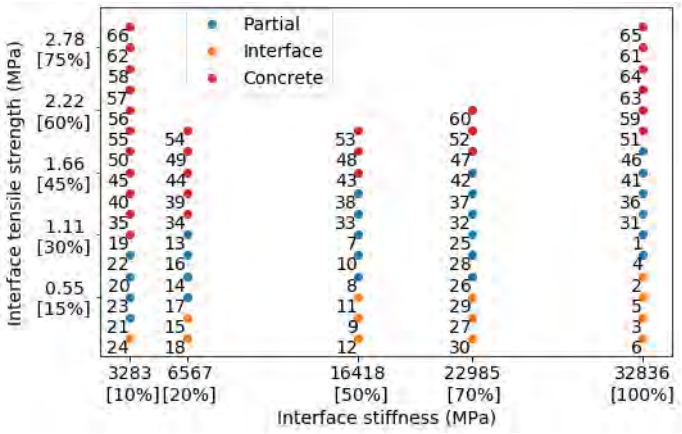

Figure 4.42: Results of unsupervised classification method time series clustering for beams with a profiled interface. Numbers indicating sample number.

For both interfaces the data is clustered well. It can be observed that for the profiled interface the interface class is small, which was predicted by the k-means method as well. In general, the partial failure and concrete failure occur at lower interface properties compared to the beams with a smooth interface. Beam sample number 21 was sometimes classified as interface failure, and sometimes as partial failure. It was more often classified as partial, also when checking the clustering with the concrete time series, this was the case. Since beam 60 and 51 are now clustered correctly, the time-series clustering result is used over the supervised method.

The time series classification is proposed to use for clustering the notched-beam test results into the different failure modes. This result is chosen over the supervised result, because for the smooth interface the main difference in classification is at the boundary. However, for the profiled interface the method shows better results in classification outside the boundaries as well. While the supervised classification method uses the data at failure only, the time series uses the information over time. This takes uncertainties in defining the point of failure away. Therefore, the time-series method will be used for both cases.

Using the classification results found above, the load-displacement curves of all beams for respectively the beams with a smooth and with a profiled interface are shown in Figures 4.43a and 4.43b. From these graphs the difference in load capacity and ductility between the different failure modes can be observed. Also, the difference in load capacity and ductility between smooth and profiled interfaces can be discussed.

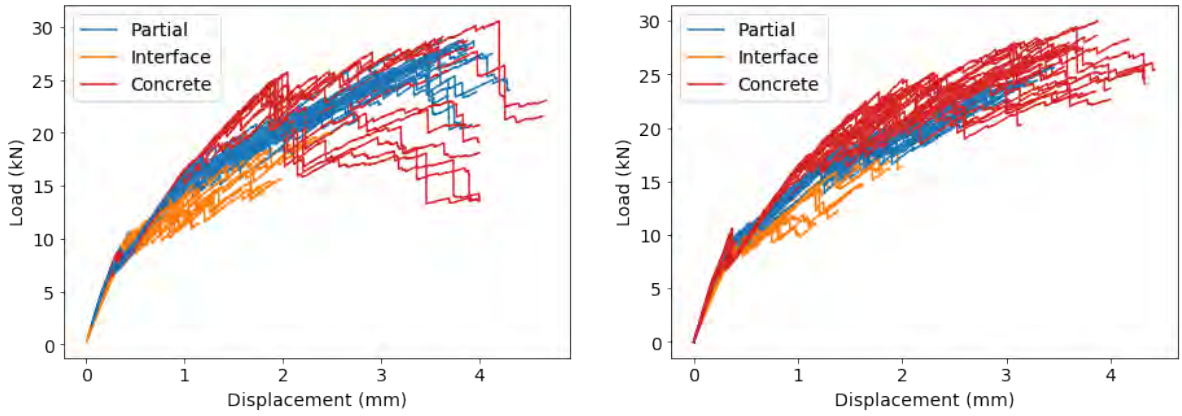

Figure 4.43: Load-displacement curve for all beams with a smooth (a) and profiled (b) interface using time series classification.

In both the smooth interface and profiled interface data a higher ductility from the partial and concrete failure class can be obtained compared to interface failure. The displacement at failure could be lower than shown in

the graphs for concrete, because a point of failure is more difficult to determine. In case of a smooth interface the partial failure reaches a higher load later on, and in some cases, higher than the concrete class. The concrete class shows some simulations with a peak and a decreasing load with increasing deformation. For the beams with a profiled interface the concrete class reaches higher loads compared to partial failure with similar shape in load-displacement curves. In general, it can be seen that the profiled interface shows less ductility compared to the smooth interface. The profiled interface will, however, already show partial failure with lower interface properties. The load and displacement could be increased for these samples compared to a smooth beam with the same interface properties but showing interface failure.

4.4. Influence interface properties per failure mode

The data at the point of failure is now investigated for the interface failure and partial failure separately. The focus is on the global behaviour, therefore, only the failure load and displacement are shown. To improve the visibility of the results, the amount of data is limited to the beams with an interface stiffness of 20%, 50% and 100% only. The results for the different interface geometry will be plotted in one graph to investigate the effect of the profile.

4.4.1. Interface failure

Figures 4.44a and 4.44b show the load and displacement at failure respectively for the beams with interface failure for both smooth and profiled interfaces. Interface failure has the lowest range in interface properties that can lead to interface failure. For the profiled interface even at lower interface properties compared to the smooth interface the failure mode would change from interface failure to partial failure.

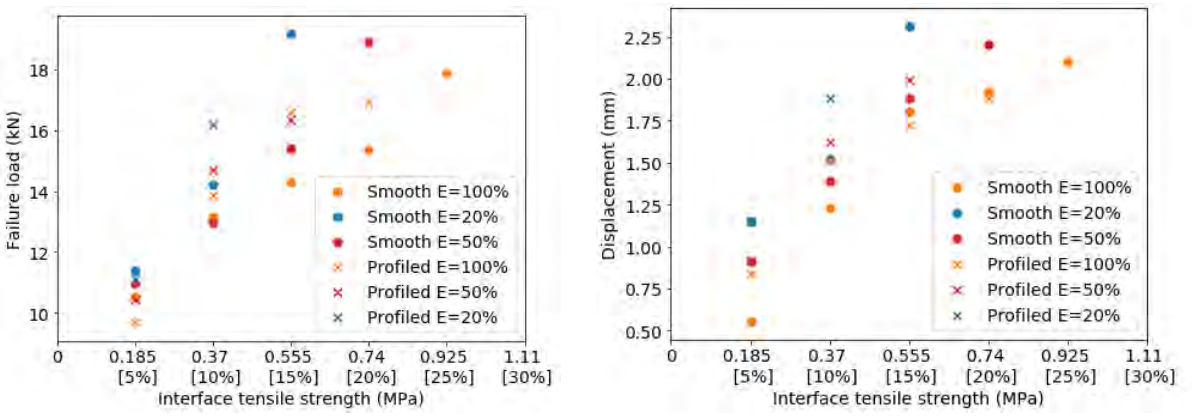

(a) (b)

Figure 4.44: Scatter plot failure load (a) and displacement at failure (b) vs. interface tensile strength and stiffness for beams with smooth and profiled interface showing interface failure.

The general trend that was obtained for the total data set in Section 4.2.1 is achieved within the interface failure data set as well. An increase in interface tensile strength and a decrease in interface stiffness leads to an increase in failure load and displacement. For a smooth interface it is seen that for a decrease in interface stiffness from 50% to 20% the increase in failure load is significantly higher compared to the decrease in interface stiffness form 100% to 50%. This is also seen for the profiled interface, although only two data points are present with 20% interface stiffness. Higher interface properties already lead to partial failure for the profiled interface. Looking at the displacement this trend is achieved, but with a minor increase compared to the failure load.

The effect of the profile on the behaviour is limited. It can be seen that for very low interface tensile strength (5%) the effect of the profile is negligible and leading to a lower failure load rather than an increase in failure load. Also, the effect on the displacement is limited for low interface properties. Moving towards higher interface tensile strength the profile leads to an increase in failure load and in some cases also to an increase in displacement. However, this increase is till minor compared to the increase that was seen from the experiments.

4.4.2. Partial failure

The results for the partial failure class are presented in Figures 4.45a and 4.45b. Both the results for smooth and profiled interface are shown. The effect of the interface properties is discusses and the effect of adding a profile is investigated.

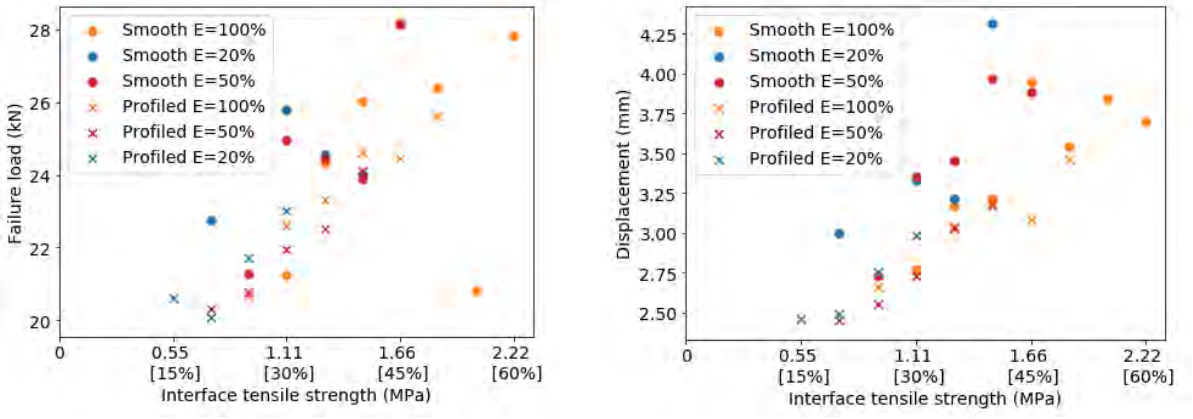

(a) (b)

Figure 4.45: Scatter plot failure load (a) and displacement at failure (b) vs. interface tensile strength and stiffness for beams with smooth and profiled interface showing partial failure.

For partial failure a larger scatter is seen in the data of the smooth interface in Figures 4.45a and 4.45b. This was already indicated when comparing the load-displacement curves from Figures 4.43a and 4.43b from the previous section. As a result, the found trends for the smooth interface are less consistent in case of partial failure. Still in most cases a lower interface stiffness leads to higher failure load and displacement, but the amount of increase differs for each interface tensile strength.

Although the profiled interface data has less spread, it still shows inconsistencies in trends. In most cases the failure load of the data with 50% interface stiffness is lower compared to the interface stiffness of 100%. On the other hand, an interface stiffness of 20% does show an increase in failure load compared to the other two stiffness values. Also, the difference in displacement for different interface stiffness is now lower compared to the smooth interface and compared to the profiled interface showing interface failure. This indicates that for partial failure the stiffness has minor effect in case of a profiled interface. Additionally, it can be seen that in the minority of the cases the application of the profiled interface leads to an increase in failure load and displacement. This means that with partial failure the influence of the profile has decreased compared to interface failure.

To gain even better insight into the effect of the interface properties and to express the difference in dependency between failure modes and interface roughness a regression analysis is carried out in the next chapter.

4.5. Suitability of the test method

In this chapter the notched beam test was modelled with the lattice mode to investigate the effect of different interface properties on the interface and structural behaviour.

With the range of interface properties used both interface, partial and concrete failure were obtained. This means that the test method is suitable to obtain different failure mechanisms. The effect of changing the interface properties on interface failure and partial failure can be investigated. Trends were found on the effect of the interface properties and the addition of a profile on the interface and global behaviour as discussed in the previous section.

For the smooth and profiled interface a set of interface properties were found with similar results to experiments. However, in case of an interface preparation with epoxy resin the lattice model shows an overestimation of the stiffness. This is due to the activation of the SHCC, which has an overestimated stiffness in the lattice model. The SHCC is in interface failure and in the majority of the cases of partial failure not activated. The model can predict the experimental findings for those cases.

The goal of this chapter was not to calibrate the model to the actual behaviour found in experiments. Although the found results might differ, the effect of the different interface properties and the addition of the

profile can still be investigated. For interface failure the found trends are consistent throughout the data set. For partial failure in a smooth interface more scatter occurs. The interface properties are in those case not the only parameter determining the structural behaviour. The adjacent materials gain an increasing role, influencing the results. For a low interface stiffness the range of interface tensile strength in the interface failure class is small. This makes it difficult to investigate the effect of the interface tensile strength in combination with low interface stiffness. Partial failure still shows dependency on the interface properties. Compared to some cases of the small-scale test, the bond test will provide a higher range of interface properties to investigate the effect of the interface behaviour.

5

Regression analysis

In this chapter the data from the notched-beam simulations from the previous chapter are used to carry out a regression analysis. This chapter starts with explaining the principle of a regression analysis using linear regression. For the regression analysis additional data is simulated to obtain a good fit. To classify this new data, support vector machine is used to determine the boundaries between different failure modes. After which for each failure mode different regression models will be used to find the best fit between the interface properties and the model outputs. The goal of the regression analysis is to find out what the role of each interface property is on the structural behaviour. Also, it is investigated how this influence differs per failure mode and interface roughness. The regression analysis is used to further explore the visually found trends from the data. For all regression analysis the Python package sklearn is used.

5.1. Simple and multiple regression

The basis for all classification and regression methods in this chapter is the linear regression. This method will be explained first to provide the basic understanding of a regression analysis. The linear regression method itself will also be used as a regression method. To indicate how well the regression model predicts the data different evaluation methods can be used. In this section different evaluation methods will be discussed.

5.1.1. Linear regression

With regression a line is described, which represents the relationship between variables [46]. In linear regression the line is described with the standard formula for a line:

$$y = ax + b + e \tag{5.1}$$

With y the dependent variable, a the slope of the line, also the regression coefficient, x the independent variable and e the error.

One way to fit the model to the data is by using least squares. With least squares coefficients of the model are chosen to minimize the residual sum of squares [47]. The residual sum of squares indicates a variability of the data that cannot be explained by the model. It is a measure for indicating how close the predicted data is to the original data [46]. It is calculated in the following way:

$$RSS = \sum_{i=1}^{n} (y_i - \hat{y}_i)^2 \tag{5.2}$$

With y_i the original data and $\hat{y}_i$ the predicted value from the regression formula.

Since there are multiple interface properties describing the beam behaviour, multiple regression is needed. In case of multiple regression there will be more independent variables and with each independent variable comes a regression coefficient [46]. The formula from Equation 5.1 changes to Equation 5.3. Each regression coefficient shows the dependence of the dependent variable on the independent variable. The regression coefficients say something about the influence of the independent variable compared to each other. This is what is needed for the regression analysis of the beam simulation data. There are two independent variables, interface stiffness and interface bond strength. A multiple regression analysis will indicate the interface property most influencing the structural behaviour of the notched-beam.

$$y_i = \alpha + \beta_1 x_{i1} + \beta_2 x_{i2} ... \beta_p x_{ip} + e \tag{5.3}$$

5.1.2. Evaluation methods

In this chapter multiple regression methods will be used. To compare which method fits the data best, multiple evaluation methods are available. The most used validations method is the coefficient of determination, also known as R^2. The coefficient of determination represents the variation in the outcome that can be predicted from the model [46]. The value of the coefficient of determination is between zero and one, with a value of one indicating a perfect prediction. In reality this is not possible. A value of zero indicates no relation is present between the outcome and the variables. The coefficient of determination is calculated by:

$$R^2 = 1 - \frac{RSS}{SS} \tag{5.4}$$

With RSS being the residual sum of squares as defined before and SS being the sum of squares. Sum of squares is a measure of the deviation from the mean and thus indicates the variation of the dependent variable [46]. In formula form it is noted as:

$$SS = \sum_{i=1}^{n} (y_i - \overline{y})^2 \tag{5.5}$$

With y_i the data value and $\overline{y}$ the mean of the data.

Other evaluation methods are the mean squared error (MSE) or root mean squared error (RMSE) and mean absolute error (MAE). The Equations 5.6, 5.7 and 5.8 respectively show the definition of these evaluation methods. The mean squared error and root mean squared error show the residual sum of squares as part of the formula. All methods indicate how large the residuals are. The mean squared error averages the expected prediction error over all samples used to determine the residual sum of squared [47]. It provides a larger value compared to the root mean squared error. The residual in the mean squared error is squared. while in the root mean squared error the mean squared error is rooted to go back to the order of the residuals. The root mean squared error might be more relatable to the data. In the mean absolute error the absolute values of the residuals are summed and not squared. Eventually all of these evaluation methods indicate the same. A low value indicates a better fit of the regression model. Because the values of this method can take any value, depending on the error of the data, it is beforehand not known what value to expect. For the coefficient of determination, R2-score, it is always a value between 0 and 1. Therefore, R2-scores are used as evaluation method.

$$MSE = \frac{1}{n} \sum_{i=1}^{n} (y_i - \hat{y}_i)^2 \tag{5.6}$$

$$RMSE = \sqrt{\frac{1}{n} \sum_{i=1}^{n} (y_i - \hat{y}_i)^2} \tag{5.7}$$

$$MAE = \frac{1}{n} \sum_{i=1}^{n} |y_i - \hat{y}_i| \tag{5.8}$$

5.2. Classification boundaries with SVM

For the regression analysis additional data is needed for accurate regression models. Time series classification has a large computational time. Therefore, a method is searched for to classify new data based on the already classified data. To determine the boundaries of the classes, support vector machine is used. Support vector machine (SVM) is a classification method that can define the boundaries of the classes and label new data into these classes. This method was introduced by [48].

5.2.1. SVM algorithm

The simple form is a two-dimensional linear separation case, where a surface is described which separates two classes. This surface is called a hyperplane. Multiple hyperplanes could separate the data; therefore, the hyperplane is determined by maximizing the distance between the hyperplane and the data points. This means a greater stability, since the change of a data point being on the wrong side of the boundary decreases with this increased distance. In Figure 5.1 the idea of how the hyperplane is formed is shown.

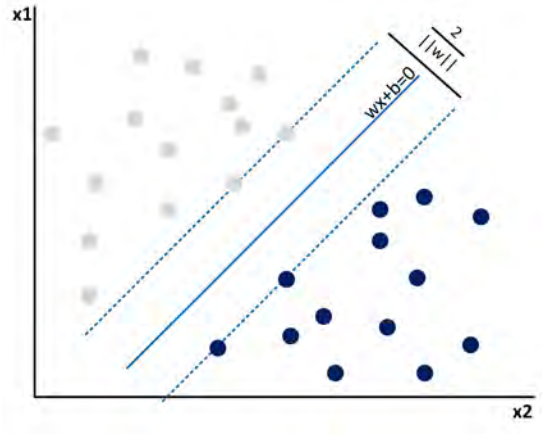

Figure 5.1: Support vector machine visualization with on axis input properties, different coloured dots indicating different clusters, solid line indicating hyperplane and dotted lines the supporting hyperplanes.

Support vector machine starts with the formula of a line, which is rewritten in vector form to the equation shown in Figure 5.1, where w is the vector (a,-1) and x is the vector (x,y). Two more lines are drawn to the nearest data points. The nearest data points are called support vectors. The two lines are the boundaries indicating the maximum distance between the hyperplane and the data points. These lines divide the data with y labelled as 1 or -1. This means for the top and bottom line the following counts respectively:

$$wx_i + b \geq 1 \text{ with } y_i = 1 \tag{5.9}$$

$$wx_i + b \leq -1 \text{ with } y_i = -1 \tag{5.10}$$

Combining the formulas leads to:

$$y_i(wx_i + b) - 1 \geq 0 \; y_i = 1, -1 \tag{5.11}$$

The space between the boundary lines and the hyperplane is called the margin. The margin needs to be maximized, which means minimizing the value of $||w||$ or $||w||^2$. This needs to be done such that Equation 5.11 is achieved. This means a constrained optimization needs to be solved, for which Lagrange's multiplier can be used. This is a dual optimization algorithm. For the primal optimization problem, meaning without a solution, the Lagrange's multiplier is used. In the next step the derivatives are set to zero for finding the minimum. These steps are shown below:

$$L = \frac{||w||^2}{2} - \sum_{i=1}^{n} (\lambda_i (y_i (wx_i + b) - 1) \tag{5.12}$$

$$\begin{gathered} \frac{\partial L}{\partial w} = w - \sum_{i=1}^{n} \lambda_i y_i x_i = 0 \\ \text{leads to } w = \sum_{i=1}^{n} \lambda_i y_i x_i \end{gathered} \tag{5.13}$$

$$\frac{\partial L}{\partial b} = \sum_{i=1}^{n} \lambda_i y_i = 0 \tag{5.14}$$

The dual optimization problem is found by substituting Equation 5.13 into Equation 5.12. After simplifying the equations an algorithm needs to be used to find the values of w and b.

5.2.2. Soft-margin boundaries

The above method used hard boundary lines. In some cases the classification could benefit from a soft margin to prevent overfitting of the data. A soft margin allows points to be present in the margin, which means allowing for misclassification. In case of a soft margin a second constraint is added to the calculation. This second constraint is minimizing the misclassification error. The misclassification error should be minimized, while still maximizing the margin. This is contradicting and an optimum should be searched for.

5.2.3. Multi-class classification

Since three different failure modes are distinguished, a multi-class classification is needed. The multi-class classification is based on the binary SVM. The same method is used but multiple times. Two multi-class methods can be distinguished namely one-to-one and one-to-rest. Both methods are shown in Figure 5.2. In one-to-one a hyperplane is determined between two classes ignoring the other classes. This is done for all pairs possible. This will cause the hyperplanes to intersect. In the one-to-rest method a hyperplane is drawn between one class and all other data points, ignoring the distinction between classes of the other data points. This is repeated for all classes. In this method the hyperplanes will not intersect together in one point but will form a shape between the classes based on the number of classes. In case of three classes a triangle will form.

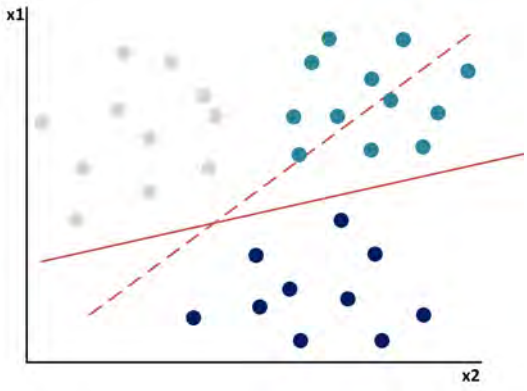

Figure 5.2: Support vector machine visualization one-to-one (red dashed line) and one-to-rest (red solid line).

5.2.4. Classification boundaries

The SVM classification method will be used to find the classification boundaries of the data. The data is labelled, as explained in the previous chapter, according to the classification from the time series data. Python is now used to find the boundaries. In Figures 5.3 and 5.4 the data is plotted showing the three classes for the different interface properties on the axis in different colours for the beams with a smooth and profiled interface respectively. The boundaries found using support vector machine are shown. Using one-to-one or one-to-rest will in both cases lead to the same outcome due to the way the data is clustered. For the class with partial failure the method for both one-to-one or one-to-rest is not possible because the cluster is surrounded by other clusters. Therefore, the method leads to the middle line, which is the centre of the class data having the maximum distance to both the concrete class and the interface class. For this data only two boundaries are now needed, namely the top, red line and bottom, orange line. Everything below the orange line, will be interface failure, between the lines is classified as partial failure and above the top line is part of the concrete failure class.

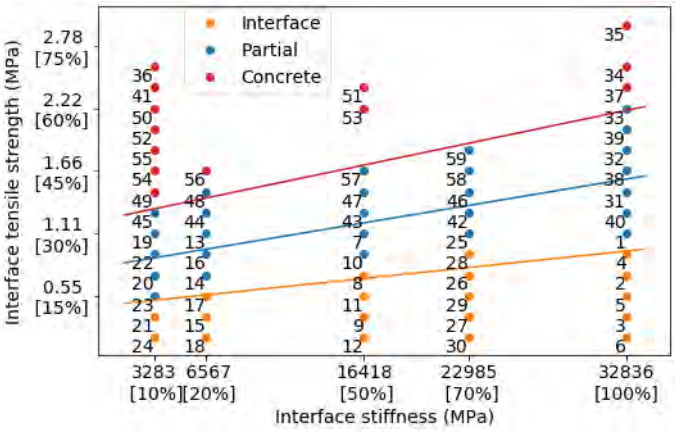

Figure 5.3: Support vector machine result for classification boundaries of the beams with a smooth interface.

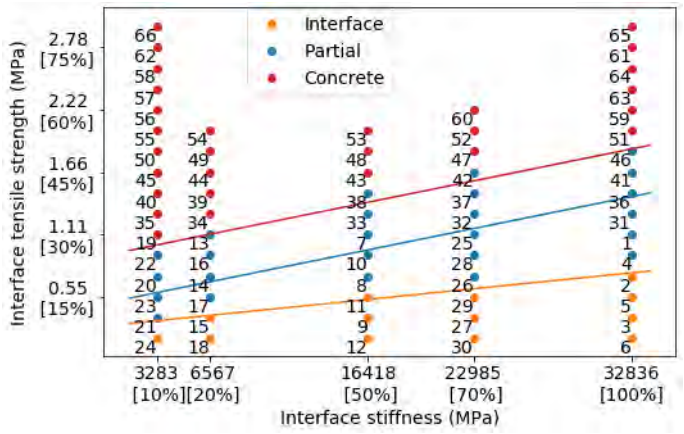

Figure 5.4: Support vector machine result for classification boundaries of the beams with a profiled interface.

5.2.5. Classification new data

Support vector classification is also used to classify data that is added later. Based on the known classification and the interface input values, new samples can be classified based on their input values. This saves time compared to redoing the time series clustering. In the Figures below the classification of the existing and new data is shown using the support vector machine. Figure 5.5 shows the total classified data for beams with a smooth interface. The figure below, Figure 5.6, shows the classified data for all beams with a profiled interface.

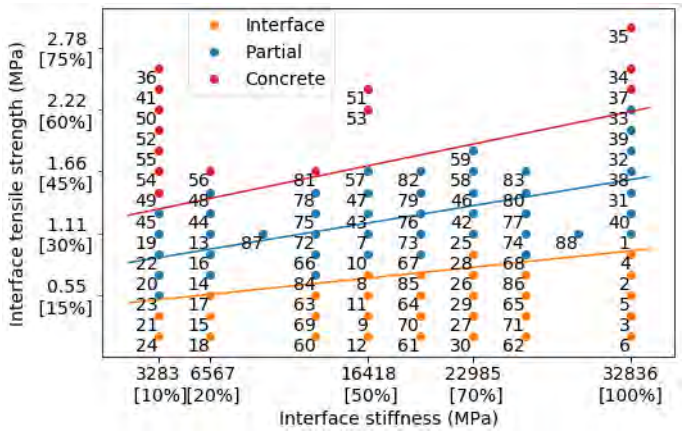

Figure 5.5: Support vector machine result for classification of the beams with a smooth interface.

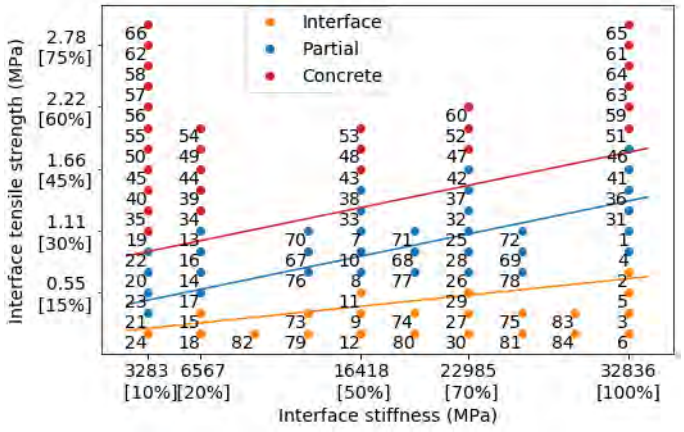

Figure 5.6: Support vector machine result for classification of the beams with a profiled interface.

5.3. Regression methods

In this thesis different regression methods will be used, which will be carried out using the Python package scikit learn. The linear regression method has already been explained. LASSO, ridge and SVR will be explained before applying the different methods on the data. The LASSO method is chosen because of its ability to shrink different parameters to zero. This could indicate if one interface property does not show any effect. Ridge is a similar method also using shrinkage of the coefficients. SVR is used since it provided good results in [49] on a data set of slant shear test on NSC-UHPC interfaces. Each method will be explained in this section.

5.3.1. LASSO regression

LASSO stands for least absolute shrinkage and selection operator. In LASSO regression a linear regression is carried out with the ability to shrink coefficients. In case of large number of predictors, the number of predictors could be minimized instead of trying to fit all predictors as with linear regression. This reduces the possibility of overfitting the data. The definition of the LASSO regression in formula form defined by [50], is stated in Equation 5.15. LASSO is also called a L_1-optimization problem.

$$(\hat{\alpha}, \hat{\beta}) = argmin \sum_{i=1}^{n} \left(y_i - \alpha - \sum_{j=1}^{n} \beta_j x_j^{(i)} \right)^2 \text{ subjected to } \sum_{j=1}^{n} |\beta_j| \leq t \tag{5.15}$$

With $\hat{\alpha}$ and $\hat{\beta}$ the LASSO estimates, α being the constant coefficient, β the coefficient vector and t the tuning parameter that determines the amount of shrinkage. The tuning parameter sets an upper bound for the regression coefficients and thus penalizes the solution is this upper bound is exceeded.

If the data is standardized, meaning $\sum_i^n x_{ij}/N = 0$, the mean of the response, $\overline{y}$, will be equal to zero. This means that the constant coefficient will also be zero and α can be left out of the equation.

LASSO is a constrained optimization problem, as was the case with SVM. Therefore, the Lagrange's multiplier can be used. Rewriting the formula using the Lagrange's multiplier, λ, gives the formula as stated in Equation 5.16. The tuning parameter from 5.15 is changed to the LASSO multiplier, λ, which is now used as the shrinkage parameter. The first part of the equation equals the residual sum of squares. A λ of zero will thus reduce the problem to an ordinary least square. If all coefficients shrink to zero, λ goes to infinity. The bias increases with increasing λ, while the variance increases with a decreasing λ. Choosing the value of λ determines the outcome of the model and should be chosen carefully by the user. The best value for the shrinkage parameter depends on the data.

$$L = min \sum_{i=1}^{n} \left(y_i - \sum_{j=0}^{n} \beta_j x_j^{(i)} \right)^2 + \lambda \sum_{j=1}^{n} |\beta_j| \tag{5.16}$$

One way to find the best λ is by using cross-validation and choose the λ with the lowest cross-validation prediction error. This method will be explained in Section 5.3.4.

An algorithm is needed to find the solution of the LASSO model for the regression coefficients. The LASSO model in Python uses coordinate descent to solve the model. This method is explained here. To solve Equation 5.16 the derivative is taken and set to zero to find the values for β that minimize the equation.

$$\frac{\partial L}{\partial \beta_j} = -\frac{2}{N} \sum_{i=1}^{n} x_j^{(i)} \left(y_i - \sum_{j=1}^{n} x_j^{(i)} \beta_j \right) + \lambda \tag{5.17}$$

The value for λ can be positive or negative depending on the value of β_j. This will be considered in the soft thresholding function at the end of this section. The equation is first rewritten to extract β_j from the summation.

$$\frac{\partial L}{\partial \beta} = -\frac{2}{N} \sum_{i=1}^{n} x_j^{(i)} \left(y_i - \sum_{k \neq j}^{n} x_k^{(i)} \beta_k - \beta_j x_j^{(i)} \right) + \lambda \tag{5.18}$$

Next, the term with β_j can be extracted from the summation.

$$\frac{\partial L}{\partial \beta} = -\frac{2}{N} \sum_{i=1}^{n} x_j^{(i)} \left(y_i - \sum_{k \neq j}^{n} x_k^{(i)} \beta_k \right) + \frac{2}{N} \beta_j \sum_{i=1}^{n} \left(x_j^{(i)} \right)^2 + \lambda \tag{5.19}$$

Now that $beta_j$ is outside the summation, the solution can be found. There are three cases that need to be considered to find the minimum. This is done by using a soft thresholding notation. The β_j value can be smaller than zero, larger than zero or equal to zero. The results are shown below:

$$\begin{cases} \beta_j = \frac{\sum_{i=1}^{n} x_j^{(i)} \left(y_i - \sum_{k\neq j}^{n} x_k^{(i)} \beta_k\right) + \lambda}{\sum_{i=1}^{n} \left(x_j^{(i)}\right)^2} & \text{for } \sum_{i=1}^{n} x_j^{(i)} \left(y_i - \sum_{k\neq j}^{n} x_k^{(i)} \beta_k\right) < -\lambda \\ \beta_j = 0 & \text{for } -\lambda \leq \sum_{i=1}^{n} x_j^{(i)} \left(y_i \sum_{k\neq j}^{n} x_k^{(i)} \beta_k\right) \leq \lambda \\ \beta_j = \frac{\sum_{i=1}^{n} x_j^{(i)} \left(y_i - \sum_{k\neq j}^{n} x_k^{(i)} \beta_k\right) - \lambda}{\sum_{i=1}^{n} \left(x_j^{(i)}\right)^2} & \text{for } \sum_{i=1}^{n} x_j^{(i)} \left(y_i - \sum_{k\neq j}^{n} x_k^{(i)} \beta_k\right) > \lambda \end{cases} \tag{5.20}$$

Next follows an iteration procedure for $j = 0, 1, ..., n$. In each step it is determined which of the equations in the soft thresholding formula from 5.20 needs to be used, after which the β_j value is determined. The iteration procedure continues until convergence or the maximum number of iterations is reached.

5.3.2. Ridge regression

In [50] alongside the LASSO regression, the ridge regression is discussed. LASSO and ridge regression are often named together, since both determine the regression coefficients by setting a penalty to the regression coefficients. The difference is that ridge regression cannot shrink the coefficients to zero. Ridge regression minimizes the following equation:

$$\begin{aligned} (\hat{\alpha}, \hat{\beta}) = argmin \sum_{i=1}^{n} \left(y_i - \alpha - \sum_{j=1}^{n} \beta_j x_j^{(i)}\right)^2 \\ \text{subjected to } \sum_{j=1}^{n} (\beta_j)^2 \leq t \end{aligned} \tag{5.21}$$

The equation looks similar to the equation for LASSO with the only difference being the penalty term. In case of a standardized data, again α can be left out. For finding the regression coefficients (β) the equation is first set to the Lagrangian form:

$$L = min \sum_{i=1}^{n} \left(y_i - \sum_{j=0}^{n} \beta_j x_j^{(i)}\right)^2 + \lambda \sum_{j=1}^{n} (\beta_j)^2 \tag{5.22}$$

Since there is a closed form solution to this task, the equation is rewritten in vector notation for simplification in reading.

$$L = (\mathbf{Y} - \mathbf{X}\beta)^T (\mathbf{Y} - \mathbf{X}\beta) + \lambda \beta^T \beta \tag{5.23}$$

To minimize β the derivative of the equation is set to zero.

$$\frac{\partial L}{\partial \beta} = -2\mathbf{X}^T\mathbf{Y} + 2\mathbf{X}^T\mathbf{X}\beta + 2\lambda\beta = 0 \tag{5.24}$$

Now, solve for β to find the coefficients of the ridge regression.

$$\beta = \mathbf{X}^T\mathbf{Y}(\mathbf{X}^T\mathbf{X} + \lambda\mathbf{I})^{-1} \tag{5.25}$$

The identity matrix (I) is included to set λ to a matrix which allows for summation with the matrix present in the brackets. The solution is the same as for the least squares with an addition of the shrinkage parameter λ.

5.3.3. Support vector regression

Based on the same idea of support vector classification, the support vector regression can be used. Instead of increasing the distance between the points of two different clusters, the distance is minimized between the linear regression line and the data points in a data set. The distance between the supporting hyperplanes now indicates the error, or precision, between the predicted and actual value. This precision is introduced with ϵ. The supporting hyperplanes are described as followed as in done in [51]:

$$y_i - wx_i - b \leq \epsilon \tag{5.26}$$

$$wx_i + b - y_i \leq \epsilon \tag{5.27}$$

The following optimization problem can be formed:

$$b = argmin(\frac{1}{2}||w||^2) \text{ subjected to } wx_i + b - y_i \leq \epsilon,\ y_i - wx_i - b \leq \epsilon \tag{5.28}$$

This means a constrained optimization needs to be performed, for which the Lagrange's multiplier can be used. Two Langrangian multipliers are needed, since there are two constraints. The same steps need to be carried out as with the support vector classification.

$$L = \frac{||w||^2}{2} - \sum_{i=1}^{n}(\lambda_i(\epsilon - y_i + wx_i + b)) - \sum_{i=1}^{n}(\lambda_i^*(\epsilon + y_i - wx_i - b)) \tag{5.29}$$

$$\frac{\partial L}{\partial w} = w - \sum_{i=1}^{n}(\lambda_i - \lambda_i^*)x_i = 0 \tag{5.30}$$

$$\frac{\partial L}{\partial b} = \sum_{i=1}^{n}(\lambda_i^* - \lambda_i) = 0 \tag{5.31}$$

The dual optimization problem can be found by substituting the derivatives into the Lagrangian function. After this an algorithm can be used to find the solution.

5.3.4. Model parameter selection

For the different regression models explained in the previous sections, the model parameters need to be determined. For LASSO and ridge regression the optimum shrinkage parameter, λ, needs to be found. For the SVR-model there are two input parameters: C and ϵ. Where C is the regularization parameter and ϵ is as is stated in the formula of Equation 5.30. In the programming package used, sklearn, cross-validation is used to determine the shrinkage parameters for LASSO and ridge. This method is explained first. The method for the SVR model parameters is discussed afterwards.

K-fold cross-validation

To find the most optimum shrinkage coefficient K-fold cross-validation is used. The method is as described in [47]. In this method the data is divided into K parts. One part is used for validation, the other $K-1$ parts are used to fit the data. This process is then repeated K times, with each time a different part of the data set as validation set. After carrying out the method K times, the cross-validation estimate of the prediction error is calculated with Equation 5.32.

$$CV(\hat{f}) = \frac{1}{N}\sum_{i=1}^{N}(y_i - \hat{f}^{-\kappa(i)}(x_i))^2 \tag{5.32}$$

With $\hat{(}f)^{-\kappa}(x)$ the fitted model on the data set, X, without the k^th part.

With the method described above a prediction error is calculated. Cross-validation can be used to compare different models based on these prediction errors. To use cross-validation for estimating the model parameter, the method needs to be repeated with different model parameters each time. The model parameter with the lowest cross-validation prediction error would in that case describe the best fit. For the regression analysis in this thesis, a range from 0 to 10 is used to find the best shrinkage coefficient. Python package scikit learn has an implemented cross-validation method for determining the shrinkage parameter.

The amount of K-fold affects the solution. Splitting the data into a large number of small data sets, will decrease the bias, but increase the variance. Using a lower value of K, will lower the variance, but increase the bias. Therefore, the amount of K-fold chosen, provides different solutions. For K a value of 5 or 10 is most common. Here, the value for K will be varied from 2 to 10 for each model. The value for K with the lowest prediction error will be used.

SVR model parameters

For support vector regression two parameters need to be determined. Different as is the case for LASSO and Ridge is that Sklearn does not provide an implemented cross-validation method to compute the best parameters. Therefore, a simple method is used to find the best value. The data set is for this method not divided into parts. In this method the analysis is carried out for different values of the parameters. For both C and ϵ a range of values is used. For C a range from 100 to 900 with steps of 100 and for ϵ a range from 0.1 to 1 with steps of 0.1 is used. The regression model is used to fit the data for each value separately. A constant value for ϵ is used for determining the value of C and a constant value for C is used for determining ϵ. For each value of the different parameters the R2-score of the model is calculated. The parameter value that leads to the highest R2-score is used.

It was found that the value for C does not affect the results. For ϵ the values range from 0.3-0.5 between the model for the best R2-score. Since the value for C does not affect the result, it can be ruled out that a different combination of values would result in different results. Therefore, this method can be used. The only difference compared to cross-validation is that the complete data set is used and the result is not verified with separate parts of the data set.

5.4. Regression analysis results

The different methods described in the previous sections will now be used to carry out a regression analysis on the classified data. Interface and partial failure will be analysed. The concrete failure mode will not be considered, since this failure mode is governed by the concrete. The regression analysis will be carried out using the Python package scikit learn. For the input the interface stiffness and the interface tensile strength, are used. As output the failure load, displacement, interface opening and joint opening are used. This means multiple output regression is carried out. For the linear regression there are no additional steps required. However, for the SVR, LASSO and Ridge model the input and output data need to be scaled first. This is done to prevent the magnitude of the input values to affect the results. The value for the elastic modulus is larger compared to the tensile strength. For these models it is necessary to scale the values to have the same magnitude. After the regression analysis the regression coefficients can be unscaled to visualise the prediction models.

Each data set is divided in a train and test part with a ratio of 70/30. The training set is used to determine the model parameters as described in the previous section and to fit the model. The test data is used to evaluate the regression model. Since the data sets are small, all data is used to visualize the results. Two ways to visualize the results are used. First the evaluation of the models is shown per case by plotting the predicted values of the model vs. the values obtained from simulation. This is to evaluate the regression model visually. In this plot the R2-scores per regression method will be stated to express the fit of the models in a number. For the second evaluation method the models and the original data are plotted. The models are shown per output feature to visualize how the effect of the input parameters on the different output features differs. After the visualization the results of the regression analysis are discussed. It is concluded if the earlier found trends from visually analysis the data are supported with the regression analysis. The regression coefficients will be discussed and compared between different cases. The difference in influence of the interface properties between smooth and profiled interface is investigated and also the difference in effect between failure modes. In the next sections the results will be presented and discussed.

5.4.1. Regression results for beams with a smooth interface showing interface failure

The first class considered for the regression method is the beams with a smooth interface showing interface failure. The models will be evaluated based on their R2-scores first. For each regression analysis a plot is shown indicating the predicted values from the results versus the values obtained from the simulations. The results are shown in Figure 5.7. A line is drawn that represents a perfect fit if all simulation values were correctly predicted. The deviation from this line of the different points indicates how much the predicted value deviates from the simulations. For each model the R2-score is shown for both the test and training data set. If the R2-scores are close for the test and training data set the results can be assumed to be more accurate. A large difference between the test and training data set can be the cause of scatter in the data influencing one of the two data sets.

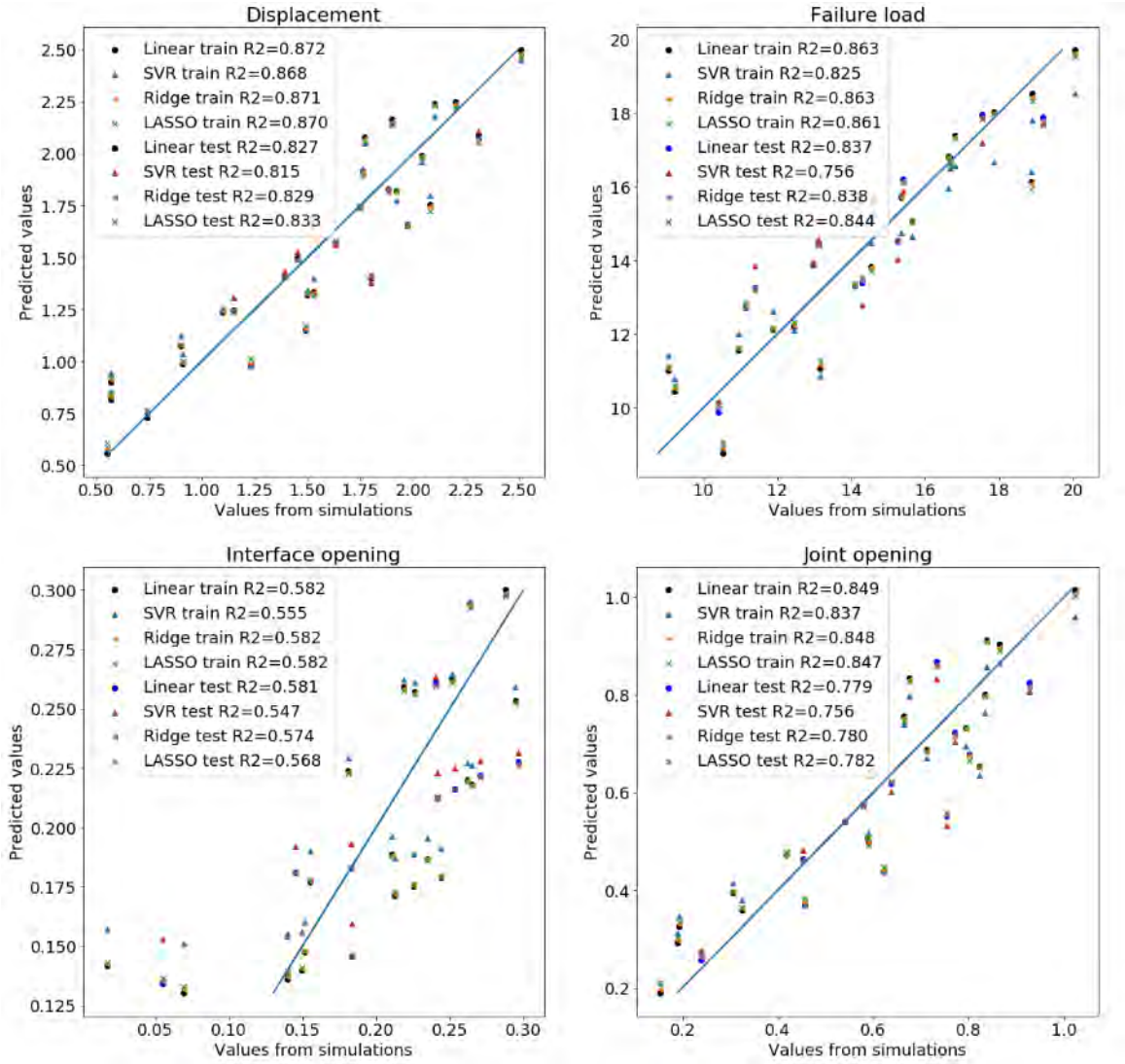

Figure 5.7: Predicted vs. simulated data for train and test data and predicted vs. predicted line for the case of smooth interface with interface failure for beam behaviour at failure (displacement, load, interface opening and joint opening).

In this case the R2-scores are above 0.75 for the displacement, load and joint opening. The scores are similar for each model. The models are accurate enough to analyse the relation between the beam behaviour and the interface properties. For the interface opening the results are very inaccurate judging from the R2-score. This is to be expected since the interface opening is measured locally and opens up fast at the point of failure. This latter means that if the point of failure is taken slightly different, the interface opening could reach very different values. It can be seen that there is a group of interface opening values in the left bottom that are overestimated in the regression models. From the data it was seen that low interface opening values are obtained with low interface properties. For very low values the interface opening is very small compared to the interface opening at higher interface properties. This deviation causes the R2-score to be low. However, also the other data points are positioned further away from the blue prediction line compared to the other output features as a result of the scatter in the data.

Now that the models are evaluated, the models will be plotted to analyse the effect of the interface properties on the beam behaviour. The fitted models are plotted together with the data set from the simulations in Figure 5.8. The models are plotted for the different output features versus the interface properties individually. Two plots will thus be presented for each output feature. This is done to analyse the effect of the interface properties on the behaviour individually. The behaviour predicted by each model is plotted for different interface properties on the x-axis and the other property is set at specific values indicated with a different colour.

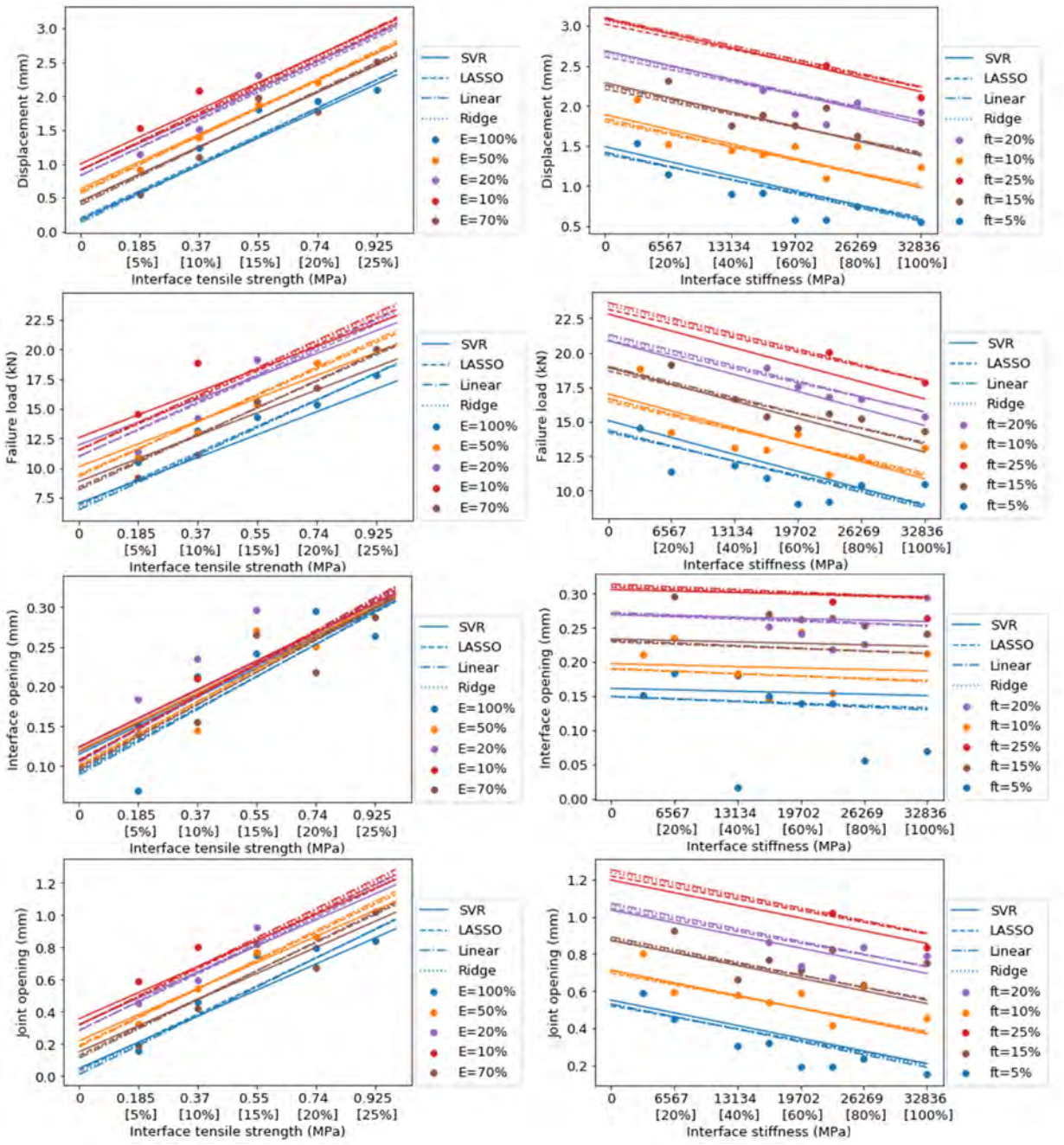

Figure 5.8: Regression models and data values for beam behaviour at failure (displacement, load, interface opening and joint opening) vs. interface tensile strength (left) and interface stiffness (right) for beams with a smooth interface showing interface failure. In brackets the interface properties as a percentage of the concrete properties.

It can be seen that the slope of the interface tensile strength is steeper, meaning a stronger dependency compared to the slope of the interface stiffness. However, it should be noted that in case of the interface stiffness the x-axis reached 100% while in case of the interface tensile strength as the main parameter the range is 25%. Looking at the distance between the lines the influence of the behaviour of the other property can also be conducted. Although there is a difference in range in y-axis this does not change the conclusion. In case of the interface tensile strength on the x-axis the lines are close together for the changing stiffness. A range of 1 mm is covered, with a range of 90% of the interface stiffness. A range of 1.5 mm is covered by the interface tensile strength in the right graph for a range of 20% in interface tensile strength. This indicates that the influence of the stiffness is limited and minor compared to the interface tensile strength.

From the plots the scatter of the interface opening is again visible. The models do catch some of the

behaviour, however, the scatter lowers the R2-score. Between the models, the results differ slightly, which indicates that the models found similar effect of the interface properties on the structural behaviour. Only in case of SVR a more distinct difference can be observed for predicting the failure load. This was also indicated by a lower R2-score for this model on predicting the behaviour.

5.4.2. Regression results for beams with a profiled interface showing interface failure

The regression results are presented for the beams with a profiled interface showing interface failure. The data set of this case is small because the boundary between the interface failure and partial failure occurs at lower interface properties, leaving a limited range of data left. Therefore, more data was generated for the interface failure class with a profiled interface as could be seen in the classification using SVM in Section 5.2.5. For this increased data set the results are shown in Figure 5.9.

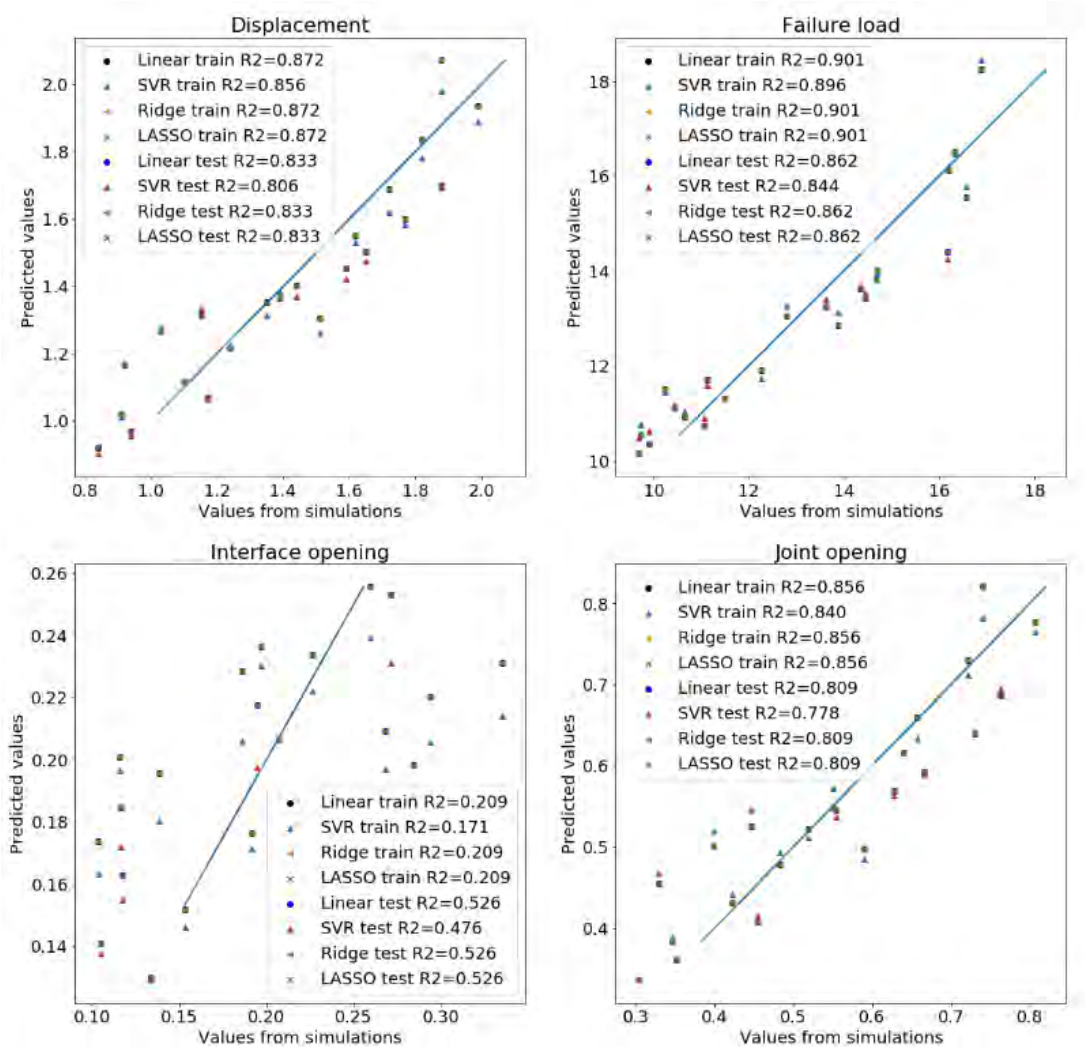

Figure 5.9: Predicted vs. simulated data for train and test data and predicted vs. predicted line of profiled interface with interface failure for beam behaviour at failure (displacement, failure load, interface opening and joint opening).

For the interface failure class for beams with a profiled interface the R2-scores are in the same ratio as for the beams with a smooth interface. Except for the interface opening for which the R2-score is now even almost zero. For the other cases the models can be considered accurate, judging from their R2-scores. With this R2-score the results can be used to investigate the dependency of the output on the interface properties. The model results for the interface opening should be neglected since the R2-scores are very low. In other cases SVR has the lowest R2-score. The models are plotted together with the data set in Figure 5.10.

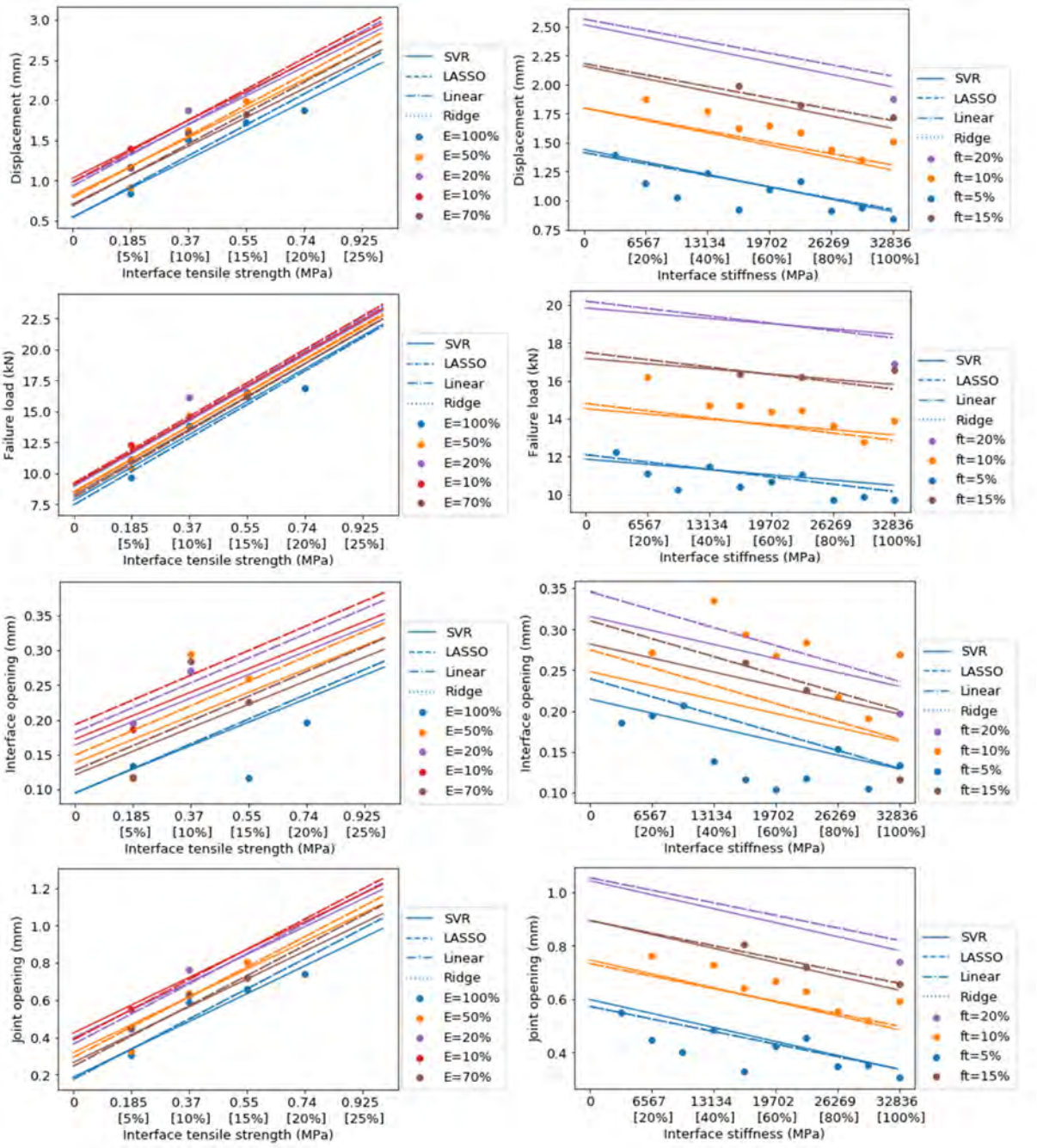

Figure 5.10: Regression models and data values for beam behaviour at failure (displacement, load, interface opening and joint opening) vs. interface tensile strength (left) and interface stiffness (right) for beams with a profiled interface showing interface failure. In brackets the interface properties as a percentage of the concrete properties.

From the plots in Figure 5.10 it can be concluded that the interface tensile strength is dominant for the behaviour. This is not only indicated by the slope of the graphs, but also by the close distance between the curves for different interface stiffness in the left graphs. From the graphs of the interface opening it can clearly be seen that the SVR model has a curve differing from the other models. Since the interface opening has more scatter, because of its local behaviour, it is to be expected that the models have difficulty fitting a line representing the data. It is also visible that the other models do not catch the behaviour. The data points are scattered throughout the graph not showing any relation by itself. For the global behaviour indicated by the failure load and displacement it can be concluded that the interface tensile strength is governing for the behaviour. An increase in interface tensile strength increases the global behaviour. For the stiffness this relation is negative but also very limited.

From the plots on the right sides showing the output versus the interface stiffness, it is seen that there is only one data point for the highest interface tensile strength in the class (the purple dot). For the displacement the models are close to this value, for the failure load however, the distance between the data point and the model is larger. It is difficult to conclude the correctness of the model based on one data point. However, given the overall accuracy of the models, indicated by the R2-score, the model is reliable. This means that the model is useful to indicate the dependency, which is not possible to obtain with one data point.

5.4.3. Comparison of results for interface failure of smooth and profiled interface

To indicate if the dependency of the beam behaviour on the interface properties differs between a smooth and profiled interfaces for beams showing interface failure, a comparison of the results is made. First the fitted models and simulation data are plotted in one graph. This is done for linear regression only to increase the visibility of the graphs. Only the global behaviour, the failure load and displacement, are plotted. These plots are shown in Figure 5.11. It should, however, be noted that the regression model does not consider the boundary between interface failure and partial failure. It, therefore, disregards the fact that the profiled interface moves to partial interface at lower interface properties compared to smooth interface. The best way to indicate up to what point the models can be considered, is by looking at the simulation data. If there is no data point above a certain interface tensile strength or below a certain stiffness, it is because the failure mode has changed.

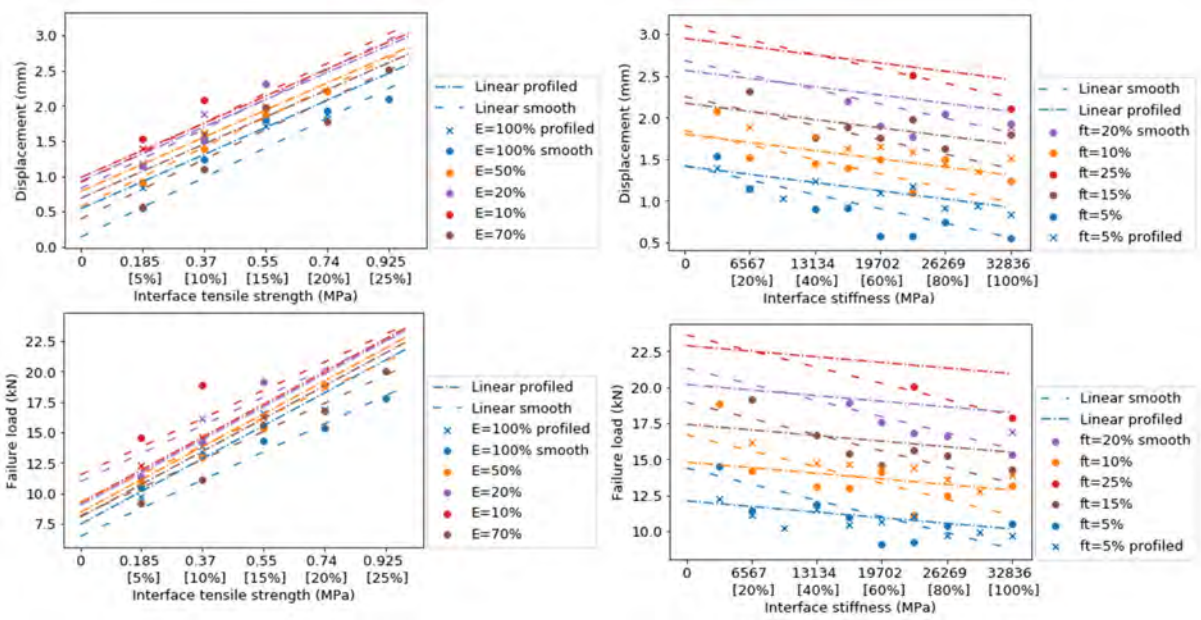

Figure 5.11: Linear regression model and data values for different interface properties and for beam behaviour at failure for smooth and profiled interface. In brackets the percentage of the concrete properties.

Comparing the plots the difference in dependency of the beam behaviour on the interface properties between a smooth and profiled interface can be determined. It is spoken of dependency to analyse the results from the regression coefficients. The regression coefficients, however, do not represent the dependency, but it is an indication for the dependency. The regression coefficients indicate with what factor of the input value the output can be described. In the regression analysis there were two parameters set as input that, while there are more factors that can affect the outcome. For example, the interface compression strength is altered along with the interface tensile strength. If more concrete would crack, the concrete properties would also influence the results. However, the amount of concrete cracking cannot be expressed as an input property. The concrete material properties are constant and will not indicate change of the beam behaviour. Therefore, the regression coefficients should not be solely defined as dependency, but rather how they describe the observed behaviour.

From the plots it can be seen that the interface tensile strength has a higher influence on the displacement in case of a smooth interface. This is obtained by comparing the slope of the curves. For the interface stiffness the dependency is higher in case of a smooth interface compared to a profiled interface. For the failure load the stiffness also has a higher influence for describing the behaviour in case of a smooth interface. However, for the tensile strength it seems that the profiled interface is influenced more. The failure load shows a wider range in values for the smooth interface with for higher interface stiffness lower values compared to the profiled interface. For the lower interface stiffness the smooth profile has slightly higher values. This was not obtained in the comparison of the data visually. The reason is that the data of 10% interface stiffness was not plotted, which shows a higher increase in failure load for the smooth interface compared to the profiled interface.

From the load-displacement curves in Figures 4.43a and 4.43b, it was concluded that the profiled interface does not reach higher structural behaviour values compared to the beams with a smooth interface. From the regression model it can be seen that a profiled interface would indeed not reach higher values at the same or increasing interface properties.

All in all, the effect of the profiled interface on the output is minor. A slight increase in failure load is seen for low interface tensile strength in case of a profiled interface compared to a smooth interface. Beams with a smooth interface are more prone to changes in interface stiffness compared to beams with a profiled interface. The interface tensile strength is governing in both cases, but shows a slightly stronger effect for a profiled interface. This latter can be seen when comparing the regression coefficients more in depth. A clear overview of the different regression coefficients can be found in Figures 5.12a and 5.12b.

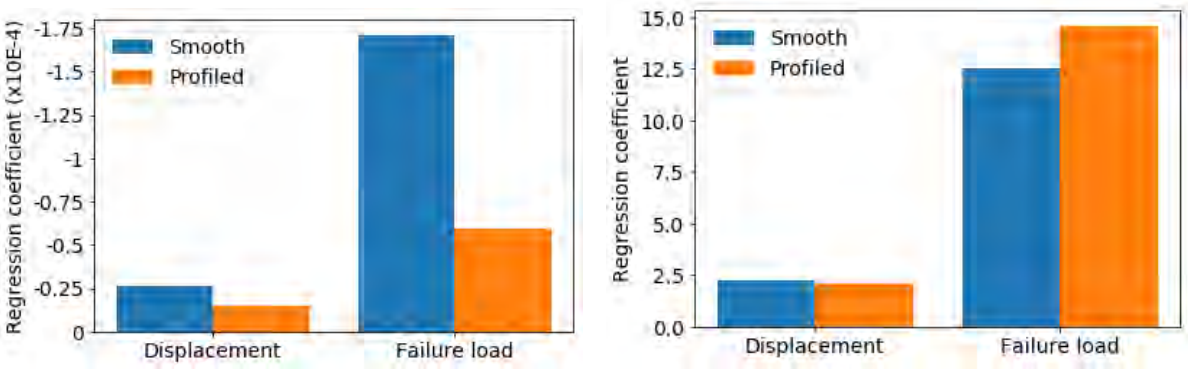

(a) (b)

Figure 5.12: Bar plot indicating regression coefficients of interface stiffness (a) and interface tensile strength (b) of the linear regression model for smooth and profiled interface showing interface failure.

The plots support the already concluded difference in dependency on the interface properties for different interface geometries. It is seen that the difference in dependency between the smooth and profiled interface differs significantly on the interface stiffness compared to the interface tensile strength. The failure load of a smooth interface seems to be significantly more dependent on the interface stiffness compared to the profiled interface. The smooth interface is almost 3 times more dependent on the interface stiffness compared to the profiled interface. For the interface tensile strength it is seen that the failure load of beams with a profiled interface is influenced more compared to the smooth interface.

5.4.4. Regression results for beams with a smooth interface showing partial failure

The same regression methods are used to predict the beam behaviour for a smooth interface showing partial failure. The obtained modelled will first be evaluated using the R2-scores. The regression models can be evaluated using Figure 5.13.

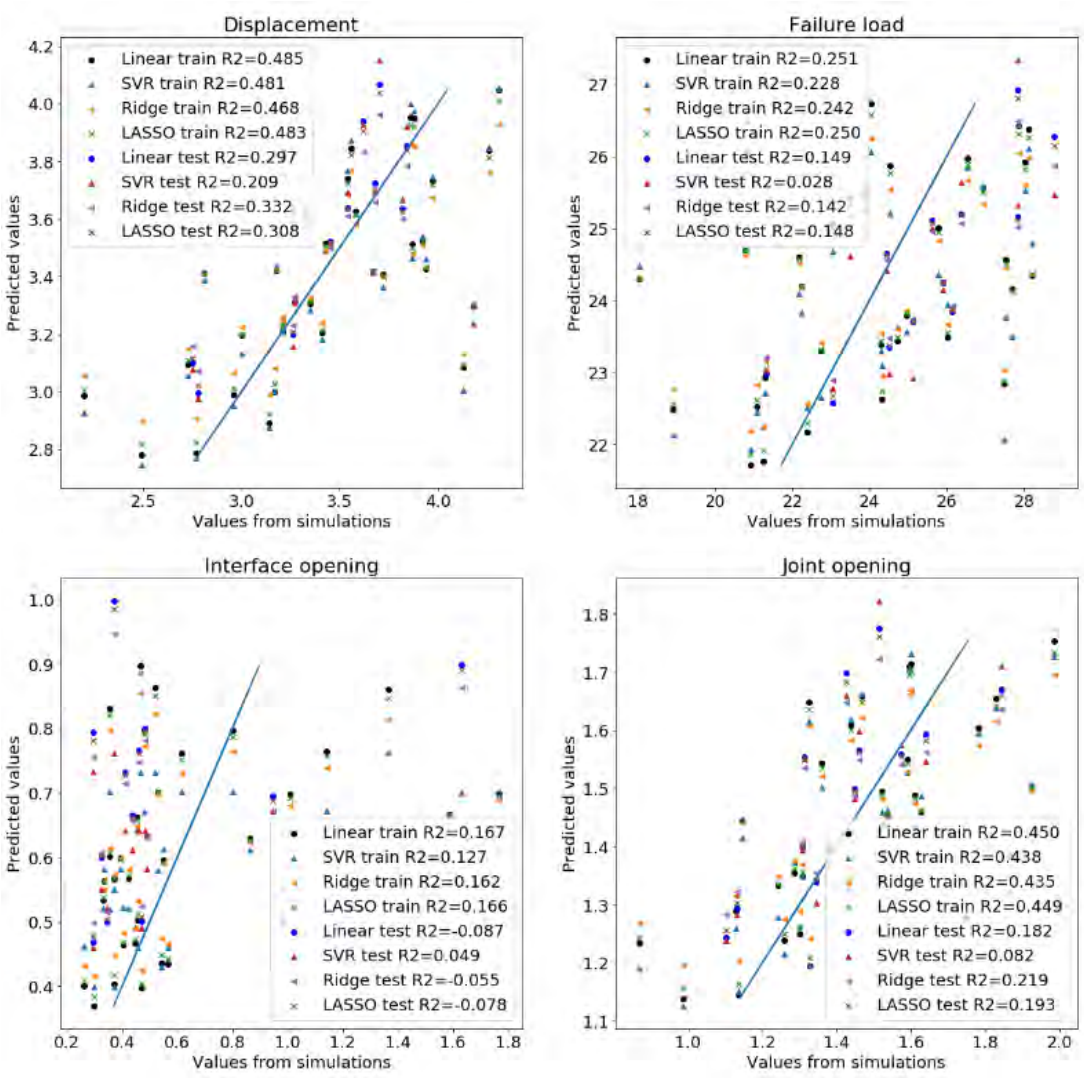

Figure 5.13: Predicted vs. simulated data for train and test data and predicted vs. predicted line for smooth interface showing partial failure for beam behaviour at failure (displacement, failure load, interface opening and joint opening).

The predicted values show a higher deviation from the simulations compared to the previous cases. It can also be seen that the R2-scores are very poor for this data set. Although this data set is the largest of all sets generated, it results in low R2-scores. This can be explained by looking at the load-displacement curves of all smooth beams in Figure 4.43a in the previous chapter. The load-displacement curves of the beams with partial failure have a wide range in failure points. A high number of beams have drops at the end of the curve. These drops are too small to satisfy the failure criteria, but do influence the outcome of the simulation. Due to this scatter, the regression model has difficulty in finding a linear model to represent the behaviour. Although the scores are poor, the data is presented in Figure 5.8 to visualize the relation between the interface properties and the different output features. These conclusions should, however, not stand on their own because of the poor scoring.

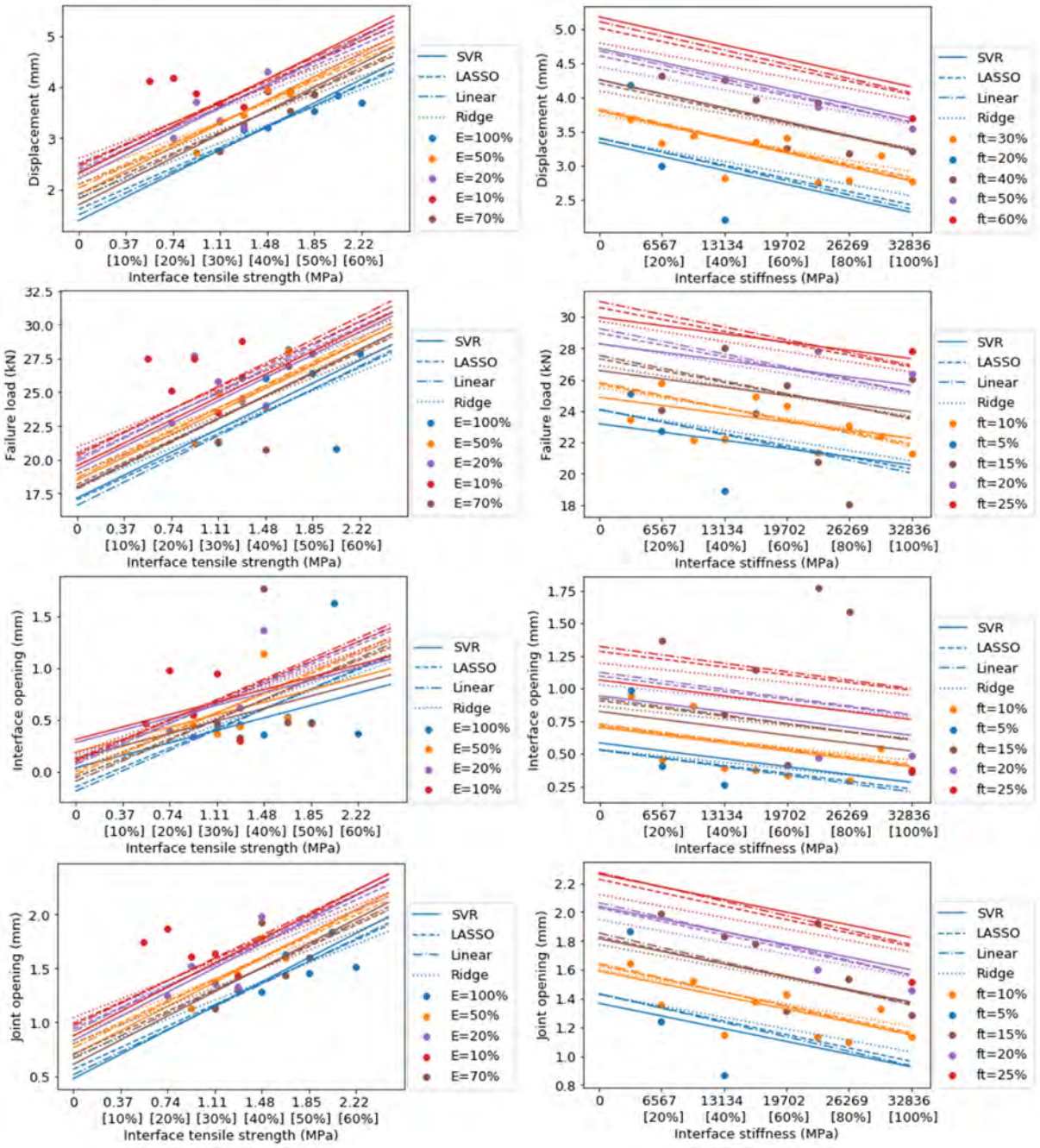

Figure 5.14: Regression models and data values for beam behaviour at failure (displacement, load, interface opening and joint opening) vs. interface tensile strength (left) and interface stiffness (right) for beams with a smooth interface showing partial failure. In brackets the interface properties as a percentage of the concrete properties.

For all features it can be said that an increase in interface tensile strength results in an increase of the output value. On the other hand, an increase of interface stiffness will cause a decrease in the output values. From the slope and spacing between the different lines it can be concluded that the interface tensile strength is governing for predicting the behaviour of the beam. It is seen that all models have a slightly different slope. This indicates that the models have difficulty capturing the data correctly. Even with different slopes the R2-scores do not increase. In the right graphs there is one red data point. This data point does not cross the fitted models, except for the failure load. This is because the model fits the general trend and the general trend would expect higher values than obtained in the simulations. The one data point deviates from this overall trend.

5.4.5. Regression results for beams with a profiled interface showing partial failure

The last regression analysis is carried out for the beams with a profiled interface classified as partial failure. The model results will first be evaluated based on their R2-scores. The predicted values are plotted against the simulated values in Figure 5.15.

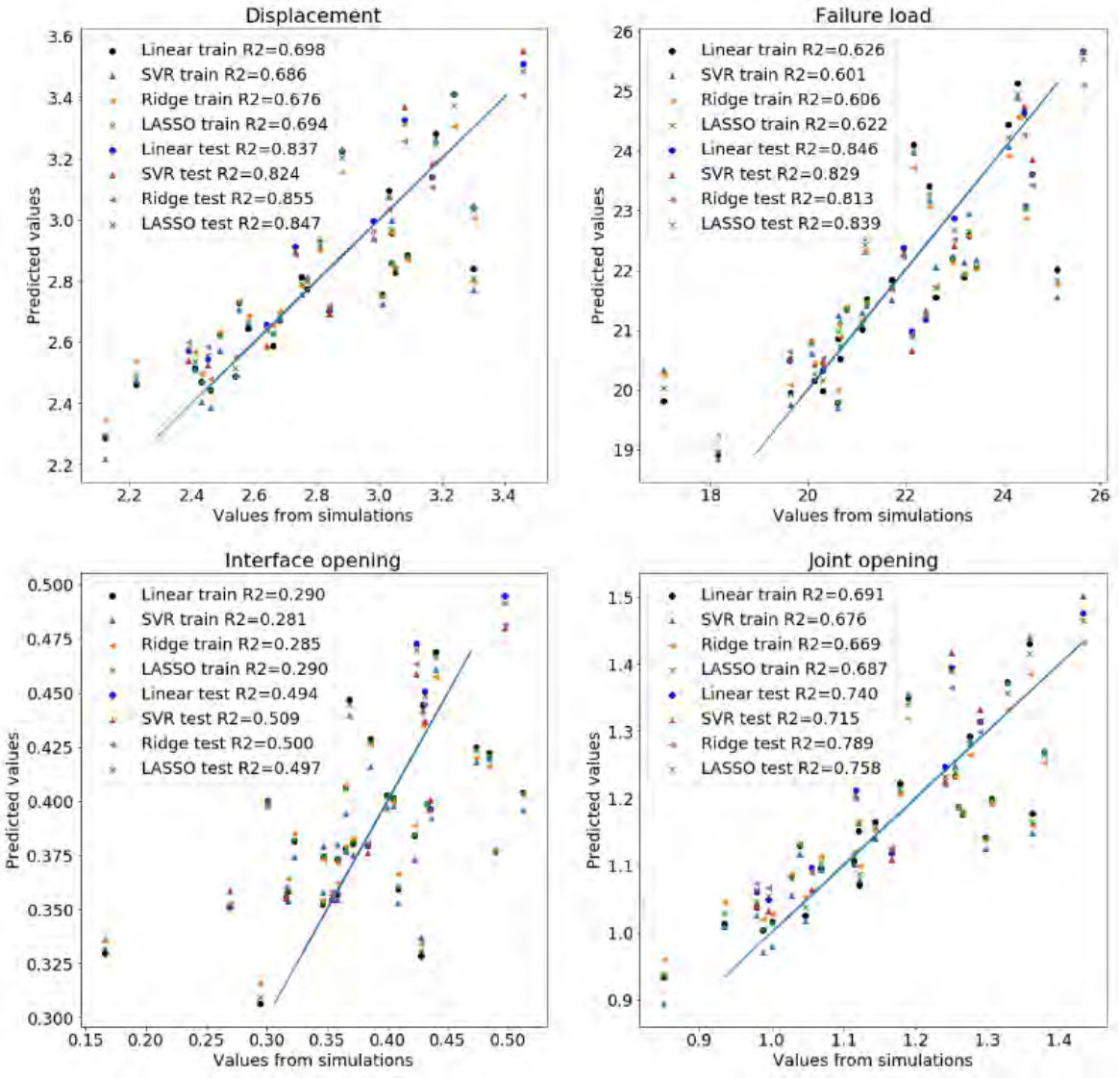

Figure 5.15: Predicted vs. simulated data for train and test data and predicted vs. predicted line of profiled interface showing partial failure for beam behaviour at failure (displacement, failure load, interface opening and joint opening).

The R2-scores of the regression analysis are considered good. The scores are higher compared to the smooth interface, meaning that for a profiled interface partial failure is better predictable. The values are higher for the test set in case of the displacement and failure load. This means that a few scatters were present in the training data set. There are a few data points that deviate from the prediction line. It was already expected that this class would provide better scores compared to the smooth profile, judging from the less scatter of the data. Looking at Figure 4.43b the reason for this can be conducted. It can be seen that partial failure for beams with a profiled interface shows less drops at the end of the load-displacement curves, providing more stable results compared to the drops present in the partial failure for beams with a smooth interface as seen in Figure 4.43a. Again, the interface opening should be neglected, since these scores are almost zero.

Lastly, the dependencies of the results on the interface properties can be visualised by plotting the models and the data sets. The plots are presented in Figure 5.16.

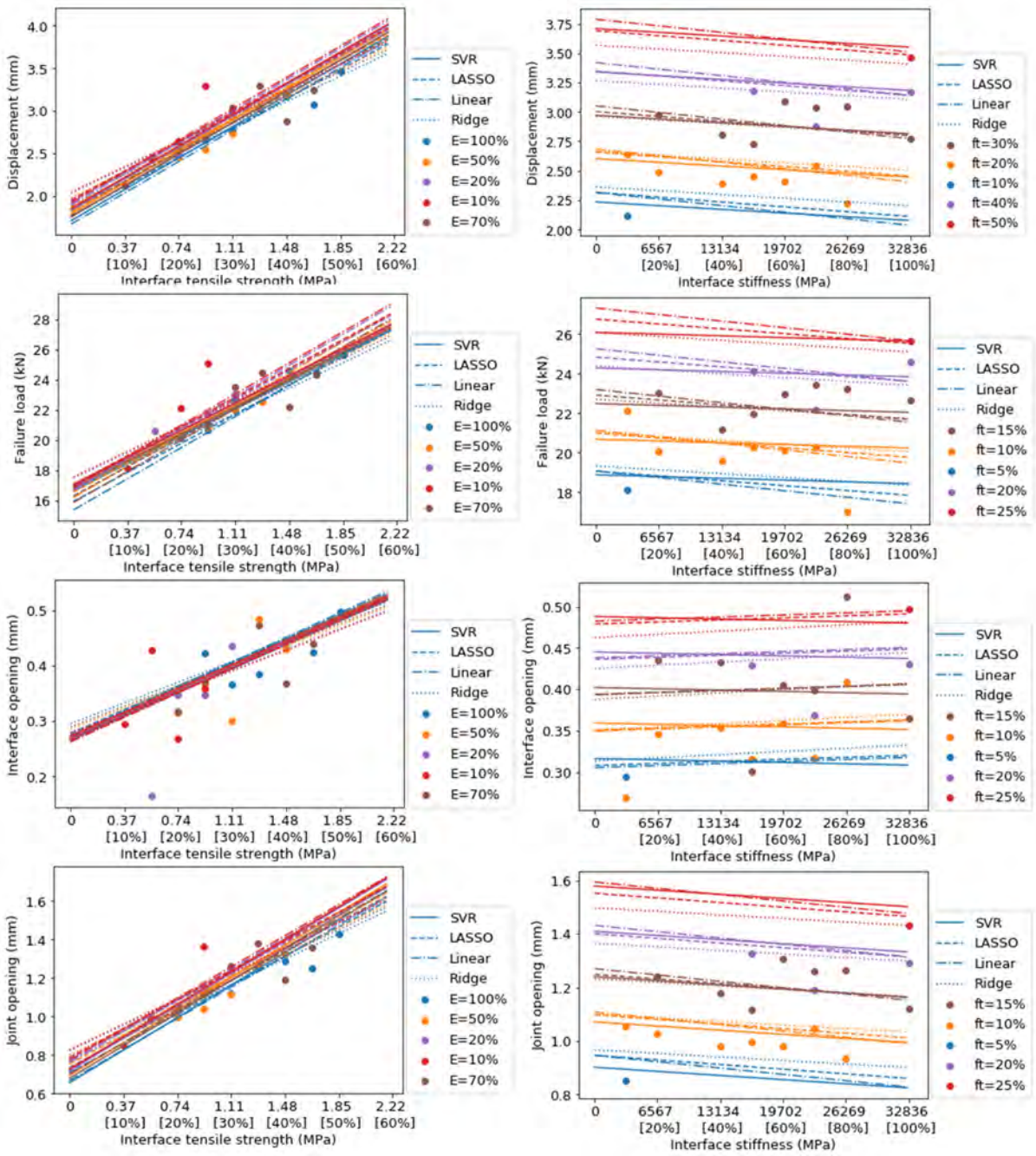

Figure 5.16: Regression models and data values for beam behaviour at failure (displacement, load, interface opening and joint opening) vs. interface tensile strength (left) and interface stiffness (right) for beams with a profiled interface showing partial failure. In brackets the interface properties as a percentage of the concrete properties.

Similar as to the other failure modes, the governing interface property is the interface tensile strength. In the graphs on the left in Figure 5.16 the lines for different interface stiffness are very close together, indicating a low effect of changing the interface stiffness. The plots on the right provide a better visibility of the graph to compare the different models. The models do have different slopes and, in some cases, a different intercept. This again shows that partial failure is more difficult to grasp with the regression models. SVR shows a more moderate influence of the interface properties on the beam behaviour. This time the models do cross the red data point, but show more difficulty in capturing the blue data point with a low interface tensile strength.

5.4.6. Comparison of results for partial failure of smooth and profiled interface

The effect of the interface properties on the structural behaviour of the beams becomes clear from the individual regression analysis. Comparing the results of a smooth and profiled interface allows for investigating the effect of a profiled interface. Also, the effect of the interface properties between a smooth and profiled interface can be concluded. In Figure 5.17 the linear regression models for interface failure of both the beams with a smooth interface as well as for the beams with a profiled interface are shown for partial failure. Only the displacement and failure load are shown for different interface properties to compare the global behaviour. The linear regression model is chosen for simplicity and visibility of the graphs. The models are plotted in Figure 5.17

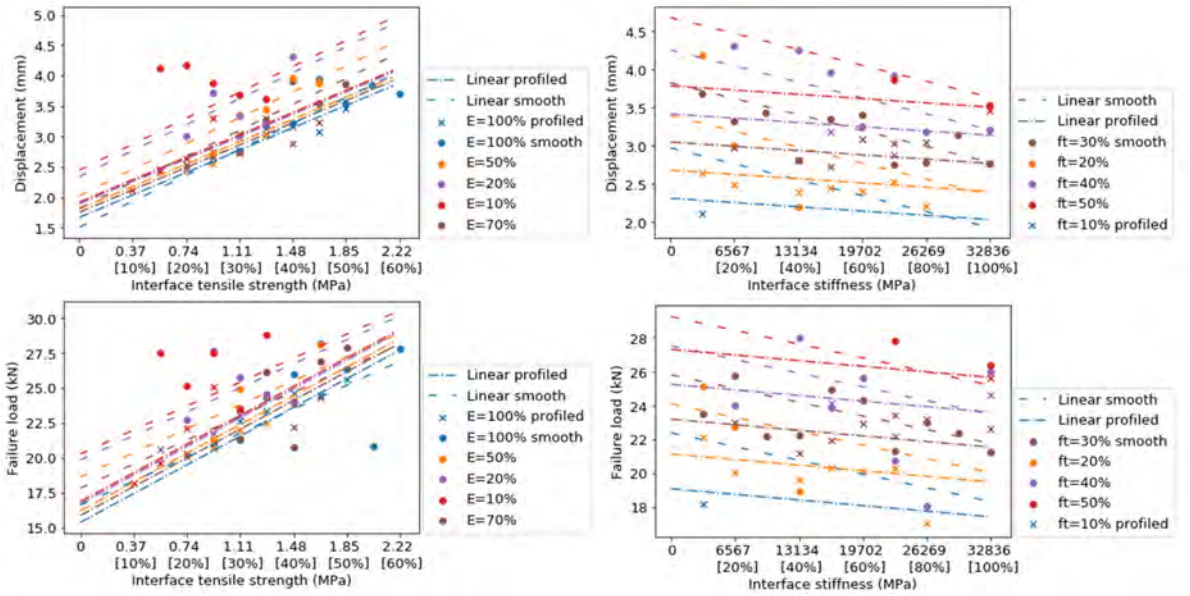

Figure 5.17: Regression models and data values for different interface properties and for beam behaviour at failure for both smooth and profiled interface showing partial failure. In brackets the percentage of the concrete properties.

Due to the scatter in the results of the smooth interface for partial failure, the results should be compared with caution. The smooth profile shows a higher range of failure load and displacement to be reached with the same interface properties. Looking at the slope of the curves, the displacement shows a higher dependency to the interface tensile strength and stiffness for a smooth interface compared to the profiled interface. Due to this it seems that the profiled interface reaches lower displacement and load values. Especially for low interface stiffness the models seem to predict a higher displacement and load for a smooth interface compared to a profiled interface. For the failure load the profiled interface shows a higher dependency on the interface tensile strength compared to the smooth interface. These trends in dependencies were also found for interface failure.

The dependencies are indicated by the regression coefficients, which are shown in the bar plots of Figure 5.18a and 5.18b. The bar plot shows the main difference is in the interface stiffness, where the smooth interface shows a higher dependency compared to the profiled interface. For both displacement and failure load the regression coefficients for the smooth interface reach more than twice the coefficient values to the profiled interface. For the interface tensile strength the dependencies are more similar. Again, the profiled interface seems to show a slightly higher dependency on the interface tensile strength compared to the smooth interface. In partial failure the concrete becomes more governing. With increasing interface tensile strength the concrete cracks and becomes more governing. The higher regression coefficient might include this effect. For the displacement the difference is negligible.

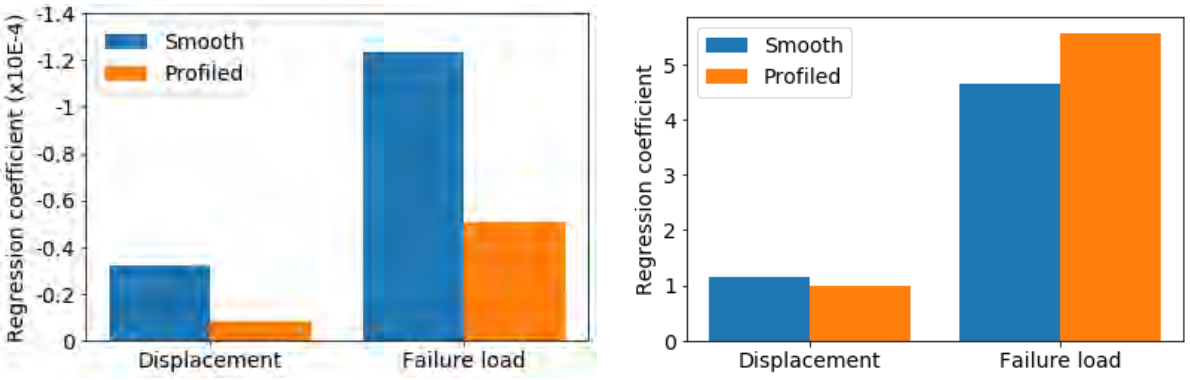

(a) (b)

Figure 5.18: Bar plot indicating regression coefficients of interface stiffness (a) and interface tensile strength (b) of the linear regression model for smooth and profiled interface showing partial failure.

5.4.7. Comparison interface and partial failure smooth interface

A comparison of the dependencies of the interface properties between interface and partial failure for a smooth interface will be made. Again, the results of the partial failure of the smooth interface should be used with caution. Only the coefficients are compared, because plotting the data and models in one graph will disregards the class boundaries. The regression coefficients are shown in Figures 5.19a and 5.19b for the interface stiffness and interface tensile strength respectively.

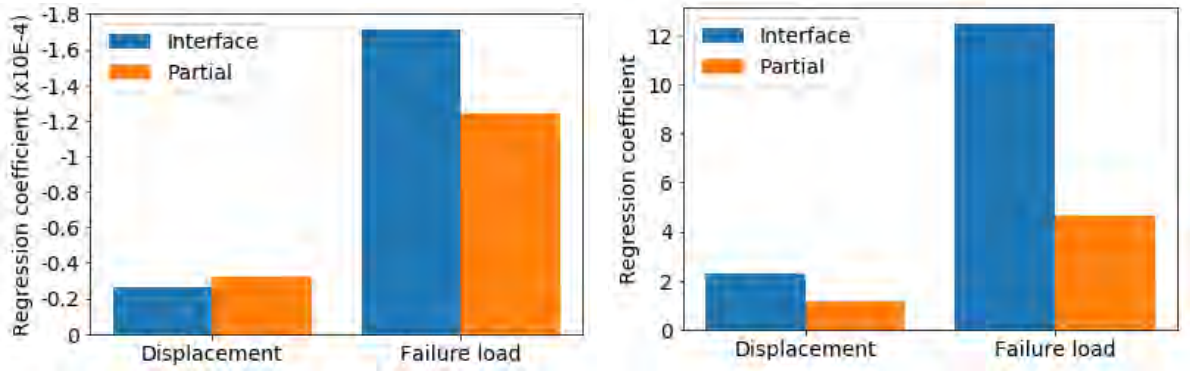

(a) (b)

Figure 5.19: Bar plot indicating regression coefficients of interface stiffness (a) and interface tensile strength (b) of the linear regression model for smooth interface for interface and partial failure.

It can be observed that in most cases a higher dependency is found when the failure mode is interface failure. Only for the displacement the dependency on the interface stiffness is higher for partial failure. It is to be expected that interface failure shows higher dependency, since in partial failure the adjacent materials, concrete and SHCC, start to become more and more involved with increasing interface properties. In case of the interface tensile strength it is seen that for the failure load the dependency for interface failure is even three times the dependency for partial failure.

5.4.8. Comparison interface and partial failure profiled interface

A comparison of the dependencies of the behaviour on the interface properties between interface and partial failure for a profiled interface will be made. The results for a profiled interface were good, allowing for an accurate comparison. Only the coefficients are compared, because plotting the data and models in one graph will disregards the class boundaries. The coefficients are shown in the Figures 5.20a and 5.20b for the interface stiffness and interface tensile strength respectively.

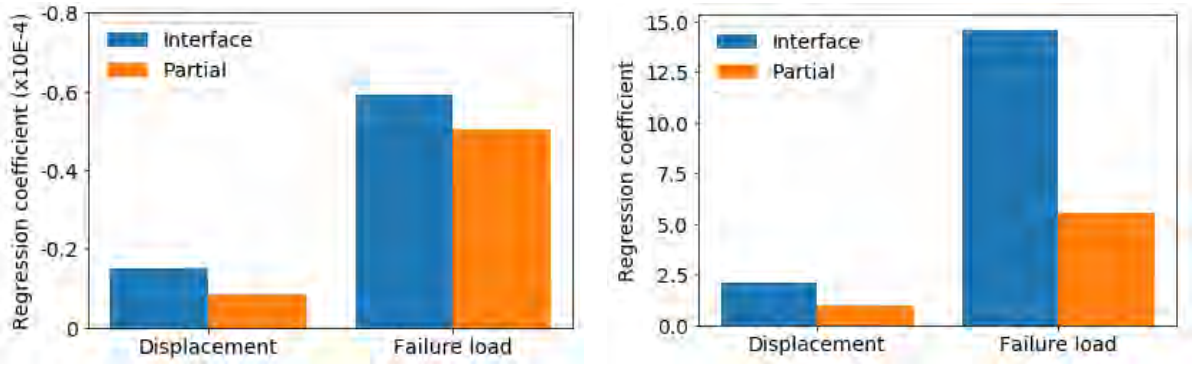

(a) (b)

Figure 5.20: Bar plot indicating regression coefficients of interface stiffness (a) and interface tensile strength (b) of the linear regression model for profiled interface for interface and partial failure.

For the profiled interface the dependency on the interface properties is the highest in case of interface failure. This is to be expected, since in partial failure the adjacent materials start to crack and become governing for the behaviour. For the displacement the regression coefficients are almost twice as high for interface failure compared to partial failure. For the failure load the dependency on the interface tensile strength is three times higher for interface failure compared to partial failure. For the stiffness the difference between failure mode is minor.

6

Conclusion and Recommendations

In this thesis a research question was proposed together with five sub-questions. The answers to these questions are stated in this chapter. Next to answering the questions, recommendations will be given for future work.

6.1. Conclusion

In this thesis the main research question is:

What is the effect of the interface properties between NSC and SHCC in different bond tests using the Lattice model?

The answer to this question is given by answering the sub-questions.

What is the effect of the interface tensile strength on the load capacity and ductility in different bond tests?

In the small-scale test a linear relation is obtained between an increase in tensile strength of the interface and the maximum stress. This holds for both the direct tension and direct shear test in case of interface failure on a smooth interface. In the small-scale test this relation is almost one to one. If the interface tensile strength is doubled, the maximum stress is doubled. If the interface tensile strength is increased further, the adjacent materials start to crack. The strength still increases, but the relation is no longer one to one. The adjacent materials govern the maximum stress. For both direct tension and direct shear on a smooth interface the behaviour is brittle, when failure localizes in the interface.

For a profiled interface in the direct tension test a second peak occurred. The firs peak was observed from failure in the interface on the top of the profile. The second peak is attributed to the failure of the shear planes of the profile. For intermediate interface properties, the final crack propagates from the top of the profile to the concrete. The behaviour is less brittle due to this failure mechanism with the profiled interface. The profile results in a higher maximum stress and fracture energy compared to the smooth interface. However, because the second peak was governing in low interface tensile strength, the effect of increasing the interface tensile strength is limited. Due to this the maximum stress and fracture energy are less influenced by the interface tensile strength compared to the smooth interface.

The direct shear test for a profiled interface showed an increased ductility compared to the smooth interface. The ductility and load capacity increased with increasing interface. Also, the interface tensile strength showed a higher influence on the maximum stress compared to the direct tension test. With an increase in interface tensile strength, more of the adjacent materials cracked. This mechanism benefits from an increase in interface tensile strength, increasing the maximum stress. However, due to the activation of the adjacent materials, these materials become governing for the maximum stress. With the adjacent members starting to crack the ductility is increased even more.

In the interface of a notched-beam test a combination of shear and tensile stresses are present. In case of the notch-beam test the structural behaviour is analysed using the load-displacement response and the crack propagation of the beams. In general, an increase in interface tensile strength leads to an increase of

the failure load and displacement. For low interface tensile strength the cracking follows the geometry of the interface (smooth or profiled) with straight vertical cracks to the concrete. With increasing interface tensile strength the adjacent materials started to crack, leading to more cracks and scatter around the interface. Eventually a plateau in failure load and displacement is reached, after which an increase in interface tensile strength will lead to concrete failure. When partial failure is obtained, the interface tensile strength has already limited effect and the concrete starts to govern the failure mechanism and load capacity. The effect of the interface tensile strength is reduced even further in case of concrete failure. In that case the concrete is governing and the results are not used to investigate the effect of the interface properties anymore.

From the regression analysis it was obtained that the dependency of the beam behaviour on the interface tensile strength regarding the failure load. The regression coefficient is three times higher for interface failure compared to partial failure for both smooth and profiled interfaces. For the displacement this is reduced to two times.

What is the effect of the interface stiffness on the load capacity and ductility in different bond tests?

It should be noted that the interface stiffness in the lattice model is a collection of the stiffness of the three materials present. Altering the interface stiffness will indicate a difference in contribution of the three materials.

From the direct tension test it was found that a high interface stiffness leads to localized cracking for both a smooth and profiled interface. With a decreasing in interface stiffness the damage was smeared out over the interface. This resulted in a slight increase in maximum stress for a smooth interface and a higher increase of the first peak stress in case of a profiled interface. In case of a smooth interface the fracture energy was increased due to the softening and ductility from the scattered failure in the interface. For the profiled interface the effect of changing the interface stiffness on the ductility and fracture energy was limited.

In the direct shear test an increase in the maximum load was found with decreasing the interface stiffness. The activation of the adjacent members was the cause of the increased load capacity with decreasing interface stiffness. For the profiled interface the reduction in interface stiffness caused an increase in activation of the adjacent materials with an increased softening and peak stress as a result.

In the notched beam test a decrease in stiffness increases the failure load and displacement. A decrease in interface stiffness leads to cracking of the adjacent materials. With a decreased interface stiffness the failure mode moves from interface failure to partial failure and from partial failure to concrete failure at a lower interface tensile strength.

From the regression analysis it was seen that the interface stiffness shows a minor effect on the failure load and displacement of the beams. For the profiled interface this is even reduced and also moving from interface failure to partial failure the effect of the interface stiffness reduces even more.

What is the influence of the interface roughness on the load capacity and ductility in different bond tests?

In this thesis the roughness was modelled with a profile. In the small-scale test the addition of the profile led to an increase in load capacity and ductility. In the small-scale test the shapes of the stress-strain curves changed. Often a higher softening was obtained. With a profiled interface the activation of the adjacent materials took place at lower interface properties.

Adding a profile in the direct tension test introduced a second peak, which governed the behaviour at low interface tensile strength. With the application of the profile the fracture energy increased with a factor 10 compared to the smooth interface for the case of 30% interface tensile strength and 100% interface stiffness. But the increase in fracture energy with increasing interface tensile strength or decrease in interface stiffness was limited. For the direct shear test adding a profile had almost no effect on the maximum stress for very low and very high interface properties. The same stress values were obtained for smooth and profiled interfaces in those cases. For intermediate interface properties adding a profile resulted in higher maximum stress. For the direct shear tests the softening was increased with the addition of the profile.

In the notched beam test the failure would localize in the interface for low interface tensile strength. Increasing the interface tensile strength and decreasing the interface stiffness results in partial failure at lower interface properties compared to a smooth interface. The cracks propagate through the concrete, connecting the profile on top.

From the load-displacement curve the smooth interface even showed a higher peak displacement and slightly higher maximum failure load compared to the profiled interface. This means the profiled interface

does not result in higher peak load and displacement values. The maximum capacity of the beam is governed by the concrete and SHCC in both cases. The difference in failure load and displacement seems to increase with decreasing interface stiffness. Eventually higher values are obtained for a smooth interface.

What is the interface parameter with the most significant effect on the load capacity and ductility in different bond tests?

This sub-question can be divided into two parts. First, it is discussed what is seen from the modelled test results itself. Secondly, the results of the regression analysis on the notched-beam data are discussed.

In both the small-scale test and the notched-beam test a strong relation is found between the interface tensile strength and the structural behaviour. In case of the small-scale tests with a smooth interface an increase of interface tensile strength shows the most significant effect on the peak stress. This effect is limited for the direct tension test with a profiled interface, where mainly the first peak is affected. For the fracture energy of the direct tension test, the stiffness plays a more significant role. A decrease in stiffness prevents cracks from localizing, resulting in higher softening of the stress-train curve and an increase in fracture energy. In case of the profiled interface the addition of the profile caused already an increased softening, limiting the effect of the stiffness. In the direct shear test softening was not obtained with changing the interface properties for the smooth interface. In that case softening was obtained with applying a profile. For a profiled interface the softening was increased with increasing interface tensile strength.

In the notched beam test the interface tensile strength has a high influence on the structural behaviour of the beams. Both the displacement and failure load increase and show a strong dependency. This is found for both the smooth and the profiled interface. The profile does not influence the load and displacement at failure. However, a difference in load-displacement response is obtained. For a smooth interface the stress-strain curve showed multiple drops in load from cracking. In case of a profiled interface these drops did not occur and a more consistent load-displacement curve is obtained.

To apply a regression analysis on the data, the data should first be categorized. To categorize the data different classification methods were used. It was found that using k-means time series clustering with dynamic time warping provided the best classification. For this, the time series of the displacement, the ratio of damaged interface elements and ratio of coupling elements were used. These dimensions are best to be used for clustering the data.

From the clustered data it is observed that a lower range of interface tensile strength can reach different failure modes. Changing the interface stiffness over a larger range does not always result in a different failure mode with the same interface tensile strength. However, with a lower interface stiffness the failure mode does change at a lower interface tensile strength compared to a high interface stiffness.

With the clustered data multiple regression analysis have been carried out to find the most significant interface parameter. Different models were used to compare the effect of the interface properties to the structural behaviour of the notched-beam test. All models provided similar results. An increase in interface tensile strength would show a higher increase in the output features compared to decreasing the interface stiffness. This relation was found for both interfaces and both failure modes.

For interface failure the interface properties showed a higher influence on the load-displacement behaviour compared to partial failure. This was for both a smooth and profiled interface. For a profiled interface the interface stiffness showed a lower influence on the output compared to the smooth interface. Only for the interface tensile strength the profiled interface showed a higher regression coefficient compared to the smooth interface for both failure modes.

All in all, it can be stated that the interface properties influence the structural behaviour of the notched-beam. Both interface stiffness and interface tensile strength affect the load-displacement response of the beams. Multiple combinations of interface properties can result in the same beam behaviour. With adding a profile in the interface the influence of the interface properties decreases, but the same relation is found. An increase in interface tensile strength often has more influence in increasing the failure load and displacement compared to the interface stiffness. This general influence is also found in the small-scale tests. However, in the small-scale test the softening is influenced by different interface properties for different test methods. One significant parameter cannot be assigned for the ductility.

What bond test is recommended for investigating the effect of different interface properties?

The suitability of the different bond test modelled with the lattice model can be divided into two parts. It is concluded if the lattice model is suitable for modelling the different bond tests by comparing the results with literature and it is concluded what bond test can be used best to investigate the effect of different interface properties.

With regard to the direct tension method, the results in terms of failure mode were comparable to results found in literature, especially for the smooth interface. For the profiled interface the results showed a second peak in the stress-crack opening curve. This peak is obtained in literature, but is often lower compared to the first peak. This could be due to the modelling, the used interface properties or the shape of the profile. The fracture energy was found to be lower compared to values in literature. This had two reasons. One is that the cracks localize in the weaker interface resulting in a brittle behaviour. This especially counts for the smooth interface. This is the cause of how the interface is modelled in the lattice model. The randomness of the element orientation is reduced with modelling the interface with one row. However, it was seen that for cracking in the concrete, the fracture energy was still lower compared to literature. This indicates that in general the lattice model has a more brittle behaviour.

For the direct shear method the smooth interface showed a brittle behaviour of the stress-strain curve as well. In literature a higher ductility was obtained. In this test method a few interface elements were loaded under compression, dominating the behaviour. The ratio between the tensile strength and compressive strength was already lowered in this thesis compared to the actual ratio of normal strength concrete. Because of these aspects the applicability of the lattice model for the direct shear test is arguable. The effect of the different interface properties on the behaviour can still be investigated. The addition of a profile in the interface provided results comparable to experiments. This effect is, therefore, found suitable to investigate with the direct shear test and the lattice model.

For the notched-beam test the three different interface cases, smooth, epoxy resin and profiled, were compared to the experimental testing results.

Preparing the interface with roughness will increase the interface performance and can lead to partial failure as is the case with an epoxy resin layer. A sample with corresponding load-displacement curve was not found from the data set formed in this thesis. A similar crack propagation was found in one case, but the load was over-estimated and the displacement was underestimated. This stiffness difference comes from the modelling of the SHCC with the lattice model. For failure modes, where the SHCC is activated, the results will thus be differentiating from the actual behaviour.

Low interface properties in case of smooth interfaces would compare to the reality in both crack behaviour and load-displacement curve. In case of the profiled interface, higher interface properties are found to give equal behaviour in load-displacement and crack propagation. For these two cases the lattice model was found to predict the behaviour found from experiments. It is, however, expected that the same interface properties would provide results comparable to the experiments. There was a combination of interface properties found that resulted in interface failure in the smooth interface and partial failure for the profiled interface. The load-displacement response was in these cases not comparable to experiments.

Although the simulations do not match the experimental results completely, the effect of the interface properties can be investigated. With the range of interface properties used both interface and partial failure with the adjacent materials were obtained in all the different tests used. This means that the test methods are suitable to obtain different failure mechanisms. The effect of changing the interface properties on the interface individually and on the complete specimen can be investigated. Trends were found on the effect of the interface properties and the addition of a profile on the interface and global behaviour. The stiffness was seen to influence the failure mode the least. With the same interface tensile strength a changing stiffness reaching from 20 to 100% did not always change the failure mode, while the interface tensile strength in a smaller range does. With a low interface stiffness it is, however, more difficult to investigate the interface failure, since a small range of interface tensile strength remains. The test set-up with the widest range is the direct tension test on a smooth interface. Up to 50% interface tensile strength can be reached to still have interface failure. This allows to investigate both the interface and partial failure. For the other test method the tensile strength was limited to 15% or even 7.5% with an interface stiffness of 100%. For the notched beam test the ranges are higher allowing for up to 25% and 30% interface tensile strength at 100% interface stiffness for smooth and profiled interface respectively. This range reduces with decreasing interface stiffness. From this point of view

the notched-beam test allows for a wider range of interface properties to be tested for interface failure. This means that in both modelling and experimental testing, the notched-beam test will be able to have failure localized in the interface for higher interface properties.

The notch beam test provides information on difference in crack pattern and load-displacement response. This is for the combination of shear and tension stresses. The small-scale tests allow for testing tension and shear individually. Additionally, the softening effect can be measured in these tests. On top of this, the small-scale tests have the advantage of being simple to analyse. The computational time of the small-scale test was significantly lower compared to the notch-beam test, generating more information in a short period of time.

6.2. Recommendations

In this thesis the lattice model is used to investigated the effect of the interface properties on the interface behaviour in different bond tests. The interface properties considered are interface stiffness and interface tensile strength. There is, however, one more parameter that is defined for the material properties of the beam elements in the lattice model. The interface compressive strength is in this thesis set to be ten times the interface tensile strength. This input ratio was found from calibrating the shear stress from the direct shear test to be two times the tensile strength from the direct tension test. Still the direct shear test with a smooth interface showed too brittle behaviour due to the interface elements loaded in compression governing the behaviour. The ratio found from the small-scale test is applied to the notched-beam test. However, this ratio is an assumption and could be found to change the notched-beam behaviour. This effect is left out in this thesis but might bring new insights and better modelling behaviour. Also, modelling of the interface with one row of elements leads to a more brittle behaviour in the direct tension test, reducing the fracture energy.

In the small-scale tests a brittle behaviour was observed in case of a smooth interface for both direct tension and direct shear. In literature a more ductile behaviour and higher fracture energy was found. This can be due to the more brittle behaviour of the lattice model or due to modelling of the interface with one row of elements. For a more accurate behaviour, alterations of the model should be investigated to gain a more ductile behaviour.

In this thesis a micro-scale roughness is modelled by changing the interface properties of a smooth interface. It was found that for the use of an epoxy layer on the interface the data generated in this study could not reach the same load-displacement curve. This was due to the SHCC being modelled for accurately representing crack widths, overestimating the stiffness of the SHCC. It was however seen that there are limited cracks in the SHCC. Therefore, it is recommended to try to see what the effect is of modelling the SHCC with correct stiffness rather than focusing on crack widths.

Next to micro-scale roughness a profile is used to simulate a macro-scale roughness. Different roughness profiles are not considered, while it is interesting to dig deeper into the effect of adding a profile in the interface. In this thesis it was seen that the effect of the interface properties reduces with the presence of the profile. How this relate to different roughness parameter is not considered. From literature it was seen that different profiles already influence the softening of the stress-strain curve [37]. Investigating different profiles might help in finding the most efficient profile for the wanted global behaviour or more efficient material use.

The reason why this is not considered is mainly due to time limits. The lattice model takes three to five days to generate the output of a single beam model. With limit computational time the effect of the compressive strength and the roughness parameter is left out. The lattice model does show good results looking at crack propagation and structural behaviour output. However, a faster method would be useful to generate more data in a shorter period of time. This could be with the use of other modelling programs, or adjusting the lattice model.

Lastly, a regression analysis was carried out in this thesis with different regression models. For the limited number of input properties a simple linear regression already provides a good insight into the effect of the interface properties on the beam behaviour. In case of more interface properties the use of LASSO could be useful. It is recommended to focus on the global behaviour of the beams for an accurate prediction of the behaviour.

Bibliography

[1] Luković, M., Dong, H., Šavija, B., Schlangen, E., Ye, G., & Breugel, K. van. (2014). Tailoring strain-hardening cementitious composite repair systems through numerical experimentation. Cement and Concrete Composites, 53, 200–213. https://doi.org/10.1016/j.cemconcomp.2014.06.017

[2] Mustafa, S., Singh, S., Hordijk, D., Schlangen, E., & Luković, M. (2022). Experimental and numerical investigation on the role of interface for crack-width control of hybrid SHCC concrete beams. Engineering Structures, 251. https://doi.org/10.1016/j.engstruct.2021.113378

[3] Van Zijl GPAG, Slowik V. (2017). A Framework for Durability Design with Strain-Hardening Cement-Based Composites (SHCC) State-of-the-Art Report of the RILEM Technical Committee; 22. https://doi.org/10.1007/978-94-024-1013-6

[4] Mechtcherine, V. (2013). Novel cement-based composites for the strengthening and repair of concrete structures. In Construction and Building Materials, 41, 365–373. https://doi.org/10.1016/j.conbuildmat.2012.11.117

[5] Singh, S. (2019). Influence of Interface and Type of Strain Hardening Cementitious Composite (SHCC) on Crack Control in SHCC-Concrete Hybrid Beams. (Master thesis) http://resolver.tudelft.nl/uuid:5d59fd89-6ec4-405e-9fda-b247f1ae8789

[6] Aysha, H., Murugesan, A., Ramsundar, K. R., & Velrajkumar, G. (2014). An Overview of Interface Behaviour between Concrete to Concrete. In International Journal of Advanced Structures and Geotechnical Engineering 3(2). https://www.researchgate.net/publication/307429938

[7] Zanotti, C., & Randl, N. (2019). Are concrete-concrete bond tests comparable? Cement and Concrete Composites, 99, 80–88. https://doi.org/10.1016/j.cemconcomp.2019.02.012

[8] Harrass, O. (2020). Interfacial behavior of hybrid SHCC-Concrete beams with a joint at midspan. (Master thesis) http://resolver.tudelft.nl/uuid:f5b2c7f1-fc84-459b-8a61-3eb3bc43254e

[9] Akçaoğlu, T., Tokyay, M., & Çelik, T. (2005). Assessing the ITZ microcracking via scanning electron microscope and its effect on the failure behavior of concrete. Cement and Concrete Research, 35(2), 358–363. https://doi.org/10.1016/j.cemconres.2004.05.042

[10] Muslim, F. (2020). A Review on The Microstructure of Interfaces in Reinforced Concrete and Its Effect on The Bond Strength. CSID Journal of Infrastructure Development, 3(1), 102. https://doi.org/10.32783/csid-jid.v3i1.105

[11] Hui-cai, X., Geng-ying, L. & Guang-jing, X. (2002) Microstructure model of the interfacial zone between fresh and old concrete. J. Wuhan Univ. Technol. Mat. Sci. Ed. 17(4), 64–68. https://doi.org/10.1007/BF02838421

[12] Zhang, Y., Zhu, P., Liao, Z., &; Wang, L. (2020). Interfacial bond properties between normal strength concrete substrate and ultra-high performance concrete as a repair material. Construction and Building Materials, 235. https://doi.org/10.1016/j.conbuildmat.2019.117431

[13] Feng, S., Xiao, H., Liu, R., &; Liu, M. (2022). The bond properties between ultra-high-performance concrete and normal strength concrete substrate: Bond macro-performance and overlay transition zone microstructure. Cement and Concrete Composites, 128. https://doi.org/10.1016/j.cemconcomp.2022.104436

[14] Gao, S., Jin, J., Hu, G., &; Qi, L. (2019). Experimental investigation of the interface bond properties between SHCC and concrete under sulfate attack. Construction and Building Materials, 217, 651–663. https://doi.org/10.1016/j.conbuildmat.2019.05.121

[15] EN1992-1-1 (2004). Eurocode2: Design of Concrete Structures-Part1: General Rules and Rules for Buildings, CEN, Brussels(BE)

[16] Wagner, C., Slowik, V., &; Bretschneider, N. (2013). Characterization of the interface between strain hardening cementitious repair layers and concrete subgrade. Proceedings of the 8th International Conference on Fracture Mechanics of Concrete and Concrete Structures, FraMCoS 2013

[17] Sahmaran, M., Yücel, H. E., Yildirim, G., Al-Emam, M., &; Lachemi, M. (2014). Investigation of the Bond between Concrete Substrate and ECC Overlays. Journal of Materials in Civil Engineering, 26(1), 167–174. https://doi.org/10.1061/(asce)mt.1943-5533.0000805

[18] Júlio, E. N. B. S., Branco, F. A. B., & Silva, V. D. (2005). Concrete-to-concrete bond strength: influence of an epoxy-based bonding agent on a roughened substrate surface. Magazine of Concrete Research, 57(8), 463–468. https://doi.org/10.1680/macr.2005.57.8.463

[19] Feng, S., Xiao, H., Liu, R., Dong, X., Liu, Z., & Liu, H. (2021). The influence of different bond primers on the bond strength of concrete overlays and the microstructure of the overlays transition zone. Cement and Concrete Composites, 119. https://doi.org/10.1016/j.cemconcomp.2021.104023

[20] He, Y., Zhang, X., Hooton, R. D., & Zhang, X. (2017). Effects of interface roughness and interface adhesion on new-to-old concrete bonding. Construction and Building Material, 151, 582–590. https://doi.org/10.1016/j.conbuildmat.2017.05.049

[21] Santos, D. S., Santos, P. M. D., & Dias-Da-Costa, D. (2012). Effect of surface preparation and bonding agent on the concrete-to-concrete interface strength. Construction and Building Materials, 37, 102–110. https://doi.org/10.1016/j.conbuildmat.2012.07.028

[22] Bentz, D. P., de la Varga, I., Muñoz, J. F., Spragg, R. P., Graybeal, B. A., Hussey, D. S., Jacobson, D. L., Jones, S. Z., & LaManna, J. M. (2018). Influence of substrate moisture state and roughness on interface microstructure and bond strength: Slant shear vs. pull-off testing. <i>Cement and Concrete Composite, 87, 63–72. https://doi.org/10.1016/j.cemconcomp.2017.12.005

[23] Neville, A. M. & Neville, A. M. (2011). Properties of Concrete. Pearson.

[24] Dudziak, S., Jackiewicz-Rek, W., & Kozyra, Z. (2021). On the calibration of a numerical model for concrete-to-concrete interface. Materials, 14(23). https://doi.org/10.3390/ma14237204

[25] Bocca, P., &; Valente, S. (1991). Mixed mode fracture of concrete. International journal of Solids Structures, 27(9), 1139-1153.

[26] Ballatore, E., Carpinteri, A, Ferrara, G., &; Melchiorri, G. (1990). Mixed mode fracture energy of concrete. Engineering Fracture Mechanics, 35(3), 145-157

[27] Charalambides, P. G., Cao, H. C., Lund, J., &; Evans, A. G. (1990). Development of a test method for measuring the mixed mode fracture resistance of bi-material interfaces. In Mechanics of Materials (Vol. 8).

[28] Labuz, J. F., & Zang, A. (2012). Mohr-Coulomb failure criterion. Rock Mechanics and Rock Engineering, 45(6), 975–979. https://doi.org/10.1007/s00603-012-0281-7

[29] Carol, I., Prat, P. C., & López, C. M. (1997). Normal/Shear Cracking Model: Application to Discrete Crack Analysis. Journal of Engineering Mechanics, 123(8), 765–773. https://doi.org/10.1061/(asce)0733-9399(1997)123:8(765)

[30] Wagner, C., Bretschneider, N., Villmann, B., & Slowik, V. (2014). Modeling of the bond between strain hardening cementitious repair layers and concrete substrate. SHCC3: Proceedings of the 3rd International RILEM Conference on Strain Hardening Cementitious Composites, Dordrecht, The Netherlands, 3-5 November 2014;

[31] Espeche, A. D., & León, J. (2011). Estimation of bond strength envelopes for old-to-new concrete interfaces based on a cylinder splitting test. Construction and Building Materials, 25(3), 1222–1235. https://doi.org/10.1016/j.conbuildmat.2010.09.032

[32] Yin, H., Shirai, K., & Teo, W. (2019). Numerical model for predicting the structural response of composite UHPC–concrete members considering the bond strength at the interface. Composite Structures, 215, 185–197. https://doi.org/10.1016/j.compstruct.2019.02.040

[33] Savino, V., Lanzoni, L., Tarantino, A. M., & Viviani, M. (2020). A cohesive FE model for simulating the cracking/debonding pattern of composite NSC-HPFRC/UHPFRC members. Construction and Building Materials, 258. https://doi.org/10.1016/j.conbuildmat.2020.119516

[34] Pan, Z., Ma, R., Wang, D., &; Chen, A. (2018). A review of lattice type model in fracture mechanics: theory, applications, and perspectives. Engineering Fracture Mechanics, 190, 382–409. https://doi.org/10.1016/j.engfracmech.2017.12.037

[35] Schlangen, H. E. J. G. (1993). Experimental and Numerical Analysis of Fracture Processes in Concrete [Dissertation, Delft University of Technology]. TU Delft Repository. http://resolver.tudelft.nl/uuid:8e0d58b0-b5d0-4471-89a3-607ee4d6f7da

[36] Lilliu, G., & Van Mier, J. (2003). 3D lattice type fracture model for concrete. Engineering Fracture Mechanics, 70(7–8), 927–941. https://doi.org/10.1016/s0013-7944(02)00158-3

[37] Luković, M., Schlangen, E., Ye, G., & Šavija, Bo. (2013). Impact of surface roughness on the debonding mechanism in concrete repairs. Proceedings of the 8th International Conference on Fracture Mechanics of Concrete and Concrete Structures, FraMCoS 2013.

[38] Stander, H. (2007). Interfactial bond properties for ECC overlay systems. MSc thesis, University of Stellenbosch

[39] Hordijk, D. A. (1989). Deformation-controlled uniaxial tensile tests on concrete (25.5-89-15/VFA).

[40] Akita, H., Koide, H., Tomon, M., &; Sohn, D. (2003). A practical method for uniaxial tension test of concrete. In Materials and Structures / Matdriaux et Constructions, 36, 365-371.

[41] Gu, D., Mustafa, S., Pan, J., & Luković, M. (2022). Reinforcement-concrete bond in discrete modeling of structural concrete. Computer-Aided Civil and Infrastructure Engineering, 00, 1– 22. https://doi.org/10.1111/mice.12937

[42] Lloyd, S. (1982). Least squares quantization in PCM. IEEE Transactions on Information Theory, 28(2), 129-137. doi: 10.1109/TIT.1982.1056489

[43] Arthur, David & Vassilvitskii, Sergei. (2007). K-Means++: The Advantages of Careful Seeding. Proc. of the Annu. ACM-SIAM Symp. on Discrete Algorithms, 8, 1027-1035. https://doi.org/10.1145/1283383.1283494.

[44] Tavenard, R., Faouzi, J., Vandewiele, G., Divo, F., Androz, G., Holtz, C., Payne, M., Yurchak, R., Rußwurm, M., Kolar, K. & Wood, E. (2020). Tslearn, A Machine Learning Toolkit for Time Series Data. Journal of Machine Learning Research, 21(118), 1-6. http://jmlr.org/papers/v21/20-091.html

[45] F. Petitjean, A. Ketterlin & P. Gancarski (2011). A global averaging method for dynamic time warping, with applications to clustering. Pattern Recognition, Elsevier, 44(3), 678-693. https://doi.org/10.1016/j.patcog.2010.09.013

[46] Field, A. (2018). Discovering Statistics Using IBM SPSS Statistics, fifth edition. SAGE Publications.

[47] Hastie, T., Tibshirani, R. & Friedman, J. (2017). The Elements of Statistical Learning: Data Mining, Inference, and Prediction, Second Edition. Springer Publishing

[48] Cortes, C., Vapnik, V., &; Saitta, L. (1995). Support-Vector Networks Editor. Machine Leaming, 20. Kluwer Academic Publishers

[49] Farouk, A. I. B., & Jinsong, Z. (2022). Prediction of Interface Bond Strength Between Ultra-High-Performance Concrete (UHPC) and Normal Strength Concrete (NSC) Using a Machine Learning Approach. Arabian Journal for Science and Engineering. https://doi.org/10.1007/s13369-021-06433-6

[50] Tibshirani, R. (1996). Regression Shrinkage and Selection via the Lasso. Journal of the Royal Statistical Society. Series B (Methodological), 58(1)).

[51] Smola, A. J., Schölkopf, B., & Schölkopf, S. (2004). A tutorial on support vector regression. In Statistics and Computing, 14, Kluwer Academic Publishers.

A

Data set small-scale test simulations

In this appendix the sample interface properties are stated together with the maximum stress obtained from the simulations of the small-scale tests.

Table A.1: Small-scale test input interface properties

Sample number	Interface stiffness (MPa)	Interface tensile strength (MPa)	Interface compressive strength (MPa)
1	32836	1.11	-11.1
2	16418	1.11	-11.1
3	6567.2	1.11	-11.1
4	32836	0.55	-5.55
5	32836	0.2775	-2.775
6	16418	0.555	-5.55
7	16418	0.2775	-2.775
8	6567.2	0.555	-5.55
9	6567.2	0.2775	-2.775
10	16418	0.185	-1.85
11	32836	1.85	-18.5
12	32836	3.7	-37
13	32836	2.59	-25.9
14	32836	3.33	-33.3
15	3283.6	1.85	-18.5
16	3283.6	2.59	-25.9

Table A.2: Small-scale test simulation output data

Test method	Direct shear test		Direct tension test	
Interface geometry	Smooth	Profiled	Smooth	Profiled
Sample number	Peak stress		Peak stress	
1	2.231933	2.983567	1.029254	1.422133
2	2.536311	3.753122	1.096538	1.467467
3	2.857733	4.239033	1.157244	1.4443
4	1.175	1.543778	0.508701	1.359278
5	0.546113	0.746383	0.259249	0.857531
6	1.284744	2.031522	0.543923	1.3131
7	0.62072	1.028184	0.274134	0.934137
8	1.427244	2.516189	0.57323	1.304
9	0.780012	1.415456	0.284606	0.78917
10	0.398773	0.651509	0.1846	0.621416
11	3.908578	5.012511	1.715422	1.748289
12	9.000222	8.635478	3.101511	3.088711
13	5.557289	6.584067	2.401167	2.435178
14	8.031789	7.887111	2.978711	2.9932
15	5.704389	7.277156	1.916678	2.429944
16	8.3623	7.357333	2.679422	2.595567

B

Boundary conditions direct shear test

In the Figures B.1a-B.1d shows the results of the direct shear test on a smooth interface for sample 1 with different boundary conditions.

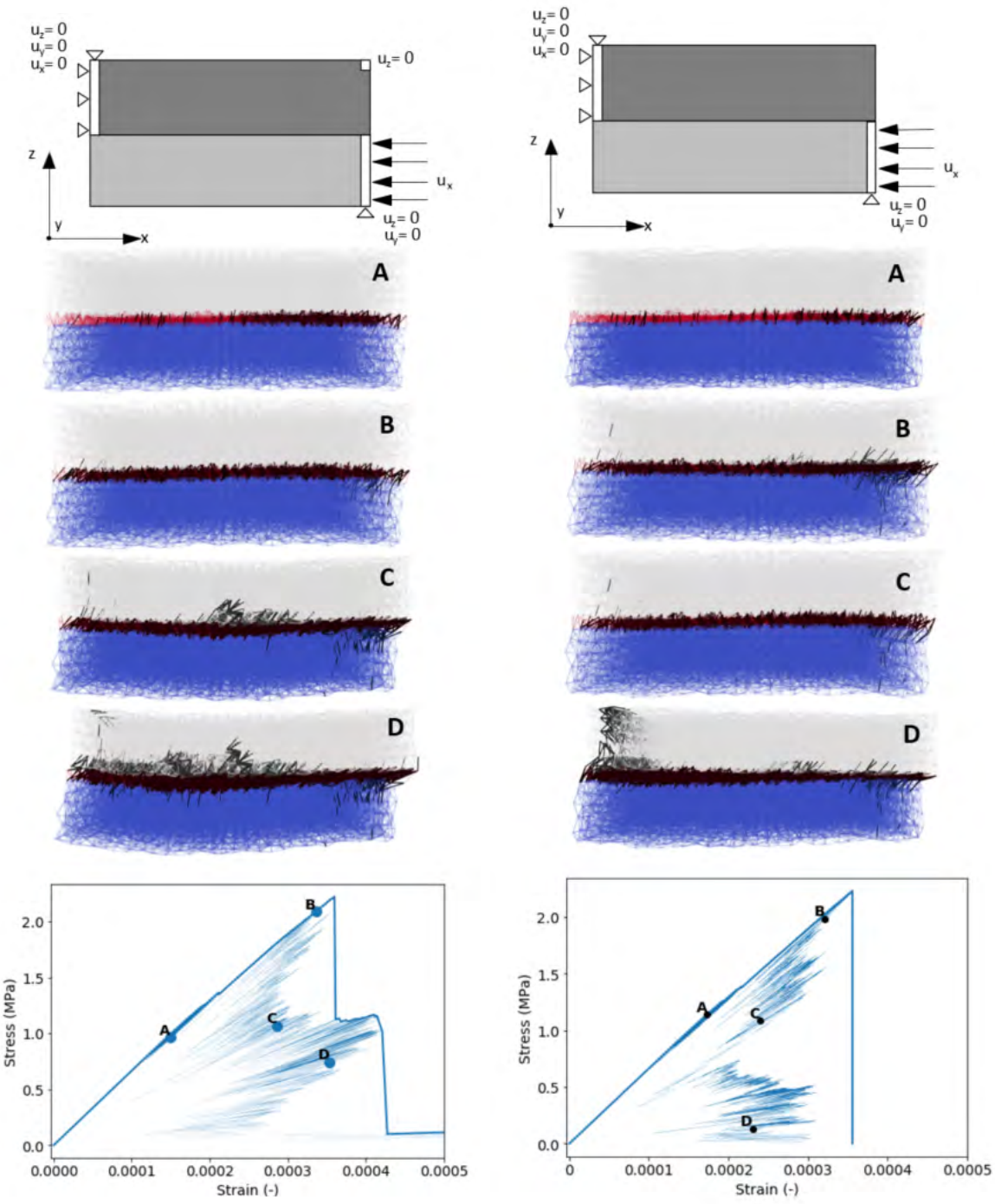
$u_z = 0$
$u_y = 0$
$u_x = 0$
$u_z = 0$
u_x
$u_z = 0$
$u_y = 0$
z
y
x
A
B
C
D
Stress (MPa)
Strain (-)
0.0
0.5
1.0
1.5
2.0
0.0000
0.0001
0.0002
0.0003
0.0004
0.0005
0

(a) (b)

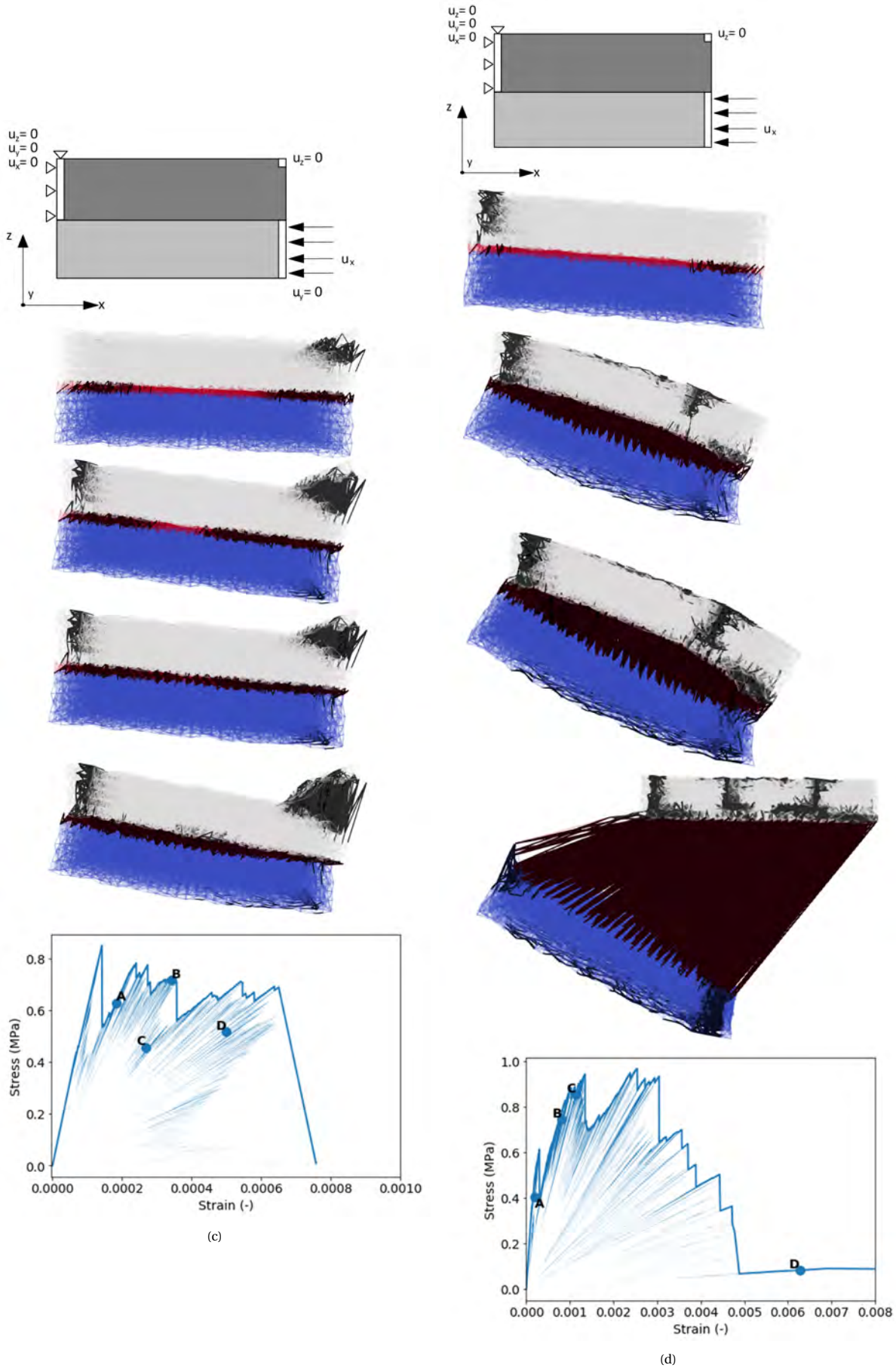

(c)

(d)

Figure B.1: Deformed damaged lattice x200 (a,b) x100 (c,d) and stress strain curve for different boundary conditions (a-d)

C

Data set beam simulations

In this appendix the input and output of the beam simulations are stated. Empty data is for samples failing in concrete. In these cases a point of failure with the set criteria was not met. A displacement was set to which the data for classification was used.

Table C.1: Input data beams simulations with smooth interface

Sample number	E interface (MPa)	f_t interface (MPa)	f_c interface (MPa)
1	32836	1.11	-11.1
2	32836	0.74	-7.4
3	32836	0.37	-3.7
4	32836	0.925	-9.25
5	32836	0.555	-5.55
6	32836	0.185	-1.85
7	16418	1.11	-11.1
8	16418	0.74	-7.4
9	16418	0.37	-3.7
10	16418	0.925	-9.25
11	16418	0.555	-5.55
12	16418	0.185	-1.85
13	6567.2	1.11	-11.1
14	6567.2	0.74	-7.4
15	6567.2	0.37	-3.7
16	6567.2	0.925	-9.25
17	6567.2	0.555	-5.55
18	6567.2	0.185	-1.85
19	3283.6	1.11	-11.1
20	3283.6	0.74	-7.4
21	3283.6	0.37	-3.7
22	3283.6	0.925	-9.25
23	3283.6	0.555	-5.55
24	3283.6	0.185	-1.85
25	22985.2	1.11	-11.1
26	22985.2	0.74	-7.4
27	22985.2	0.37	-3.7
28	22985.2	0.925	-9.25
29	22985.2	0.555	-5.55
30	22985.2	0.185	-1.85
31	32836	1.48	-14.8
32	32836	1.85	-18.5
33	32836	2.22	-22.2

Sample number	E interface (MPa)	f_t interface (MPa)	f_c interface (MPa)
34	32836	2.59	-25.9
35	32836	2.96	-29.6
36	3283.6	2.59	-25.9
37	32836	2.405	-24.05
38	32836	1.665	-16.65
39	32836	2.035	-20.35
40	32836	1.295	-12.95
41	3283.6	2.405	-24.05
42	22985.2	1.295	-12.95
43	16418	1.295	-12.95
44	6567.2	1.295	-12.95
45	3283.6	1.295	-12.95
46	22985.2	1.48	-14.8
47	16418	1.48	-14.8
48	6567.2	1.48	-14.8
49	3283.6	1.48	-14.8
50	3283.6	2.22	-22.2
51	16418	2.405	-24.05
52	3283.6	2.035	-20.35
53	16418	2.22	-22.2
54	3283.6	1.665	-16.65
55	3283.6	1.85	-18.5
56	6567.2	1.665	-16.65
57	16418	1.665	-16.65
58	22985.2	1.665	-16.65
59	22985.2	1.85	-18.5
60	13134.4	0.185	-1.85
61	19701.6	0.185	-1.85
62	26268.8	0.185	-1.85
63	13134.4	0.555	-5.55
64	19701.6	0.555	-5.55
65	26268.8	0.555	-5.55
66	13134.4	0.925	-9.25
67	19701.6	0.925	-9.25
68	26268.8	0.925	-9.25
69	13134.4	0.37	-3.7
70	19701.6	0.37	-3.7
71	26268.8	0.37	-3.7
72	13134.4	1.11	-11.1
73	19701.6	1.11	-11.1
74	26268.8	1.11	-11.1
75	13134.4	1.295	-12.95
76	19701.6	1.295	-12.95
77	26268.8	1.295	-12.95
78	13134.4	1.48	-14.8
79	19701.6	1.48	-14.8
80	26268.8	1.48	-14.8
81	13134.4	1.665	-16.65
82	19701.6	1.665	-16.65
83	26268.8	1.665	-16.65
84	13134.4	0.74	-7.4
85	19701.6	0.74	-7.4
86	26268.8	0.74	-7.4
87	9850.8	1.11	-11.1
88	29552.4	1.11	-11.1

Table C.2: Output beam simulations with smooth interface

Sample number	Failure load (kN)	Displacement (mm)	Interface opening (mm)	Joint opening (mm)
1	21.25	2.77	0.37057	1.136086
2	15.36	1.92	0.29477	0.793088
3	13.15	1.23	0.2128	0.457001
4	17.87	2.10	0.26358	0.838464
5	14.29	1.80	0.24131	0.752832
6	10.52	0.55	0.069532	0.153956
7	24.95	3.35	0.37065	1.379556
8	18.90	2.20	0.25117	0.864804
9	12.96	1.39	0.14502	0.540253
10	21.29	2.73	0.44814	1.128174
11	15.39	1.88	0.27044	0.769961
12	10.94	0.91	0.1494	0.323871
13	20.72	3.79	1.77038	1.831842
14	22.75	3.00	0.40237	1.240815
15	14.23	1.52	0.23462	0.594842
16	27.70	3.72	0.33414	1.521154
17	19.18	2.31	0.29661	0.926432
18	11.39	1.15	0.18355	0.452001
19	23.49	3.68	0.94624	1.640222
20	25.13	4.18	0.98101	1.864862
21	18.86	2.08	0.21044	0.801772
22	27.52	3.87	0.55117	1.611403
23	27.48	4.13	0.4707	1.747399
24	14.53	1.53	0.15152	0.590139
25	21.33	2.75	0.47043	1.13203
26	16.79	1.77	0.21862	0.675605
27	11.15	1.10	0.15529	0.417774
28	20.04	2.51	0.28777	1.021802
29	15.64	1.97	0.26471	0.822352
30	9.22	0.57	0.139629	0.189654
31	26.02	3.21	0.35455	1.286361
32	20.03	3.68	1.76996	1.796484
33	27.84	3.70	0.3718	1.515156
34		4.00		
35		4.00		
36	21.56	4.65	0.68872	1.620923
37	28.08	3.93	0.50801	1.566168
38	28.21	3.94	0.52806	1.628649
39	20.82	3.84	1.63024	1.843123
40	24.33	3.17	0.45557	1.300948
41		3.68		
42	26.13	3.27	0.32486	1.307473
43	13.24	3.80	2.92873	2.122955
44	27.42	3.73	0.43789	1.55476
45	28.78	3.62	0.29491	1.425342
46	25.64	3.46	0.49664	1.431787
47	26.17	3.52	0.50052	1.461775
48	24.03	4.31	1.3673	1.986042
49	29.09	3.63	0.30973	1.423501
50	23.10	4.68	0.51648	1.758933
51		4.00		
52		1.78		
53		4.00		
54	28.71	3.88	0.42671	1.4965
55		4.00		

Sample number	Failure load (kN)	Displacement (mm)	Interface opening (mm)	Joint opening (mm)
56	22.00	3.90	1.576	1.828787
57	28.12	3.88	0.52043	1.595865
58	26.94	3.54	0.48164	1.438761
59	27.86	3.86	0.46536	1.600221
60	11.87	0.90	0.017263	0.304845
61	9.06	0.57	0.139488	0.19223
62	10.40	0.74	0.055354	0.238822
63	16.67	1.76	0.18107	0.663533
64	14.58	1.75	0.26198	0.712384
65	15.26	1.63	0.2531	0.636749
66	24.51	3.26	0.34483	1.344562
67	21.09	2.96	0.56624	1.259691
68	20.91	2.49	0.29876	0.98645
69	13.10	1.45	0.18283	0.577866
70	14.10	1.50	0.24405	0.587681
71	12.44	1.49	0.22567	0.621257
72	22.24	2.81	0.39313	1.145345
73	24.30	3.41	0.33127	1.431302
74	23.04	2.78	0.29337	1.100822
75	23.04	3.58	1.00858	1.589954
76	25.91	3.67	0.49079	1.539639
77	24.73	3.21	0.4228	1.308326
78	28.03	4.26	0.80049	1.829348
79	25.62	3.26	0.41016	1.314174
80	18.03	3.18	1.58862	1.537337
81	24.26	3.54	0.70942	1.523066
82	26.55	3.56	0.35497	1.467262
83	27.83	3.82	0.46033	1.574691
84	18.91	2.20	0.26178	0.867805
85	17.54	1.90	0.24049	0.733124
86	16.63	2.04	0.22636	0.834664
87	22.17	3.43	0.86426	1.522268
88	22.38	3.14	0.5421	1.328342

Table C.3: Input data beams simulations with profiled interface

Sample number	E interface (MPa)	f_t interface (MPa)	f_c interface (MPa)
1	32836	1.11	-11.1
2	32836	0.74	-7.4
3	32836	0.37	-3.7
4	32836	0.925	-9.25
5	32836	0.555	-5.55
6	32836	0.185	-1.85
7	16418	1.11	-11.1
8	16418	0.74	-7.4
9	16418	0.37	-3.7
10	16418	0.925	-9.25
11	16418	0.555	-5.55
12	16418	0.185	-1.85
13	6567.2	1.11	-11.1
14	6567.2	0.74	-7.4
15	6567.2	0.37	-3.7
16	6567.2	0.925	-9.25

Sample number	E interface (MPa)	f_t interface (MPa)	f_c interface (MPa)
17	6567.2	0.555	-5.55
18	6567.2	0.185	-1.85
19	3283.6	1.11	-11.1
20	3283.6	0.74	-7.4
21	3283.6	0.37	-3.7
22	3283.6	0.925	-9.25
23	3283.6	0.555	-5.55
24	3283.6	0.185	-1.85
25	22985.2	1.11	-11.1
26	22985.2	0.74	-7.4
27	22985.2	0.37	-3.7
28	22985.2	0.925	-9.25
29	22985.2	0.555	-5.55
30	22985.2	0.185	-1.85
31	32836	1.295	-12.95
32	22985.2	1.295	-12.95
33	16418	1.295	-12.95
34	6567.2	1.295	-12.95
35	3283.6	1.295	-12.95
36	32836	1.48	-14.8
37	22985.2	1.48	-14.8
38	16418	1.48	-14.8
39	6567.2	1.48	-14.8
40	3283.6	1.48	-14.8
41	32836	1.665	-16.65
42	22985.2	1.665	-16.65
43	16418	1.665	-16.65
44	6567.2	1.665	-16.65
45	3283.6	1.665	-16.65
46	32836	1.85	-18.5
47	22985.2	1.85	-18.5
48	16418	1.85	-18.5
49	6567.2	1.85	-18.5
50	3283.6	1.85	-18.5
51	32836	2.035	-20.35
52	22985.2	2.035	-20.35
53	16418	2.035	-20.35
54	6567.2	2.035	-20.35
55	3283.6	2.035	-20.35
56	3283.6	2.22	-22.2
57	3283.6	2.405	-24.05
58	3283.6	2.59	-25.9
59	32836	2.22	-22.2
60	22985.2	2.22	-22.2
61	32836	2.775	-27.75
62	3283.6	2.775	-27.75
63	32836	2.405	-24.05
64	32836	2.59	-25.9
65	32836	2.96	-29.6
66	3283.6	2.96	-29.6
67	13134.4	0.925	-9.25
68	19701.6	0.925	-9.25
69	26268.8	0.925	-9.25
70	13134.4	1.11	-11.1
71	19701.6	1.11	-11.1

Sample number	E interface (MPa)	f_t interface (MPa)	f_c interface (MPa)
72	26268.8	1.11	-11.1
73	13134.4	0.37	-3.7
74	19701.6	0.37	-3.7
75	26268.8	0.37	-3.7
76	13134.4	0.74	-7.4
77	19701.6	0.74	-7.4
78	26268.8	0.74	-7.4
79	13134.4	0.185	-1.85
80	19701.6	0.185	-1.85
81	26268.8	0.185	-1.85
82	9850.8	0.185	-1.85
83	29552.4	0.37	-3.7
84	29552.4	0.185	-1.85

Table C.4: Output beam simulations with profiled interface

Sample number	Failure load (kN)	Displacement (mm)	Interface opening (mm)	Joint opening (mm)
1	22.63	2.77	0.36544	1.120741
2	16.88	1.88	0.19694	0.740312
3	13.87	1.51	0.26929	0.59035
4	20.66	2.66	0.4227	1.122448
5	16.56	1.72	0.1157	0.656926
6	9.69	0.84	0.133482	0.304451
7	21.96	2.73	0.30074	1.116862
8	20.31	2.45	0.31609	0.995029
9	14.68	1.62	0.29363	0.639902
10	20.79	2.55	0.36546	1.039432
11	16.34	1.99	0.25932	0.806858
12	10.42	0.92	0.116397	0.329101
13	17.80	6.17	7.03352	3.120998
14	20.08	2.49	0.34649	1.026972
15	16.17	1.88	0.27107	0.763476
16	21.71	2.75	0.34733	1.143919
17	20.61	2.46	0.16554	0.98755
18	11.12	1.15	0.19459	0.446115
19	22.31	4.79	2.62616	2.235183
20	16.67	3.76	2.78919	2.012833
21	18.15	2.12	0.2942	0.850392
22	18.82	4.99	3.91205	2.543921
23	19.65	2.43	0.42771	1.000259
24	12.25	1.39	0.18587	0.550374
25	23.46	3.04	0.39912	1.259909
26	20.30	2.54	0.31754	1.046752
27	14.45	1.59	0.28386	0.62786
28	21.11	2.68	0.37121	1.113695
29	16.20	1.82	0.22607	0.721072
30	11.05	1.17	0.11771	0.454109
31	23.30	3.04	0.38542	1.255094
32	24.48	3.30	0.47329	1.378497
33	22.50	3.03	0.48375	1.274516
34	25.20	3.53	0.44082	1.499569

Sample number	Failure load (kN)	Displacement (mm)	Interface opening (mm)	Joint opening (mm)
35		3.58		
36	24.61	3.17	0.43071	1.289709
37		2.88		
38	24.12	3.18	0.42911	1.32728
39	25.76	3.56	0.53341	1.498938
40	24.82	3.57	0.58983	1.524063
41	24.44	3.08	0.4237	1.24993
42	24.30	3.24	0.4398	1.357669
43	13.24	3.80	2.92873	2.122955
44	27.42	3.73	0.43789	1.55476
45	27.02	3.58	0.58292	1.449701
46	25.64	3.46	0.49664	1.431787
47	26.17	3.52	0.50052	1.461775
48	27.97	3.60	0.42201	1.454529
49	28.60	3.87	0.3812	1.583377
50	29.98	3.88	0.50941	1.547506
51	26.35	3.31	0.44076	1.330677
52	23.33	3.59	1.00191	1.574827
53		3.34		
54	28.29	4.17	0.57291	1.521696
55	25.18	4.33	0.58183	1.583016
56	25.44	4.42	0.53993	1.577184
57	24.05	4.33	0.67254	1.590113
58		4.33		
59	27.20	3.40	0.48236	1.362116
60	24.17	2.97	0.49587	1.199423
61	23.41	3.85	0.53368	1.336379
62	23.19	3.77	0.5126	1.289925
63	22.94	3.60	0.44552	1.264168
64	24.69	3.38	0.51035	1.255725
65	23.66	3.99	0.47138	1.385058
66		4.00		
67	21.20	3.01	0.48913	1.29705
68	22.42	2.84	0.38343	1.166422
69	20.62	2.58	0.32223	1.067781
70	21.17	2.81	0.43304	1.178341
71	22.96	3.09	0.40472	1.305256
72	23.21	3.05	0.51212	1.265293
73	14.70	1.77	0.33513	0.730171
74	14.35	1.65	0.26789	0.666186
75	13.61	1.44	0.21729	0.554715
76	19.62	2.39	0.35368	0.979168
77	20.13	2.41	0.35865	0.979277
78	17.04	2.22	0.40881	0.934651
79	11.50	1.24	0.13856	0.483441
80	10.65	1.10	0.10358	0.422236
81	9.72	0.91	0.153353	0.34653
82	10.24	1.03	0.20682	0.399035
83	12.79	1.35	0.19141	0.519038
84	9.90	0.94	0.105372	0.351756